UNIVERSITÀ DEGLI STUDI DELLA TUSCIA DI VITERBO

Dipartimento di Ecologia e Sviluppo Economico Sostenibile

Corso di Dottorato in Ecologia e Gestione delle risorse Biologiche - XXI CICLO

Physical-biological variability and covariability in the Algero-Provençal basin by means of multisensor satellite and *in situ* data

BIO/07

Coordinatore: Dott.ssa Roberta Cimmaruta

Firma

Dottorando: Antonio Olita

Firma

Tutor: Dott. Angelo Perilli

Firma

A Paola e Michele

Ringraziamenti

Desidero ringraziare innanzitutto i miei genitori.

Un grazie al tutor della mia tesi, Angelo, per l'aiuto datomi in questi tre anni nello sviluppo del progetto di dottorato e nell'elaborazione del presente manoscritto e ad Alberto per la revisione dei vari capitoli.

Alberto, Andrea C., Andrea S., Dino, Paolo, Roberto, Salvatore, Serena, Simone e tutti gli amici e colleghi del CNR e dell'IMC meritano un particolare ringraziamento per l'amicizia dimostratami e per le interessanti e costruttive discussioni, scientifiche e non, che hanno contribuito in questi ultimi tre anni alla mia crescita culturale, tecnica e scientifica, nonchè alla mia sopravvivenza in quel di Torregrande.

Un sentito ringraziamento al dott. Stefano Vignudelli per i preziosi consigli sull'analisi dei dati satellitari. Ringrazio inoltre il gruppo del Dipartimento di Biologia Vegetale dell'università di Firenze, nonchè tutti i partecipanti alle campagne oceanografiche MedGOOS.

Si ringrazia la NASA, il NOAA e il CLS per aver reso disponibili gratuitamente i dati satellitari.

Infine, per ultimi ma ovviamente non ultimi, vorrei ringraziare Paola e Michele per avermi sopportato (e supportato) in questi ultimi mesi, visto anche il loro impegno, incomparabilmente più importante di quanto non fosse portare a termine questo manoscritto.

A tutti loro, e a coloro che ho accidentalmente scordato di menzionare:

Grazie di cuore

Abstract

The climate change has been proved to influence marine ecosystems either in their physics and biology. The Mediterranean sea, because of its characteristics, is particularly sensitive to climatic changes and more in general to the variability of the physical forcings, as shown by several authors. In this scenario, the study of the relationships between hydrodynamics, phytoplankton distribution and primary production, becomes particularly important in order to better understand the ecological effects of eventual hydrodynamic shifts induced by climate change. The aim of the present thesis is the study of the spatial and temporal variability of the algal biomass and primary production in the Algero-Provençal Basin (Western mediterranean), as well as the study of their relationships with hydrodynamical processes. We approached the problem by analysing several remotely sensed and *in situ* datasets covering multiple temporal and spatial scales, from meso-scale to basin-scale. The seasonal and interannual variability of the chlorophyll fields has been studied by analyzing the Seawifs monthly dataset, while the AVISO/CLS and the Pathfinder AVHRR datasets have been used to analyze respectively Sea Level Anomalies (SLA) and Sea Surface Temperature (SST) over the decade 1997-2007. The main sesonal and interannual patterns of physical and biological fields have been identified through EOF decomposition and wavelet analysis, while the covariability has been studied trough Singular Value Decomposition (SVD). The seasonal variability of the algal biomass is composed by two annual cycles, timewise and spacewise shifted. The analysis also showed a significant interannual variability, and the footprint of an anomalous event, the summer 2003 heatwave, has been identified either in physical and biological fields. Significant correlations have been found between physical and biological fields permitting to perform a simple zonation of the domain, as function of the different bio-physical coupling. Three main zones have been therefore identified, north central and south. The central zone shows the lower trophic level and, at the same time, the strongest coupling between SLA and the algal biomass. The primary production (PP) has been estimated, for the same decade, by using a satellite based model. The model makes use of remotely sensed Photosyntetically Available Radiation (PAR), SST and chlorophyll, in order to estimate the PP integrated over the euphotic layer. The basin averaged annual primary production, for the period 1998-2006, is 142 $gCm^{-2}year^{-1}$, in good agreement with previous findings, with a pronounced interannual variability and no evident trends. We identified the signature of the 2003 European heatwave, which determined a marked decrease of PP in summer 2003. To better understand the relationships we hypothesized between mesoscale eddies and chlorophyll, a set of hydrological and fluorometric data, collected during two oceanographic cruises, conducted in 2001 and 2002 in the Sardinian Sea (in front of the western Sardinia coast), has been analysed. The analysis proved that the mesoscale eddies have a dominant role in modulating and redistributing the algal biomass, confirming the assumptions and the hypothesis performed in the basin scale study. The analysis of *in situ* data shows that the anticyclonic eddies infer in the concentration and distribution of the chlorophyll through several mechanisms, as function of their position (coastal or open-sea), size, relation with the continental shelf and depending on their reciprocal interaction.

Sommario

Vari autori hanno dimostrato come i cambiamenti climatici possano influenzare gli ecosistemi marini sia nella loro parte fisica che biologica. Il Mediterraneo, considerate le sue caratteristiche, è particolarmente sensibile ai cambiamenti climatici e più in generale alla variabilità dei forzanti fisici. In questo scenario, lo studio delle relazioni tra idrodinamica, distribuzione fitoplanctonica e produzione primaria, diventa di particolare importanza per poter meglio comprendere gli effetti ecologici di eventuali mutamenti nei regimi idrodinamici indotti dai cambiamenti climatici. Lo scopo della presente tesi è lo studio della variabilità spaziale e temporale della concentrazione della clorofilla e della produzione primaria nel bacino Algero-Provenzale (Mediterraneo Occidentale), nonchè lo studio delle loro relazioni con i processi idrodinamici. Il nostro approccio è stato quello di analizzare diversi dataset di misurazioni satellitari (multisensore) ed *in situ*, che ci hanno permesso di coprire differenti scale spaziali e temporali, dalla scala di bacino alla mesoscala. La variabilità stagionale e interannuale della clorofilla è stata studiata, per il decennio 1997-2007, analizzando il dataset di Clorofilla-a SeaWiFS, mentre per lo studio delle *Sea Level Anomalies (SLA)* e della *Sea Surface Temperature (SST)* sono stati utilizzati i dataset AVISO/CLS e Pathfinder AVHRR. I principali cicli stagionali e gli eventi anomali sono stati identificati tramite i metodi *EOF* e *wavelet*, mentre la covariabilità è stata studiata tramite *Singular Value Decomposition (SVD)*. La variabilità stagionale della biomassa algale è risultata composta da due cicli annuali separati temporalmente e spazialmente. L'analisi ha anche permesso di indentificare il segnale dell'ondata di calore dell'estate del 2003 sia nei campi fisici che biologici. Sono state trovate significative correlazioni tra i campi fisici e biologici, permettendo di effettuare una semplice zonazione in funzione del differente accoppiamento bio-fisico osservato. Sono state quindi identificate tre zone, settentrionale meridionale e centrale. Quest'ultima si è dimostrata la più oligotrofica ma anche quella dove la covariabilità tra le *SLA* e la biomassa algale è più forte. La produzione primaria (PP) è stata stimata tramite l'uso di un modello diagnostico basato su dati satellitari. Il modello utilizza dati satellitari di *PAR, SST* e clorofilla, al fine di stimare la PP integrata sullo strato eufotico. La produzione primaria annuale mediata sul dominio per il periodo 1996-2006 è di 142 $gCm^{-2}year^{-1}$, in buon accordo con la letteratua, con una pronunciata variabilità interannuale ma senza mostrare *trend* evidenti. E' stata identificata l'anomalia dovuta all'ondata di calore del 2003, che ha determinato un marcato decremento della PP nell'estate dello stesso anno. Per meglio comprendere le relazioni ipotizzate tra i vortici a mesoscala e la distribuzione della clorofilla abbiamo analizzato un set di dati idrologici e fluorimetrici, raccolti nel corso di una due campagne oceanografiche condotte tra il 2001 e il 2002 nel Mare di Sardegna. Dall'analisi condotta è

risultato che i vortici a mesoscala hanno un ruolo predominante nel modulare e redistribuire la biomassa algale, confermando le ipotesi fatte nello studio a larga scala. L'analisi dei dati in situ mostra che i vortici anticiclonici, in questo tratto di mare, influenzano la distribuzione e la concentrazione della biomassa algale tramite differenti meccanismi, in funzione della loro posizione (costieri o di mare aperto), della loro estensione, della interazione con la piattaforma continentale nonchè a seconda della loro reciproca interazione.

This manuscript has been generated with LaTeX

Contents

General Introduction **1**
The study area . . . 6
Manuscript aim and organization . . . 8

1 Seasonal and interannual variability and covariability of SLA, SST and phytoplanktonic biomass **11**
1.1 Introduction . . . 11
1.2 Methods . . . 12
1.2.1 Satellite Data . . . 13
1.2.2 EOFs method . . . 14
1.2.3 Time series analysis and Wavelet transform . . . 16
1.2.4 Correlation and SVD analysis . . . 17
1.3 Results . . . 18
1.3.1 SLA variability . . . 18
1.3.2 SST variability . . . 23
1.3.3 Chl variability . . . 26
1.3.4 SLA–Chl covariability . . . 36
1.3.5 SST–Chl covariability . . . 38
1.4 Discussion . . . 41

2 Satellite based estimates of Primary Production, in the decade 1997-2007: seasonal and interannual variability **47**
2.1 Introduction . . . 47
2.2 Methods . . . 49
2.2.1 Satellite Data . . . 49
2.2.2 Regional algorithm for chlorophyll . . . 49
2.2.3 Chl algorithms validation . . . 50
2.2.4 Vertically Generalized Production Model . . . 53
2.2.5 Data analysis . . . 55
2.3 Results . . . 56
2.3.1 Annual budgets of PP . . . 56
2.3.2 Seasonal and interannual variability . . . 58

2.4 Discussion 61

3 Mesoscale eddies and chlorophyll distribution in the Sardinian Sea 65

3.1 Introduction 65
3.2 Methods 66
3.2.1 Hydrological measures and water samples 66
3.2.2 Satellite Data 68
3.3 Results 68
3.3.1 Chlorophyll–salinity correlation 68
3.3.2 March 2001: hydrology and Chlf distribution 71
3.3.3 May 2002: hydrology and Chlf distribution 81
3.4 Discussion 87

4 Conclusions 91

4.1 Objectives achieved 92
4.2 Perspectives 95

Bibliography 97

Acronyms 105

List of Figures

1 The electromagnetic spectrum (courtesy of LASP/University of Colorado) . . . 5

2 Algero-Provençal Basin (red squared): the principal dynamics are indicated. Modified from Millot et al. (1999) . . . 7

1.1 Top panel: SLA basin averaged time series; Bottom panel: SLA normalized anomalies . . . 18

1.2 Wavelet analysis of SLA normalized anomalies time series . . . 19

1.3 Standard deviation map of SLA . . . 20

1.4 EOF-1 of SLA. 76% of variance is explained by this mode of variability . . . 21

1.5 SLA PC-1: its periodicity is clearly driven by seasonality . . . 22

1.6 EOF-2 of SLA. 4% of variance is explained by this mode of variability, showing a maximum with an eddy-like shape . . . 23

1.7 Wavelet plot of SLA PC-2: a long-period minimum is identified in 2003. . . . 24

1.8 EOF-3 of SLA. 2% of variance is explained by this mode of variability, mainly due to algerian current anomalies . . . 25

1.9 Wavelet plot of SLA PC-3: the signal is characterized by an anomaly at the end of the series. . . . 26

1.10 EOF-4 of SLA, explaining 2% of variance, related to the variability of the LPC and AC . . . 27

1.11 Wavelet plot of SLA PC-4: the signal seems characterized by an annual cycle, even though with a break in 2004 . . . 28

1.12 Top panel: SST basin averaged time series; Bottom panel: SST normalized anomalies . . . 28

1.13 Wavelet analysis of SST normalized anomalies time series . . . 29

1.14 Standard deviation map of the SST for the 1997-2007 period . . . 30

1.15 EOF-1 of SST. more than 97% of variance is explained by this mode of variability . . . 31

1.16 EOF-2 (left) and EOF-3 (right) of SST. 0.6% of variance is explained by EOF-2, while the EOF-3 explains the 0.2%, related to interannual mistral wind events. 32
1.17 Top to bottom, SST PC-1, 2 and 3. Seasonal cycles can be recognized in the first two PCs. 32
1.18 Top panel: Chl basin averaged time series; Bottom panel: Chl normalized anomalies 33
1.19 Wavelet analysis of Chl normalized anomalies time series 33
1.20 Left Panel: EOF-1 of Chl, explaining 44% of variance, related to the MEDOC area bloom. Right Panel: EOF-2 of Chl, explaining 14% of variance, related to the weak blooms occurring along AC and AEs area of influence 34
1.21 Chl PC-1 and PC-2: The signals are characterized by annual cycles, with maxima respectively in early spring (PC-1) and winter(PC-2) 34
1.22 EOF-3 of Chl, explaining about the 4% of variance, related to a negative anomaly occurring in Gulf of Lion and in the NW part of the Basin, while the positive signs are localized along the western coasts of Corsica 35
1.23 Wavelet plot of Chl PC-3. Some anomalies are evident:a minimum centered in spring 2001, and a shorter-period maximum in spring 2005 35
1.24 SLA–Chl correlation map($P < 0.05$). The values of r are negative on the whole basin 37
1.25 Heterogeneous correlation map for the first SVD mode (SLA expansion coefficients Vs Chl data) 38
1.26 Expansion coefficients of first SVD mode: up SLA and bottom Chl expansion coefficients 39
1.27 SST–Chl correlation map. The values of r are negative on the whole basin 40
1.28 Heterogeneous correlation map for the first SVD mode (SST expansion coefficients Vs Chl data) 41
1.29 Expansion coefficients of first SVD mode: up SST and bottom Chl expansion coefficients 42

2.1 Distribution of Chl validation data 51
2.2 Regression of regional (red line) and global (blu line) satellite chlorophyll data with *in situ* measurements. Regional algorithm shows better performances. 53
2.3 Annual PP_{eu} (1998-2006 climatology) 57
2.4 Annual budgets of PP_{eu} (1999-2006) 58
2.5 Monthly time series of PP 58
2.6 EOF-1 of PP. About the 68% of variance is explained by this mode of variability 60

2.7 EOF-2 of PP. 13% of variance is explained by this mode, showing a seasonal behaviour . . . 61
2.8 EOF-3 of PP. 0.6% of variance is explained by this EOF, related to interannual variability patterns . . . 62
2.9 Top to bottom, PC-1, 2 and 3 of PP dataset . . . 63

3.1 Sampling scheme of MedGOOS-2 (left) and MedGOOS-4. The transects along which vertical sections have been coduced, are also indicated. . . . 67
3.2 Map of Mixed Layer Depth (MLD). MLD values (meters) for single stations have been calculated using the $\Delta\sigma_\theta$ criterion of Sprintall and Tomczak (1993) . . . 70
3.3 Chlorophyll-salinity correlation profiles (left) and correspondent P value (right) for the two zones, north (blue) and south (red) of the density front at 40.5°N . . . 71
3.4 Clockwise from the left-top corner, 5 m maps of: temperature, salinity, chlorophyll-a and density. The maps are obtained by cubic interpolation on equally spaced grid . . . 72
3.5 The three eddies A1, A2 and A3, found by the analysis of CTD casts, have been also observed in the Ocean Color image. . . . 73
3.6 March 2001, clockwise from the left-top corner, 30 m maps of: temperature, salinity, chlorophyll-a and density. The maps are obtained by cubic interpolation on equally spaced grid . . . 75
3.7 March 2001, vertical section, between stations 76 and 86 (diagonal transect Td), identifying the coastal upwelling south of Sardinia. The rise of isoalines (left) and the connection between the two Chlf patches (right) seen in the $30m$ map are evident . . . 76
3.8 March 2001, Integrated chlorophyll in the upper 150 m . . . 77
3.9 March 2001, clockwise from the left-top corner, 50m (DCM depth) maps of: temperature, salinity, chlorophyll-a and density. The maps are obtained by cubic interpolation on equally spaced grid . . . 78
3.10 March 2001, salinity (left) and chlorophyll sections along transect T1. Salinity is expressed in *psu* and chlorophyll-a in mg/m^3 79
3.11 March 2001, salinity (left) and chlorophyll sections along transect T2. Salinity is expressed in *psu* and chlorophyll-a in mg/m^3 79
3.12 March 2001, salinity (left) and chlorophyll sections along transect T3. Salinity is expressed in *psu* and chlorophyll-a in mg/m^3 79
3.13 May 2002, clockwise from the left-top corner, 5m maps of: temperature, salinity, chlorophyll-a and density. The maps are obtained by cubic interpolation on equally spaced grid . . . 82
3.14 May 2002, salinity (left) and chlorophyll sections along transect T1. Salinity is expressed in *psu* and chlorophyll-a in mg/m^3 . . 83
3.15 May 2002, salinity (left) and chlorophyll sections along transect T2. Salinity is expressed in *psu* and chlorophyll-a in mg/m^3 . . 83

3.16 May 2002, salinity (left) and chlorophyll sections along transect T3. Salinity is expressed in *psu* and chlorophyll-a in mg/m^3 . . 83
3.17 The anticyclonic eddies A4, A5 and A6 are indicated in the Ocean Color image (May 25 2002). 84
3.18 May 2002, clockwise from the left-top corner, 30m maps of: temperature, salinity, chlorophyll-a and density. The maps are obtained by cubic interpolation on equally spaced grid 85
3.19 May 2002, clockwise from the left-top corner, 70m (DCM depth) maps of: temperature, salinity, chlorophyll-a and density. The maps are obtained by cubic interpolation on equally spaced grid 86
3.20 May 2002, integrated chlorophyll in the upper 150 m 87

List of Tables

3.1 Period and area sampled during the two cruises 66

General Introduction

Ocean and regional seas are dynamic and sensitive systems. Strongly coupled with lower layers of the atmosphere, the physics and the biology of seas and oceans are influenced by, and interact with, atmospheric and climate dynamics. The coupling between atmosphere and seas acquires further importance considering the scenario of increased atmospheric variability (Schär et al., 2004) and the climate change the Earth is experiencing in the last century. The Earth system is actually afflicted by a rapid climate change with changing rates, above all over the last 50 years, never seen before. This is an evidence widely recognised by the scientific community as well as ratified in documents produced by international panels and protocols (Kyoto 1997, Marrakech 2001, IPCC 2007) by the synergistic efforts of policy and science. The scientific community showed that the human activities have a large impact (probably they are the main drivers of climate change) on the abnormal warming recorded at global scale, although some uncertainty, concerning the amount of the impact of human activities on observed changes, still persists. The effects of global warming at regional and local scales are still poorly understood, although it is evident that one of the main effects at these scales is the increase in the occurrence of extreme events (Black et al., 2004; Schär et al., 2004). The sensitivity and the response of marine ecosystems to climate change, and more in general to atmospheric and climate forcing, have been demonstrated in a variety of different environments and at different spatial and temporal scales (Smith et al., 1999; Gian-Reto et al., 2002; Olita et al., 2007).

In this scenario, the deep understanding of the intrinsic variability of the physical and biological parameters of the sea becomes fundamental in order to assess the natural variability of the studied systems and to avoid the problem of the *shifting baselines*, i.e. to have inadequate reference points to evaluate anomalies crossing the systems. So, the study of the relations between the physical environment and the first trophic levels in regional seas becomes topical from a theoretical point of view as well as to understand (and possibly to prefigure) the ecological effects of hydrodynamic shifts in a climate change scenario (Turley, 1999; Schär et al., 2004; Somot et al., 2006; Olita et al., 2007). The deep understanding of the variability, the relationships and the coupling between physics and biology is essential for the desirable development of an ecosystem based management of the marine resources.

While the physics governing the ocean dynamics are quite well known, as well as the coupling between hydrodynamics and the atmospheric forcings, the biological response of the sea to the dynamics of the atmosphere (and their anomalies) and of the sea itself are poorly understood, because of the complexity of the matter and of the limited resources dedicated to this argument. This neverthless several efforts have been recently accomplished by the scientific community to fill the gap.

The nontrivial issue of the physical-biological coupling of the sea can be faced with many different approaches, spanning from paleoclimatology to climatology to experimental multi-instruments oceanography, analysis of historical time-series, remote sensing, to a variety of modeling tools (diagnostic, prognostic, spatially explicit or implicit). The difficulties of studying geo-physical processes and their biological inference lies in the complexity of the interactions involved and on the fact that these relationships take different aspects in function of the temporal and spatial scales examined. In a deterministic perspective, the investigation of these relationships could be approached by studying the roles of physical forcings in the modulation of the biogeochemical cycles (C, N, P and micronutrients), which in turn regulate the productivity of phytoplankton, together with the available energy (light). The prognostic/deterministic study of the biogeochemical cycles can be accomplished at first by using sophisticated and coupled modeling tools, which are often affected by quite large uncertainties about biomass and production of the phytoplankton. These uncertainties can be due to an incorrect modeling of the hydrodynamics (advection and diffusion) or to a bad parameterization of phytoplanktonic functional groups (Vichi et al., 2007b,a). Although these modeling tools represent the future in this field because they allow to prognostically study the processes underlying the observed features, they are still affected by uncertainties such as their affordability just lies in reproducing the seasonality of the system, in front of a huge amount of computing power needed (Zavatarelli and Pinardi, 2003; Fulton et al., 2004; Vichi et al., 2007a).

An alternative/complementary approach to the deterministic–prognostic modeling is to exploit the potentiality of the huge amount of data collected by satellite remote sensing, with the support of the data collected during multidisciplinary oceanographic cruises, which furnishes the *in situ* truth. Another approach is given by the analysis of these satellite data through diagnostic algorithm to estimate biomass and production. The availability of decadal (at least) time series of multisensor (i.e. multiple parameters) data covering the study area in its entirety is the main advantage of using satellite data for these purposes. Another helpful characteristic of satellite remotely sensed data is the synopticity which permits, in contrast with *in situ* cruises, to have a contemporary assessment of the same parameter in different points. This is not trivial as the variability of the sea is characterized by higher frequencies than the land systems. Satellite imagery of the sea surface are available since the late 60's, but only in the last two or three decades several satellites and sensors furnished, simultaneously and over the whole globe, a number of retrievals of many sea surface parameters (temperature, sea surface elevation, chlorophyll and other pigments, PAR, winds, etc.). All of these parameters substantially derived from the measurements of the radiance reflected or emitted by the sea surface, over different windows of the electromagnetic spectrum (see Fig. 1 and Box 1).

Box 1 - Satellite remote sensing of the sea

In the last 20-30 years satellite remote sensing has become an essential instrument in studying dynamical features and water mass properties of the oceans at global, regional and local scales. For example, mid-latitude global observation of ocean mesoscale features allowed us to better understand the variability and the budgets of the eddy kinetic energy of the oceans and the related transport of heat, salt and water mass. Global observations of ocean color available from the late '70s, with the launch of the Coastal Zone Color Scanner (CZCS), furnished an invaluable information about the concentration and distribution of phytoplankton biomass and therefore important suggestions about the productivity of the oceans and its variability. Although ocean satellites have been mostly regarded as *experimental*, they have nevertheless contributed to an increasing awareness that the oceans, atmosphere and ice-covered regions are coupled in a way that determines short-term weather patterns as well as longer-term climate change.

Two categories of sensors can be distinguished, Active and Passive, depending if the sensor captures the backward reflected radiation emitted by the instrument itself or that naturally reflected/emitted by the Earth (Sea) surface. The number of sensors and vectors designed to monitor the sea surface increases each year. Nevertheless this increasing number, all these sensors (installed on geostationary or polar orbiting satellites) basically give information about only four parameters of the sea surface: temperature, slope, roughness and color. These parameters are retrieved from the measurement of the radiance emitted or reflected by the sea surface at different wavelengths of the electromagnetic spectrum (Fig. 1).

Here below we furnish a brief overview of the principles governing the instruments used to retrieve the different parameters, many of which used for this manuscript.

The **synthetic aperture radar (SAR)** is an active instrument which detects small modulations of surface ripple patterns caused by winds, waves, eddies, slicks effluents or other surfactants. A moving surface feature will be shifted in the image plane due to its contribution to the Doppler signal used by SAR processor to locate a particular target. One of the main marine applications of this instrument is the oil spill detection.

The **radar altimeter** is an active instrument used to detect small changes in sea surface height due either to anomalies in the gravity field of the earth or to geostrophic currents, tides, mesoscale eddies or other oceanographic structures. The height of the waves can be also monitored by measuring the slope of the leading edge of the return pulse.

Features producing changes in surface temperature could be more difficult to track, because of cloud cover which cannot be crossed by infrared and thermic wavelengths. Nevertheless the record of the **Advanced Very High Resolution Radiometer (AVHRR)** now spans over more than two decades. The algorithm for the retrieval of the Sea Surface Temperature are based on the measurements of the emission from the sea surface on infrared and thermic bands of the electromagnetic spectrum. These sensors installed on the NOAA (National Oceanographic and Atmospheric Administration) series satellites were successively and successfully supplemented by many other sensors like the Along-Track Scanning Radiometer (ATSR) produced by the European Space Agency (ESA) and mounted on the ERS-1 satellite.

The remote sensing of the **ocean color** is, by definition, the spectral variation of the reflectance diffused from the sea surface. It permits to obtain the ocean surface Chlorophyll concentrations from reflectance measurements in the visible part of the spectrum. Clarke et al. (1970) first proposed the idea that the concentration of oceanic phytoplankton can be estimated by measuring the amount of light reflected, on certain specific wavelengths of the EM spectrum, by the ocean surface. The remote sensing of the ocean color started with the launch in 1978 of the CZCS, of which the SeaWiFS radiometer is the worthy successor.

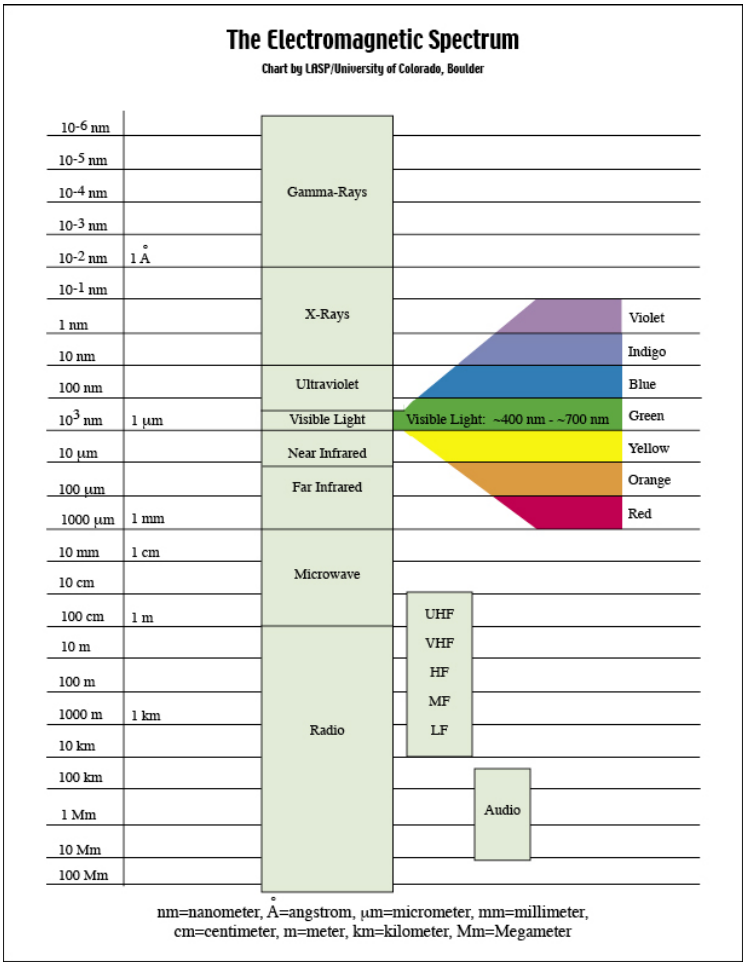

Figure 1: The electromagnetic spectrum (courtesy of LASP/University of Colorado)

The study area

The study of the biophysical relationships becomes even more important in highly dynamic seas, like the Mediterranean, where the hydrodynamic processes may strongly influence the phytoplankton distribution and concentration (Moran et al., 2001; Taupier-Letage et al., 2003; Isern-Fontanet et al., 2004; Ribotti et al., 2004; Kahru et al., 2007). The Mediterranean sea has been often considered like a small scale model of the global ocean circulation and often used as a case study to test theories and models in a wide range of disciplines of the marine sciences.

The reason for this are basically three:

- its historical anthropization has made the Mediterranean area an elected site for climate change studies;

- in the Mediterranean area a number of different dynamical features and a wide range of different trophic states can be found. This extremely variable environment, both in space and time, constitutes a good small scale model of the global ocean;

- the Mediterranean reacts more rapidly to atmospheric/climate change and to the variability of physical forcing than the global ocean.

In this framework, the Algero-Provençal Basin (APB) represents one of the most dynamic areas of the entire Mediterranean sea, and almost all the features and processes recognizable in Mediterranean can be found in this sub-basin. So, also considering the availability of *in situ* data collected during several oceanographic cruises conducted by our research group, this region has been chosen as case study. The APB can be roughly divided in two main parts, the northern and the southern one, as function of the main dynamic features and of the different circulation regimes (see Fig. 2). We adopt, partially modified, the nomenclature used by Millot et al. (1999).

The southern part of the APB, namely the Algerian Basin (AB), is characterized at the surface by the Atlantic Water (AW) flowing in the Mediterranean sea through the Gibraltar Strait (Millot et al., 1999). Along the Algerian coast the AW (Modified AW, MAW) is transported by the Algerian Current (AC Millot, 1985) from which the anticyclonic Algerian Eddies (AEs, Puillat et al.,

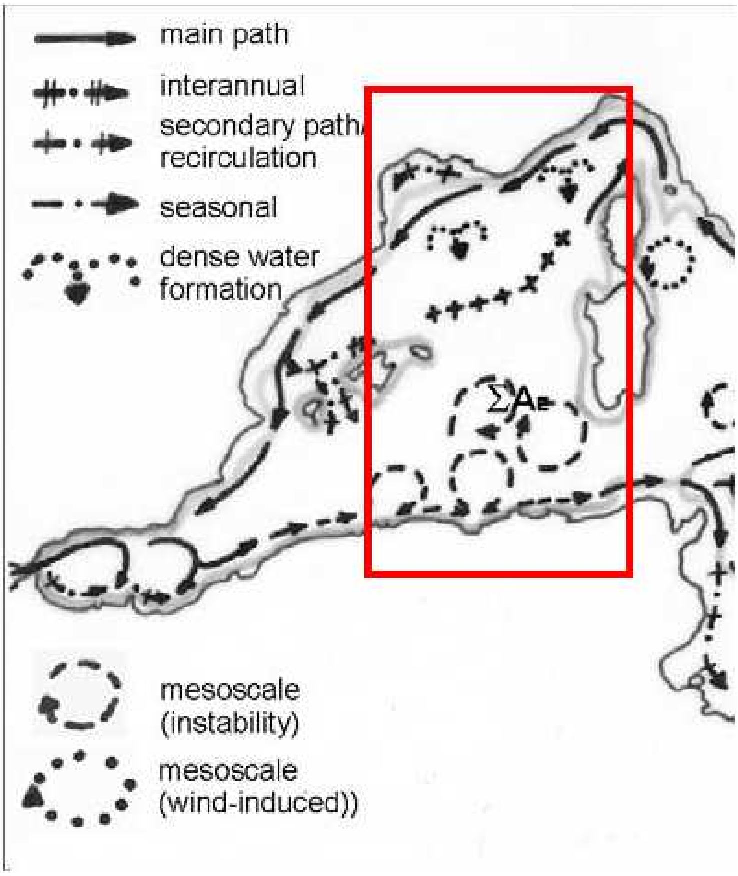

Figure 2: Algero-Provençal Basin (red squared): the principal dynamics are indicated. Modified from Millot et al. (1999)

2002; Taupier-Letage et al., 2003) are generated by baroclinic instabilities of the AC itself. The AEs generally remain more or less included in the main AC flow. Once in the Sardinia Channel (SaC) they can collapse or, strongly modified, can remain almost blocked in the SaC area for several months before collapsing (Puillat et al., 2002). In some cases (few per year) the AEs can detach from the AC moving eastward and northward. In these cases the eddies can follow the Sardinian slope northward becoming open-sea eddies. These big "old" and highly energetic AEs can accomplish one or more cyclonic cycle in the AB, not exceeding 40°N (Puillat et al., 2002). Studies focusing on the biological response of AEs (e.g. Taupier-Letage et al., 2003), suggested complicated relationships depending on the life history, path and size of such eddies, without entirely clarifying these processes and indicating that further investigations and studies are needed.

The northern part of the basin (Liguro-Provençal Basin or LPB) is also a highly dynamic region with strong mesoscale activity, studied especially because it is the most important site of deep waters formation (MEDOC group, 1969) for the whole western Mediterranean sea. The deep water formation in winter and the seasonal bloom occurring in the so called MEDOC area (MEDOC group, 1969) in spring are strictly related as stated by Jacques et al. (1973). The deep water formation is a complicated process which substantially involves three phases (MEDOC group, 1969; Levy et al., 1998). The first one is a preconditioning phase, mainly due to the sub-basin cyclonic circulation encomprising the LPB down to about 41°N and determining the rise of colder and saltier waters from the deep to the upper layers. The second one is a violent mixing phase, determined by the mistral wind, with the formation of stable columns of dense waters from surface to the bottom. These columns of dense water are also called *chymneys*. The third phase consists in the sinking of the dense chimneys, due to the weakening of the winds, with the consequent rapid restratification of the surface waters enhanced by their warming. The restratification is also responsible of the onset of an intense algal bloom as described in Jacques et al. (1973). The main sub-surface coastal current of this sub-basin is the Liguro-Provençal Current (LPC), which flows NE to SW, along the Italian and French coasts. The LPB can be separated from the AB by the Balearic Front (BF), formed by the north-south density gradient between saltier and colder waters at north (LaViolette et al., 1990; López Garciá et al., 1994; Millot et al., 1999) and fresher MAW at the south. The BF is disposed more or less longitudinally, at a latitude of about 41-42°N, with some variability on its latitudinal position which has not still deeply investigated. The buffer area between APB and LPB, partly occupied by the BF, is also called by some authors Balearic Basin. The eastern part of this sub-basin, along the western Sardinian coast, is the Sardinia Sea (SaS) while the Sardinia Channel (SaC) is the channel located between Sardinia and the African coast.

Manuscript aim and organization

The APB, broadly investigated in the past on its hydrodynamics (e.g. Vignudelli, 1997; Levy et al., 1999; Millot et al., 1999; Levy et al., 2000; Bouzinac et al., 2003; Isern-Fontanet et al., 2004), was also object of studies on the relationships between hydrodynamics and phytoplanktonic biomass distribution and production, often focusing on the biological signature associated to mesoscale processes (e.g. Lohrenz et al., 1988; Raimbault et al., 1993; Levy et al., 1998, 2000; Garcon et al., 2001; Moran et al., 2001; Taupier-Letage et al., 2003). Nevertheless, the bio-physical covariability in the APB has been poorly investigated from a statistical point of view, needing the analysis of well structured datasets and long time series. The use of both satellite and *in situ* data, sampled with a mesoscale resolving grid, permits to conduct the study at multiple spatial and temporal scales.

In the present study, the physical and biological variability is investigated through the satellite data spatially at basin and sub-basin scale while temporally at seasonal and interannual scale, also giving some clues on mesoscale processes. A set of multisensor satellite Level 3 monthly data has been analyzed making use of multivariate techniques, covering the decade 1997-2007, in order to study the variability and covariability of the main bio-physical parameters retrieved from satellite (sea surface temperature, sea level anomalies, photosynthetically available radiation, Chlorophyll-a concentration, primary production) at these scales. Three are the main gaps in the use of satellite data: the spatial resolution which can miss the smallest features; the presence of cloud cover that in visible and infrared wavelength avoids the observation of the sea surface; the total absence of information about the vertical characteristics of the water column, i.e. the satellite can see only the sea surface! The data collected during a series of oceanographic cruises conducted in the central-eastern part of the APB (namely the Sardinian Sea) has been also analysed in order to obtain any information on the main vertical features, at least in some sample sub-areas, and to study the mesoscale horizontal and vertical processes influencing the biological fields (Chlorophyll-a is universally considered the best and most helpful proxy for phytoplanktonic biomass).

The general aim of this manuscript is to depict the seasonal and interannual variability of the some key physical parameters of the water masses retrieved by satellite and understand how these fields are related to the phytoplanktonic biomass and productivity in the APB. Primary production budgets have been estimated by using a diagnostic model which make use of remotely sensed data. A series of oceanographic cruises have been analyzed and the results of this analysis related to the findings of the first two chapters, in order to understand how smaller (meso) scales features influence the phytoplankton distribution in the study area.

Different aspects of the same general problem have been faced in the first three chapters of this manuscript. By considering the diversity of the methods used and of the analyses performed, each chapter can be considered as a distinct study, although each one contributes to furnish, as much as possible, a complete picture of the variability and covariability of the physical and biological fields in the APB. Then each chapter is composed by *Introduction, Methods, Results* and *Discussion* sections, with the exception of Chapter 4 which draws the general conclusions.

The manuscript is organized as follows:

- In **Chapter 1** the seasonal and interannual variability and co-variability of remotely sensed SLA, SST and Chlorophyll-a fields in the APB is studied, for the period 1997-2007. A zoning of the area is therefore obtained in function of the co-variability patterns.

- In **Chapter 2** the Primary Production (PP) of the APB has been estimated, during the same decade, using a semi-analytical diagnostic model. All the model parameters are obtained, directly or indirectly, from remote sensing measurements. Findings about PP are therefore compared with literature.

- **Chapter 3** is devoted to the analysis of the oceanographic cruises data, aiming to investigate the mesoscale processes (with special focus on eddies) influencing the phytoplanktonic biomass distribution in the central part of the APB.

- Finally in the **Conclusions** (**Chapter 4**), the objectives achieved are synthesized and the perspectives for future developments are drawn.

Chapter 1

Seasonal and interannual variability and covariability of SLA, SST and phytoplanktonic biomass

1.1 Introduction

Recent studies (McGillicuddy and Robinson, 1997; Wilson and Adamec, 2001; Wilson and Adamec, 2002; Kahru et al., 2007) showed that, in many areas of the world ocean and at various scales, the Chlorophyll-a concentration (Chl) and/or the new production of phytoplankton biomass, are strongly related with Sea Level Anomalies (SLA). The main mechanism explaining this relationship is the shoaling (deepening) of isotherms/isopycnae due to the action of dynamical features (having a SLA signature) which produces the increase (decrease) of nutrients injection in the euphotic layer.

On the other side, the Sea Surface Temperature (SST), which can be retrieved with an ever increasing accuracy from satellite, is historically the main parameter of the sea surface used in satellite oceanography to distinguish dynamical features like currents, fronts and eddies, which are often characterized by a thermic signature. The relationships of the temperature with the dynamic structures, which in turn influence patchiness and distribution of the chlorophyll (the best proxy for phytoplanktonic biomass) field, lead many authors (e.g. Bricaud et al., 2002; Legaard and Thomas, 2006; Rivas, 2006; Nieves et al., 2007; Venegas et al., 2008) to use also SST signatures to investigate the complex relationships between phytoplanktonic biomass and dynamical features. Especially in some areas, like over the continental shelves, where dynamical processes cannot be correctly observed or deduced by satellite altimetry because of sensor or data-products limitations, the information coming from thermic sensors can be very helpful.

The availability of decadal time series (1997-2007) of remotely sensed estimates of Chl and the simultaneous availability of SLA and SST satellite data for the same period, allow us to investigate the main spatial and temporal patterns of variability of Chl, SLA and SST and the SLA–Chl and SST–Chl covariability in the APB, which is actually the main aim of this chapter.

Timewise, the seasonal and interannual variability are investigated and quantified through multivariate analysis techniques and data decomposition. Although the investigated spatial scales are mainly the basin and the sub-basin, some indication on mesoscale features, indirectly, is also given. Suggestions for a better interpretation of the observed patterns of variability are given in Chapter 3, where the analysis of *in situ* oceanographic data furnished useful indications on the mesoscale processes influencing phytoplankton concentration and distribution of the eastern sub-area.

1.2 Methods

We have analyzed three datasets of remotely sensed data (Chl, SLA and SST from September 1997 to January 2007) through decomposition of their variability by means of the Empirical Orthogonal Function (EOF) method. This method allowed us to identify and quantify the spatial and temporal variability of the three variables. The Continuous Wavelet Transform and the Fourier Transform (CWT and FT) were used to better interpret the expansion coefficients time series of secondary EOFs, often drawing complicated non-stationary patterns, as well as to analyze the basin-averaged anomalies time series for the three datasets.

The SLA–Chl and the SST–Chl covariabilities were evaluated by analyzing the r correlation coefficient maps, obtained through the integration of the data in time, and by Singular Value Decomposition (SVD) analysis. The decomposition in different modes of covariability, performed through SVD, was useful to recognize, spacewise and timewise, the processes having the largest influence on the observed covariability and to quantify them.

1.2.1 Satellite Data

The satellite SLA data used are delayed time (dt) gridded and merged products covering the entire Mediterranean Sea. They were provided by AVISO-CLS and produced in the framework of the SSALTO-DUACS (Data Unification and Altimeter Combination System) and of the Mediterranean Forecasting System (MFSPP-MFSTEP) European projects. AVISO has produced the gridded maps by processing the raw data collected from altimeters of different satellite missions (Jason-1, Topex-Poseidon, Envisat, GFO, ERS-x and Geosat Follow On). The SLA are calculated by subtracting, from the Sea Surface Height (SSH) data, the Mean Sea Surface (MSS) constructed on the basis of the Topex/Poseidon data from 1993 to 1997, which are affected by a weak orbital error. We used a set of 488 weekly SLA gridded data from September 1997 to January 2007.

SST data used are the pathfinder SST version 5. The pathfinder SST data are derived from the 5-channel Advanced Very High Resolution Radiometers (AVHRR) on board the NOAA-7, -9, -11, -14, -16 and -17 polar orbiting satellites. The monthly averaged data for the ascending pass (daytime) on equal-angle grids of 8192 pixels/360 degrees (nominally referred to as the 4 km resolution) have been used. Data have been obtained from the US National Oceanographic Data Center (NODC) of the National Oceanic and Atmospheric Administration (NOAA) and downloaded via ftp (data.nodc.noaa.gov). From the SST dataset an "anomaly" dataset has been obtained to perform the correlation and covariability analysis with Chl.

Chl data are Level-3 global composite data acquired from the SeaWiFS satellite and provided by NASA Goddard Space Flight Center through the Ocean Color Web portal. The algorithm used for the transformation of raw satellite SeaWiFS data to Chlorophyll-a concentration expressed in mg/m^3 is the NASA OC4v4 algorithm (O'Reilly et al., 1998). We further transformed these data using the regional algorithm proposed by Bricaud et al. (2002). Recently Volpe et al. (2007) showed that the MED-OC4 algorithm generates the best Chl satellite estimates for the Mediterranean Sea. Nevertheless, in our work we used the Bricaud et al. (2002) algorithm which can derive its estimates directly from the global OC4v4 L2 or L3 products, because of their prompt availability through the OceanColor web portal at the various processing levels. Moreover this study was mainly focused on low-frequency and large-scale variability rather than on the analysis of the absolute values of Chl. We excluded from the analysis the nearest-to-coast grid points supposedly containing the worst estimates of Chl (Case-2 waters). Additionally the Bricaud et al. (2002) algorithm produces quite good estimates of the Chl in the Mediterranean waters, from many points of view comparable with those of the algorithm proposed by Volpe et al. (2007). A set of 113 monthly SeaWiFS Chl composite maps from September 1997 to January 2007 have been used, almost the whole SeaWiFS level 3 dataset. For homogeneity reasons with SLA dataset we subtracted the related mean value from each pixel then obtaining a Chl anomaly dataset. This dataset of Chl anomalies (hereafter simply Chl) was used for the EOF, SVD and correlation analyses instead of the raw dataset.

Chl and SST maps have been spatially re-sampled to match the SLA grid, while the SLA maps have been temporally averaged to obtain a monthly temporal resolution fitting with SeaWiFS and AVHRR data time step (monthly). As result, three datasets of 113 monthly maps with spatial resolution of $1/8°$ have been produced and analyzed.

1.2.2 EOFs method

In order to detect the main patterns of spatial and temporal variability of the Chl, SLA and SST series, we performed the Empirical Orthogonal Functions (EOFs) analysis, also known as Principal Component Analysis (PCA). The EOF method was introduced in meteorology by Lorenz (1956). From that moment the EOFs have been widely used in climatology, meteorology and oceanography (Preisendorfer, 1988; Bretherton et al., 1992; Peng and Fyfe, 1996; Bartolacci and Luther, 1999; Baldacci et al., 2001; Bouzinac et al., 2003; Lopez-Calderon et al., 2006). This method allows to find the spatial and temporal variability patterns of the dataset and to estimate the amount of variance associated to each mode of variability in percentage terms (Preisendorfer, 1988). We would like to underline that the modes of variability, also known as EOFs (EOF-1, EOF-2,... EOF-n), contain informations about the variability of the dataset, that is not necessarily related to physical features. The interpretation of the EOF modes just aims to relate the data modes with physics. The temporal amplitudes associated with the spatial patterns, referred to as EOF expansion coefficients or simply PCs, are also object of physical interpretation. In some case further statistical analysis was needed to correctly interpret PCs, especially when the signal contains non-stationary components.

The dataset (the same was done for SLA and Chl) has been organized as follow, in order to perform the EOF analysis: At first we vectoralized the matrices (of dimension x by y) containing the monthly fields of the variable in row vectors of dimension $p = xy$. Then we formed a matrix F of dimension n columns by p rows, where: n is the number of observations (113 in our case); p is the number of grid-meshes for each observation. We can consider each of the n columns of matrix F as a time series for a given location xy, and each of the p rows as an observation (single monthly field) at a given time. The mean of each time series is then removed to obtain series with zero mean. Then R, the covariance matrix of F, is calculated by:

$$R = F^t F \tag{1.1}$$

where F^t is the transposed matrix of F.

The eigenvalue problem is solved so that:

$$R = C \Lambda C^t \tag{1.2}$$

where Λ is a diagonal matrix containing the eigenvalues λ_i of R and where each column c_i of C is the eigenvector corresponding to the λ_i eigenvalue. Each of the eigenvectors c_i is an EOF. The EOF-1 will be the c_i with the highest λ_i, i.e. the highest value of explained variance. The EOF-2 will be the c_i with the second λ_i value and so on. Each EOF, in vectorial form, is then re-converted in matrix before drawing the respective EOF map.

In order to see how an EOF evolves in time, we calculated the expansion coefficient a_j by:

$$a_j = F c_j \tag{1.3}$$

a_j is composed by n components which are the projections of the maps contained in F on c_i (EOF_j). a_j is the PC, i.e. the time evolution of each EOF_j.

1.2.3 Time series analysis and Wavelet transform

The anomalies time series of each dataset have been calculated because in many cases they may give useful information about interannual or anomalous events which cannot be correctly identified by EOF decomposition, for example due to their phase coincidence with the main seasonal signal.

The anomalies time series of each dataset has been obtained by:

$$x_n = \frac{x - x_m}{\sigma_m}, \tag{1.4}$$

where x is the monthly value, x_m is the monthly climatology for the corresponding month and σ_m is the related monthly standard deviation.

Despite the dimension reduction of the datasets performed through the EOF method, the spatial patterns and their associated PCs are not always easy to interpret, especially referring to the secondary PCs, often complicated by non-periodic signals.

For these reasons, we analyzed the spectrum of the PCs and of the anomalies time series by means of the Continuous Wavelet Transform (CWT) and of the Fourier Transform (FT). The CWT is an useful instrument to analyze time series data, especially when they contain non-stationary components. In fact the CWT allows exceptional localization both in the time domain with translations of the mother wavelet, defined as in Torrence and Compo (1998), and in the frequency domain with its dilations. The classical FT is only able to recognize the location and the magnitude of maxima in the frequency domain, without locating the frequency peaks in the time dimension. However the FT remains very appropriate for the analysis of stationary data, which do not require time localization information or, as in our case, to give an overview of the main signal components. For this reason we coupled the FT spectrum to the CWT, being the Fourier periodogram a sort of resume of the wavelet spectrum. The CWT was applied to anomalies time series (of SLA, SST and Chl) and, when necessary, to the secondary PCs to recognize where (in time-frequency) the patterns and/or the peaks recognized by the respective EOFs are located. The mother wavelets used in this study were the "Mexican hat" and the "Morlet" wavelets. The latter one is a complex function, the most used in geophysics, that constitutes a good tool to describe signals with some periodic component. The former is a real wavelet and better than the latter to precisely locate the non-stationary and non-periodic components of a series in time dimension (Torrence and Compo, 1998). Before performing the CWT and the FT we have removed the trend from the series to reduce the presence of spurious low frequency signals.

All the wavelet plots have been organized as follows: the top panel shows the analyzed series; the bottom panel shows the wavelet spectrum in the time-frequency domain with the Cone of Influence (COI, thin line indicating the area not affected by edges error) and the significance contours (95%) marked by a thick black line; the right panel shows the periodogram derived from the Fourier analysis which summarizes the frequencies of the series.

1.2.4 Correlation and SVD analysis

The r Pearson correlation coefficient between the variables has been computed in a time-integrated way (pixel by pixel) in order to describe the spatial patterns of SLA–Chl and SST–Chl covariability. We performed the Singular Value Decomposition (SVD) analysis of the coupled datasets (SLA–Chl and SST–Chl) in order to give a more accurate picture of the coupling between physical and biological variables. The SVD analysis (Bjornsson and Venegas, 1997; Bartolacci and Luther, 1999) has many common points with the EOF decomposition because it separates datasets in modes of (co-)variability. On the contrary of EOF method the SVD analysis aims to study coupled variables and to find the main patterns of covariability between two series. The explained covariability is expressed in terms of Squared Covariance Fraction (SCF) and each SCF value is associated with a pair of coupled maps drawing the coupled spatial patterns. The SVD analysis is applied on the so-called covariance matrix C. Given the two matrices S and P, containing respectively the dataset of SLA (SST) and Chl organized as matrix F for EOF method, the covariance matrix C is:

$$C = S^t P \tag{1.5}$$

where S^t is the transposed matrix of S.

Then the SVD problem is solved. We found matrices U and V and the diagonal matrix L so that:

$$C = ULV^t \tag{1.6}$$

Matrices U and V are formed by vectors u_i and v_i which are pairs of coupled modes of covariability of SLA (SST) and Chl, explaining a l_i (singular values) part of the total covariance. The expansion coefficients of the two datasets may be found, as for EOFs, by the projections of the data (S and P) on the modes of covariability (U and V). Singular values l_i contained in L can therefore be considered an estimate of how much the covariance is explained by the respective pair of coupled modes u_i and v_i. In literature u_i and v_i are often called left and right mode.

The fraction of explained covariance is expressed in terms of Squared Covariance Fraction (SCF), given by:

$$SCF_i = \frac{{l_i}^2}{\Sigma {l_i}^2} \tag{1.7}$$

1.3 Results

1.3.1 SLA variability

The time series of basin-averaged SLA and their anomalies series are shown in Fig. 1.1. The top panel shows a marked seasonal cycle with its maxima in autumn and the minima in spring. The anomalies of the bottom panel of Fig. 1.1 show a white-noise like signal which can be hardly interpreted just by looking it.

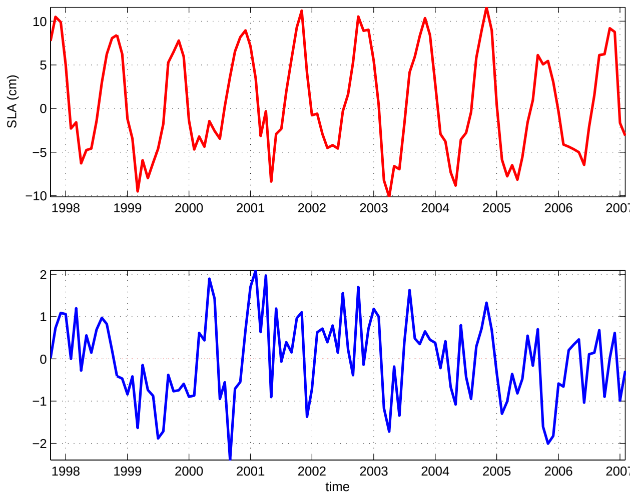

Figure 1.1: Top panel: SLA basin averaged time series; Bottom panel: SLA normalized anomalies

The wavelet analysis of the anomalies time series shown in Fig. 1.2 (computed as described is subsection 1.2.3) draws the stronger significant anomaly (negative) in 2000. Other shorter (in time) significant anomalies are found in summer 2003 and in autumn 2005.

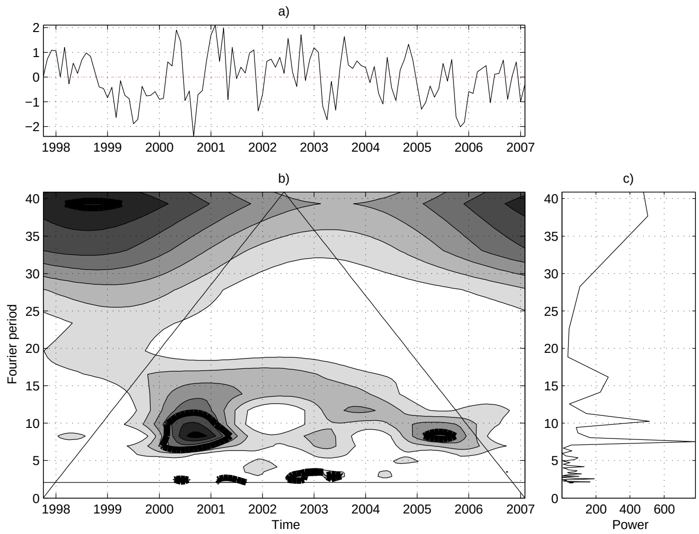

Figure 1.2: Wavelet analysis of SLA normalized anomalies time series

The standard deviation map of SLA is presented in Fig. 1.3 where a a good first look of the SLA spatial variability is given. The highest variability is identified in the southern and central part of the domain (AB and BB) while the SaC area and the LPB account the lowest variability. These last two areas are indeed interested by the presence of semi-permanent features of the circulation while the rest of the basin is mainly characterized by short-life and/or transient hydrodynamic features. In the LPB the signal, due to the Liguro-Provençal Current (LPC) and to a well known sub-basin cyclonic circulation characterizing the area, is evident. At south-east, in the SaC, another area of low variation of SLA is identified, corresponding to the western limit of a less studied cyclonic gyre located southeast of Sardinia and named South East Sardinia Gyre (Astraldi et al., 2002; Sorgente et al., 2003). However assumptions on the origin, frequency and timewise localization of the observed spatial patterns can be hardly made without a decomposition of the signals of the dataset, performed by means of EOFs.

The first four EOFs for SLAs are considered, accounting for a very large part of the total variance (85%), characterized by annual cycles and/or by anomalies having a rationale lying in physical processes.

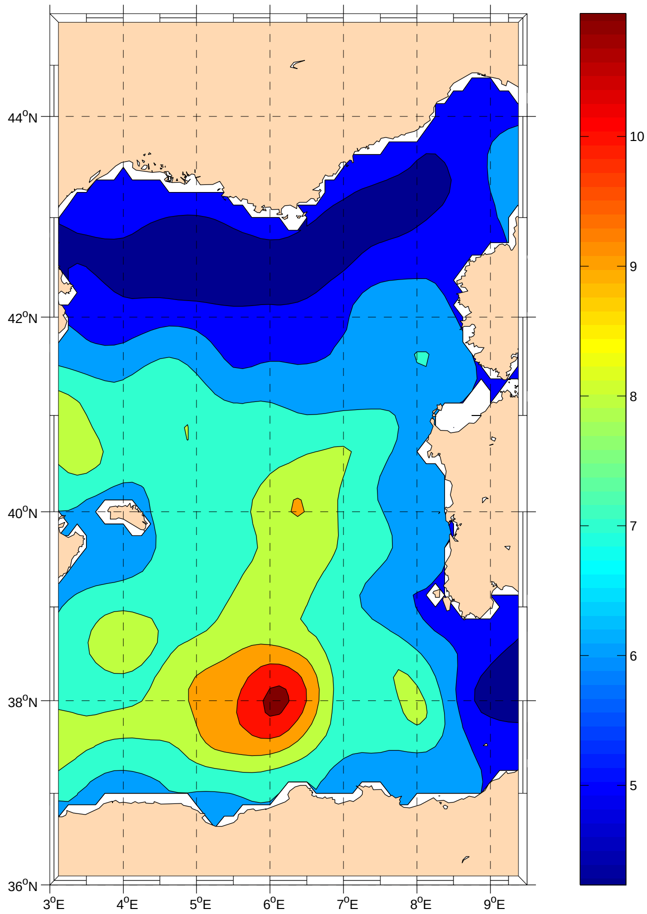

Figure 1.3: Standard deviation map of SLA

The EOF-1 (Fig. 1.4) accounts for about 76% of the total variance, explaining the seasonality (i.e. the annual cycle) of the SLA. This map shows the lowest values (loadings) in the LPB where a well known (e.g. MEDOC group, 1969; Millot et al., 1999; Pinardi and Masetti, 2000) sub-basin cyclonic circulation and the presence of the Liguro-Provençal Current drive the sea levels. As shown in the standard deviation map, the variability of SLA in this area is low. The loadings of EOF-1 are in phase in the whole domain, meaning that for this mode of variability (seasonal cycle) we have variations of the same sign over the entire domain. The homogeneous (in phase) seasonal variation of SLA over the domain is mainly due to the steric effect, quantified for the whole western Mediterranean by Bouzinac et al. (2003). The seasonality of the

EOF-1 from the PC-1 (Fig. 1.5) shows a clear annual periodicity with maxima in autumn and minima in spring, accordingly with Bouzinac et al. (2003).

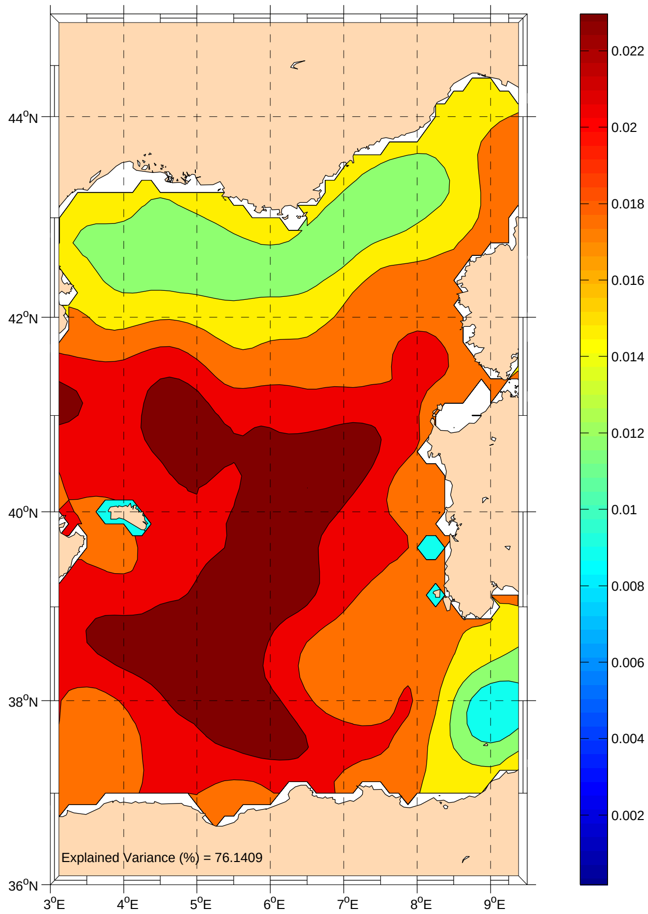

Figure 1.4: EOF-1 of SLA. 76% of variance is explained by this mode of variability

The second EOF (Fig. 1.6 explains about the 4% of the total variance, and clearly shows an eddy-like signature in a well known formation area of AEs (Puillat et al., 2002). This area shows the highest values of EOF-2 loadings, meaning that this region has the highest variability for this mode. The signal of the PC in this case is complex and characterized by inter-annual variability, needing a processing which could help its interpretation.

The wavelet spectrum in Fig. 1.7 shows that the signal of PC-2 is characterized by a pronounced minimum, temporally centered in 2003 and with

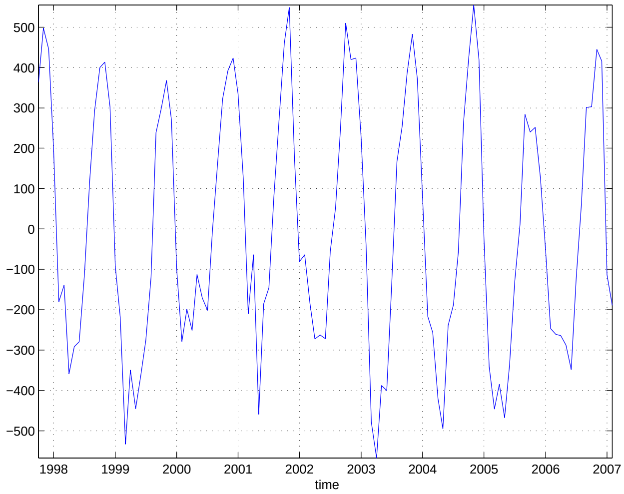

Figure 1.5: SLA PC-1: its periodicity is clearly driven by seasonality

a quite long period of persistence (about 1 year). This long-period minimum recorded in 2003 seems due to the almost total absence of formation of the above cited eddy-like structure, as verified by the screening of the 2003 map series (not shown). More in general anomalous low values of SLA over the entire domain, especially in the first six months of 2003, are recognized. Maxima, with a shorter life than the 2003 minimum, are localized at the beginning and at the end of the series, with the longest located in winter 2001. Maxima are probably due to the formation and persistence, for some months, of anticyclones of anomalously high intensity at 6°E and 37°N, determining the highest SLA values recorded for the whole decade (SLAs up to $+35cm$). This spectrum shows a recurrence of formation of this high energetic structure at the same location with apparently no periodicity.

The EOF-3 (Fig. 1.8), accounting the 2.3% of variance, is also related to an anomaly in the sea level occurring in the area of the Algerian Current at the end of the time series (2006; Fig. 1.9).

The EOF-4 of the SLA dataset (2.1% of total variance) is mainly related to the seasonal variability of the AC (south) and of the LPC (Fig. 1.10). This mode is probably driven by the variability of the two current flows, modulated seasonally both in their intensity and path. This variations have a predominant annual component, as visible from the wavelet decomposition of PC-4 (Fig. 1.11), although the annual signal is not continuous along the whole series

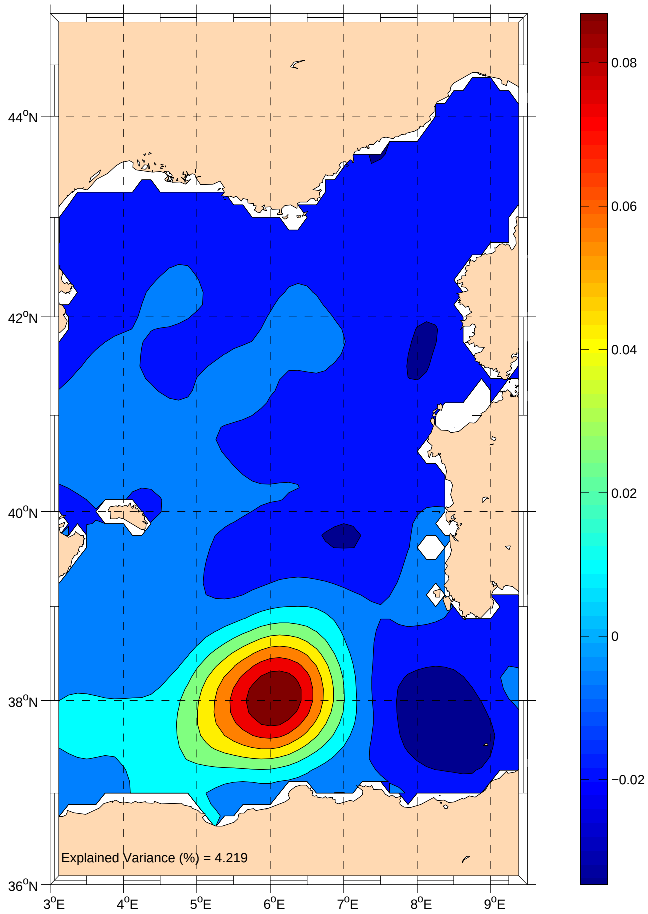

Figure 1.6: EOF-2 of SLA. 4% of variance is explained by this mode of variability, showing a maximum with an eddy-like shape

but it seems to have a break in 2004.

1.3.2 SST variability

The time series of basin averaged SST is shown in top panel of Fig. 1.12, while bottom panel shows the anomalies SST time series computed by subtracting the 10 years monthly climatological average from the monthly values. The top panel clearly depicts the seasonality of the SST in the basin, with an apparent weak interannual variability. The maximum value of the entire series is reached in summer 2003, when a strong heatwave event struck the continental Europe as well as the western and central Mediterranean areas (Marullo and

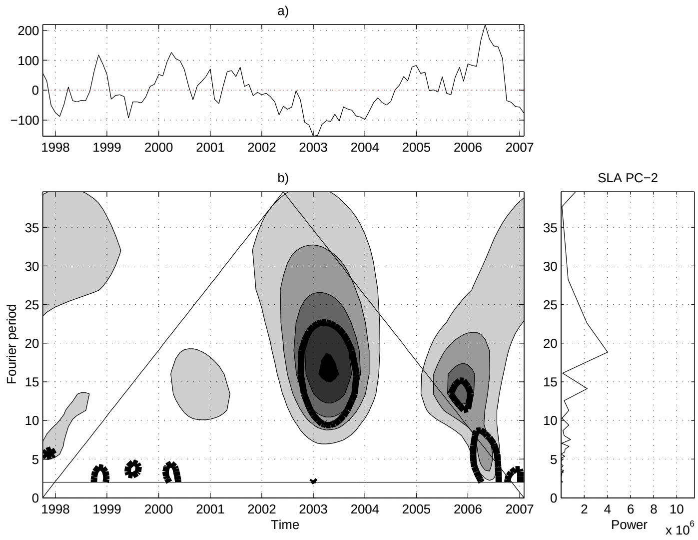

Figure 1.7: Wavelet plot of SLA PC-2: a long-period minimum is identified in 2003.

Guarracino, 2003; Black et al., 2004; Schär et al., 2004; Olita et al., 2007). This is evident by looking the bottom panel of Fig. 1.12, which demonstrates that this anomaly was the strongest interannual event for SST during the last decade. The wavelet analysis (Fig. 1.13) confirms that the main anomaly is in summer 2003. The plot shows that this event was characterized by two distinct interannual signals temporally superimposed but characterized by different Fourier periods: one shorter of about 5-6 months and one longer of about 15-16 months.

As for SLA, the main spatial patterns of variability of SST are depicted through the computation of pixel-by-pixel standard deviation. The resulting standard deviation map is shown in figure 1.14. The highest standard deviation is found around the Balearic Islands, while the lowest is in the Gulf of Lyon. The SST standard deviation ranges from 3.5 to $5C°$. Another area of relatively low standard deviation is the Algerian basin up to about 38.5° N. This last signature is probably due to the flow of MAW which is characterized by quite stable surface temperatures in comparison with local waters which are more affected by seasonal variations. The northern area of lower variability is coincident with the upwelling of the Gulf of Lyons: in this case a lower variability is due to the upwelling itself which rises colder bottom waters (especially in summer) from the deep layers then determining the smallest variability of the surface temperatures in that area, in comparison to surrounding areas where

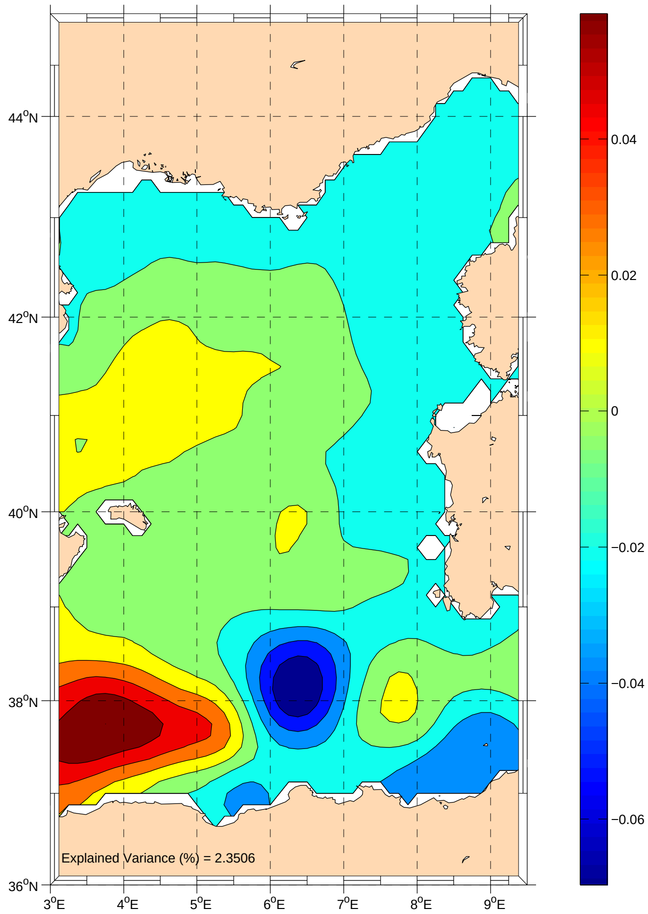

Figure 1.8: EOF-3 of SLA. 2% of variance is explained by this mode of variability, mainly due to algerian current anomalies

no upwelling is observed. For SST also the Ligurian sea shows standard deviation values comparable to those in the central part for the weak effect of the sub-basin scale upwelling due to the general cyclonic circulation of this sub-basin. Finally, the central part of the APB results, as for SLA, the area overall showing the highest variability.

The decomposotion in EOF modes emphasizes how the main part of the variability of SST is largely due to the seasonal cycle. In fact the EOF1 (Fig. 1.15) encloses more than the 97% of the total variance of the SST dataset.

This means that also the spatial patterns, as can be seen comparing the two figures, are almost equal to those depicted with small differences localized

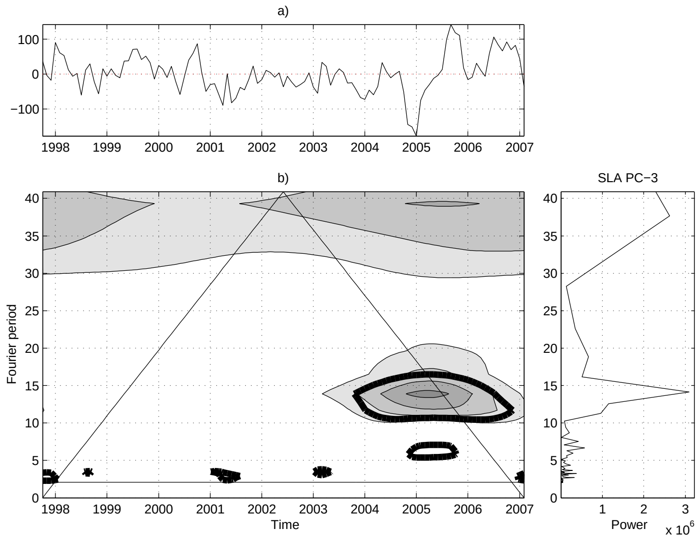

Figure 1.9: Wavelet plot of SLA PC-3: the signal is characterized by an anomaly at the end of the series.

above all along frontal areas. Second and third modes account only for the 0.6% and 0.2% of variance respectively (left panel and right panels of Fig. 1.16). Second mode of variability seems related to the variability of the southern gradient of temperature, due to the latitudes range, while the third mode shows an interannual non-periodic temporal pattern (see bottom panel of Fig. 1.17) which seems to be due, from the observation of the spatial features of the EOF-3 (right panel of Fig. 1.16), to the effects of strong mistral wind events occurring in the basin several times during the year and obviously producing a cool of the surface waters. This direct effect of mixing and cooling by the mistral wind on the surface waters accounts for only the 0.2% of total variance of SST dataset.

1.3.3 Chl variability

The maxima in phytoplanktonic biomass, as in top panel of Fig. 1.18, are reached in spring for all the years. No evident autumn blooms are emphasized by the basin-averaged monthly values. A strong interannual variability, higher than for SST or SLA, is intuitable by looking at the series. Two peaks, corresponding to the maxima of the entire series, are localized in 1999 and in 2005 when, for some reasons, the spring bloom was more intense and/or extended in time. The larger minimum is located in summer 2003, probably related

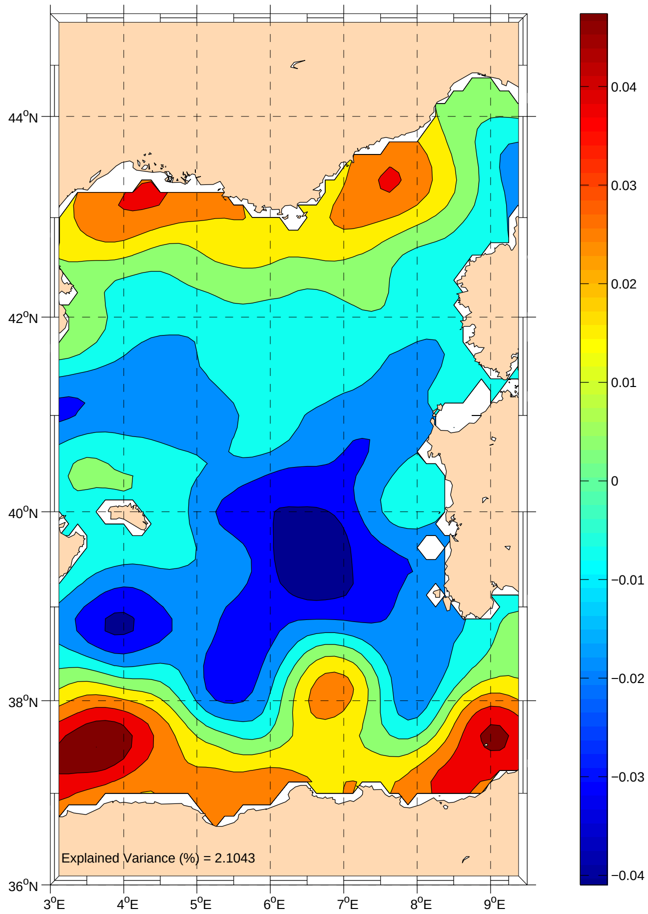

Figure 1.10: EOF-4 of SLA, explaining 2% of variance, related to the variability of the LPC and AC

to the summer heatwave we have seen in SST series. The bottom panel of Fig. 1.18 clearly shows that this anomaly was the stronger interannual event for Chl during the decade. The wavelet analysis (Fig. 1.19) confirms that the main anomaly is that of summer 2003, surprisingly coincident with the SST signal we have seen before. The plot shows in this case a single anomaly characterized by a Fourier period of about 15 months, from spring 2003 to summer 2004, and centered in the summer months of 2003. It is interesting to note that this anomaly is hardly detectable if the anomalies series is not normalized by monthly standard deviation. In facts the deviation in absolute terms from the series is not large, but the standard deviation of the summer months is

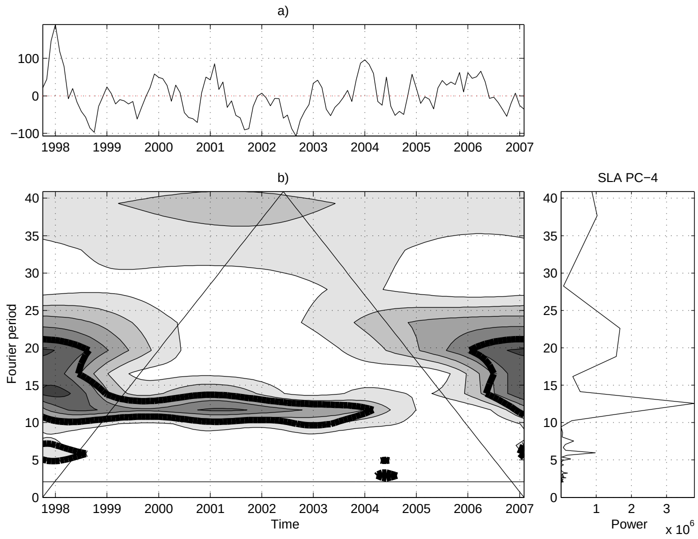

Figure 1.11: Wavelet plot of SLA PC-4: the signal seems characterized by an annual cycle, even though with a break in 2004

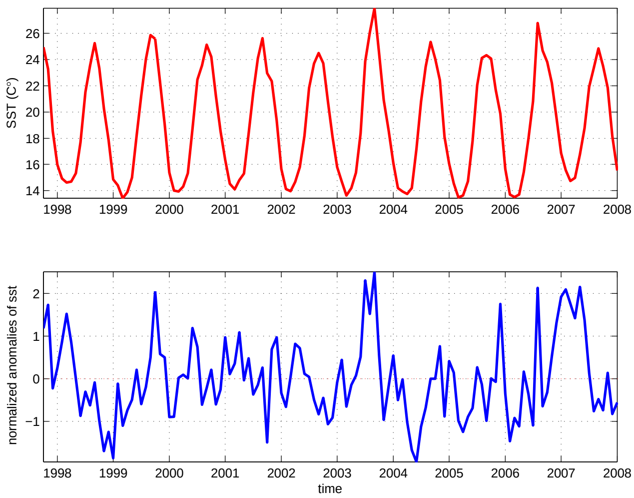

Figure 1.12: Top panel: SST basin averaged time series; Bottom panel: SST normalized anomalies

quite smaller than the winter ones.

The analysis of the EOFs is therefore performed in order to investigate the spatial variability and to quantify the amount of variance due to seasonal cycle and that due to interannual events. As for SST, only the first three EOF modes of the Chl dataset are discussed, together accounting for about the 65% of the total variance. The other lower order EOFs are not discussed because

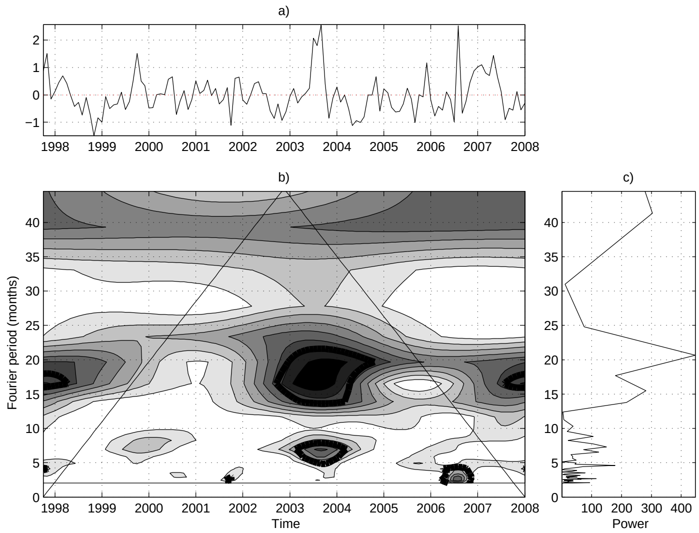

Figure 1.13: Wavelet analysis of SST normalized anomalies time series

they appear noisy-like signals.

The EOF-1 map (left panel of Fig. 1.20) accounts for about 44% of the total variance. The map clearly shows that the first mode is almost entirely due to the seasonal bloom occurring in the LPB (MEDOC area spring Bloom). The strongest signal is localized in the Gulf of Lions. Inside the Gulf the Colored Dissolved Organic Matter (CDOM) probably assume large values because of the presence of the plume of Rhone river, determining an overestimation of Chl by satellite based algorithm (Case 2 waters problem). The values of EOF-1 are all positive, meaning that this mode of variability has the same phase over the whole domain. The respective time series of expansion coefficients (PC-1, Fig. 1.21) is clearly characterized by a well defined annual cycle. PC-1 maxima are all located in early spring and minima in summer. EOF-2 (right panel of Fig. 1.20) accounts for about the 17% of the variance of the dataset. In this case positive EOF-2 loadings are reached in the AC and AEs areas, drawing a clear north-south boundary around 39.5°N. The central part of the APB, between the Balearic islands and Sardinia, shows loadings around zero, while the northern area is in phase opposition with the former, showing negative values. PC-2 (Fig. 1.21) shows a clear annual cycle with maxima in January-February in all the years, a little earlier than for PC-1, and minima in summer. The EOF-3 (Fig. 1.22), explaining the 4% of variability, draws the highest (negative) loadings in the Gulf of Lyon, probably related to anomalies of the Rhone river runoff, while positive values are localized close to the Corsica

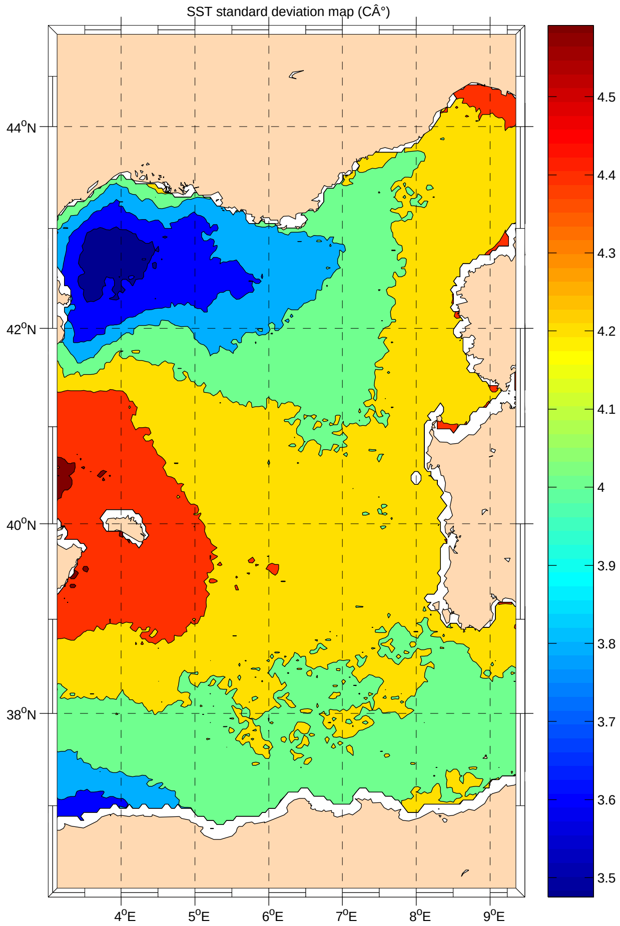

Figure 1.14: Standard deviation map of the SST for the 1997-2007 period

island and related to higher than normal chlorophyll values in 1999 and 2005. These signatures are well shown by the spectral analysis of PC-3 (Fig. 1.23). A minimum of the signal is centered in spring 2001, with a short-period signal (few months) superimposed on a longer one (more than 1 year), while the maxima are localized in spring 1999 and 2005.

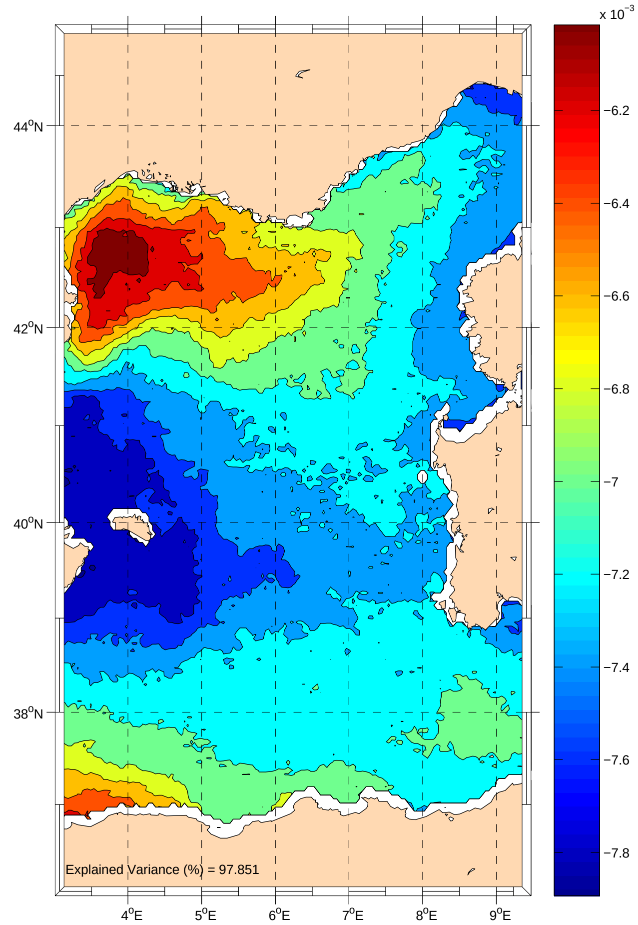

Figure 1.15: EOF-1 of SST. more than 97% of variance is explained by this mode of variability

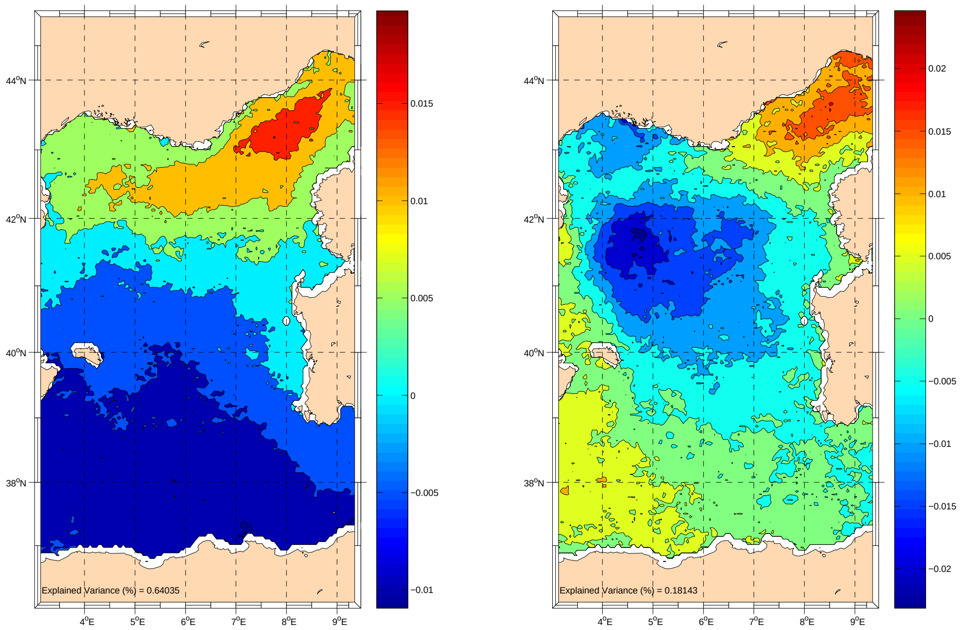

Figure 1.16: EOF-2 (left) and EOF-3 (right) of SST. 0.6% of variance is explained by EOF-2, while the EOF-3 explains the 0.2%, related to interannual mistral wind events.

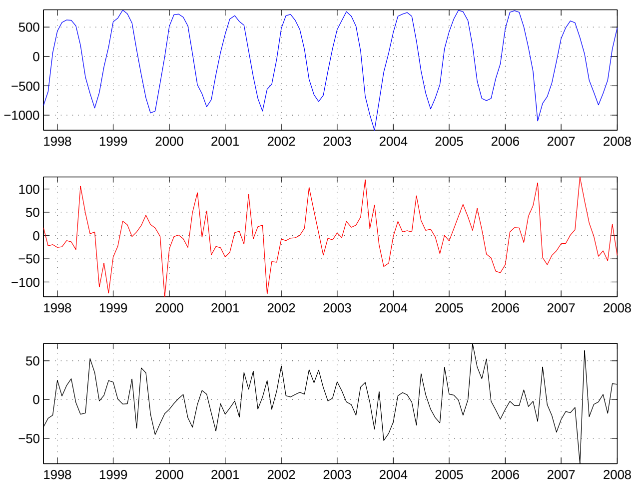

Figure 1.17: Top to bottom, SST PC-1, 2 and 3. Seasonal cycles can be recognized in the first two PCs.

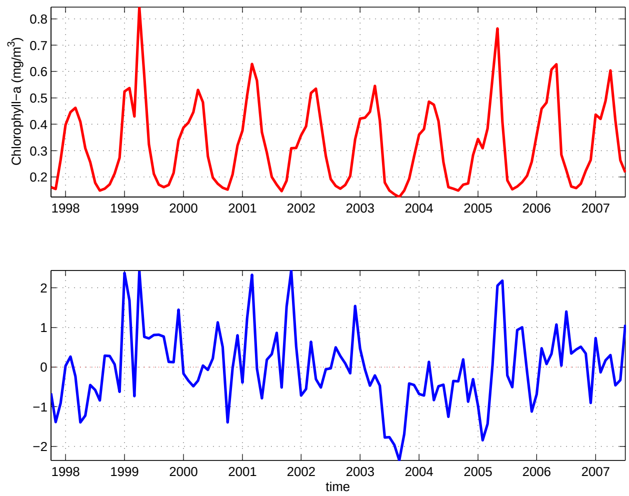

Figure 1.18: Top panel: Chl basin averaged time series; Bottom panel: Chl normalized anomalies

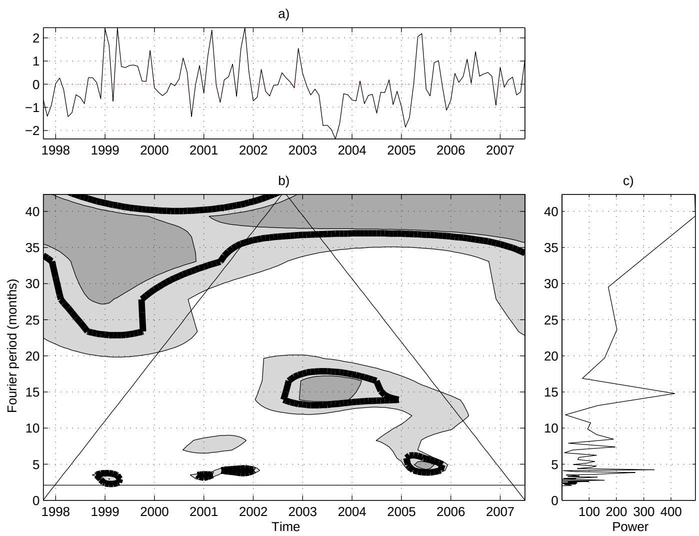

Figure 1.19: Wavelet analysis of Chl normalized anomalies time series

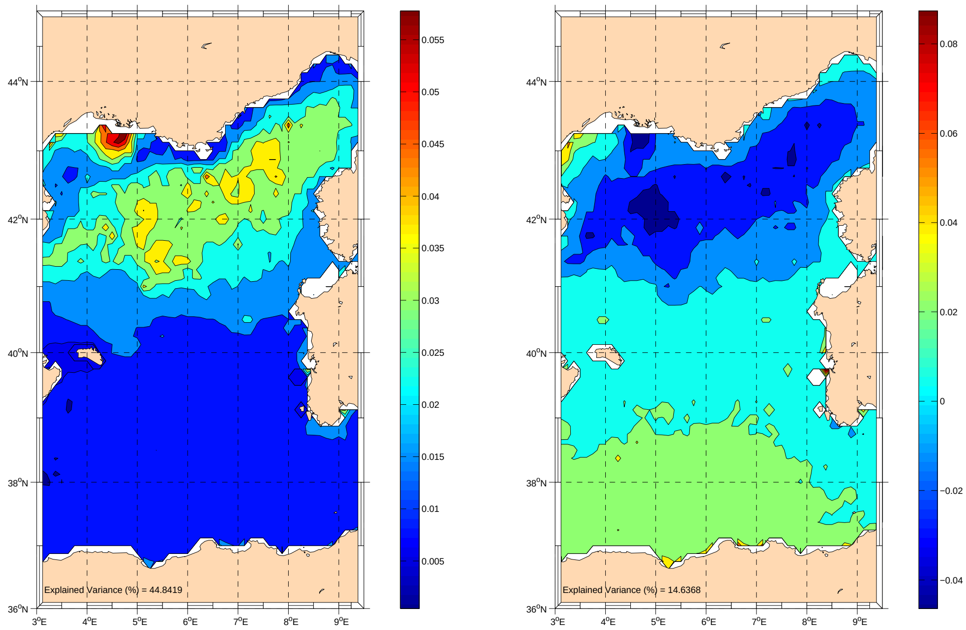

Figure 1.20: Left Panel: EOF-1 of Chl, explaining 44% of variance, related to the MEDOC area bloom. Right Panel: EOF-2 of Chl, explaining 14% of variance, related to the weak blooms occurring along AC and AEs area of influence

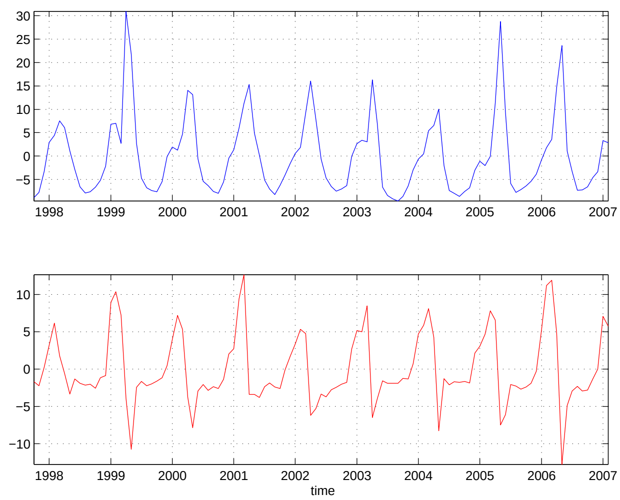

Figure 1.21: Chl PC-1 and PC-2: The signals are characterized by annual cycles, with maxima respectively in early spring (PC-1) and winter(PC-2)

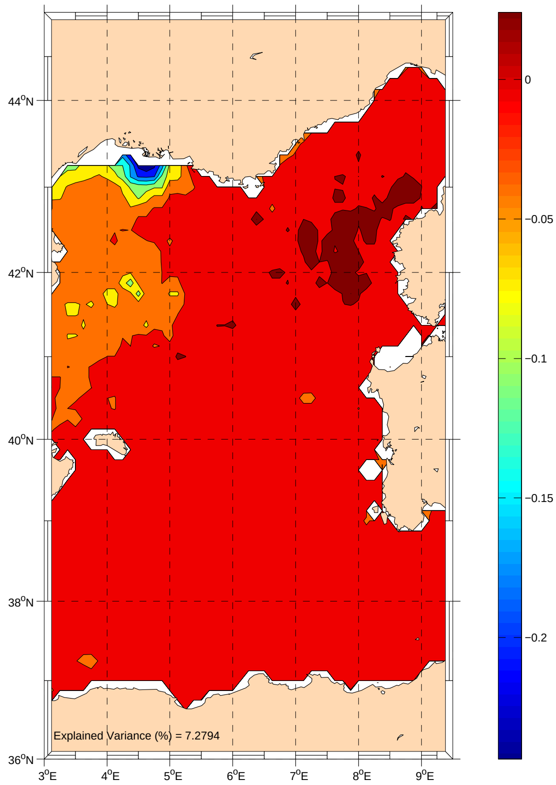

Figure 1.22: EOF-3 of Chl, explaining about the 4% of variance, related to a negative anomaly occurring in Gulf of Lion and in the NW part of the Basin, while the positive signs are localized along the western coasts of Corsica

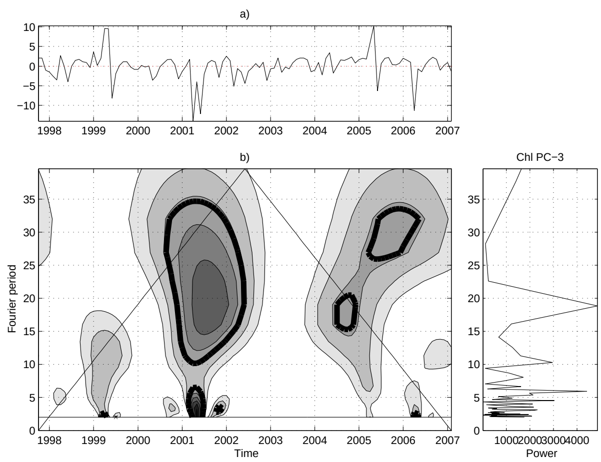

Figure 1.23: Wavelet plot of Chl PC-3. Some anomalies are evident:a minimum centered in spring 2001, and a shorter-period maximum in spring 2005

1.3.4 SLA–Chl covariability

The coupling between the two variables was studied at first by analyzing the r correlation map. The map of figure 1.24 shows that the two variables are negatively correlated over the whole domain (with significance level $P < 0.05$). The area with highest (anti-)correlation is the central part of the basin, across the Balearic Front area, with r values higher than -0.6 in some localized patches. It is also evident that a low correlation is reached along coastal boundaries (where it should be noted that errors of both dataset are highest) and in the area of interest of the AC and AEs. The variables seem almost uncorrelated in some patches (i.e. at 7°E and 37°N), meaning that in these regions the Chl is mainly driven by other forcing than SLAs.

For a better interpretation of the observed covariability, the paired maps obtained through SVD (left map or $SVD_i{-}SLA$ and right map or $SVD_i{-}Chl$) and their related expansion coefficients are studied. The SVD-1 pair of coupled maps explains more than 0.98 SCF, i.e. almost all the covariability of the two fields. The left and right SVD-1 maps (SLA and Chl respectively) roughly show the same patterns seen in the EOF-1s. Heterogeneous correlation maps of this SVD-1 mode are shown in figure 1.25. They are computed, as described in Bjornsson and Venegas (1997), by calculating correlation coefficient vectors between k^{th} expansion coefficients of one variable and the values of the other variable at each grid point. This kind of representation of SVD modes permits to show the distribution of the covariability patterns of the mode (and their centers of action) scaled as correlation coefficients. The so called "right" (SVD-1-SLA vs Chl values, Fig. 1.25) heterogeneous map shows that the center of action of the first SVD mode is located in the central part of the basin. Particularly the center of action of this SVD mode, and therefore the main pattern of covariability, is located roughly across the parallel 41°N, more or less the location of the Balearic Front. The low value of correlation shown in the heterogeneous map along AC and AEs path confirms the weak coupling existing in this region between SLA and Chl, indirectly indicating that, at these scales, horizontal advection performed by AC and AEs may be more important than vertical processes in influencing Chl concentration and distribution. The respective SVD-1 expansion coefficients (Fig. 1.26) show clear annual cycles, similar to those observed for PC-1s of the two variables. Combining the spatial and temporal information furnished by SVD analysis we can tell that the

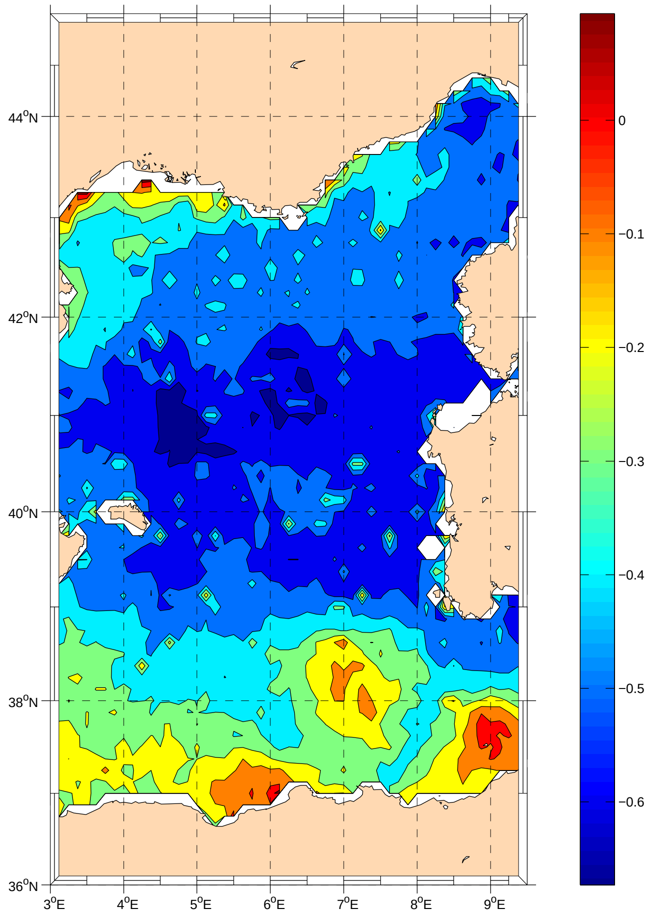

Figure 1.24: SLA–Chl correlation map($P < 0.05$). The values of r are negative on the whole basin

covariability between SLA and Chl by a seasonal cycle having its maximum expression in the central area of the basin, more or less across the location of the Balearic Front.

The second pair of coupled maps (second SVD mode, less than 0.5% of SCF explained) substantially show the patterns depicted by EOF-4 of SLA and EOF-2 of Chl, also in this case drawing annual periodicity. The centers of action in heterogeneous correlation maps (not shown) of this SVD-2 mode are located along the AC path, showing, for this mode of covariability, the influence of the AC on the spatial distribution of the weak phytoplankton bloom occurring in winter in the AB. The SCF value is, in any case, really low

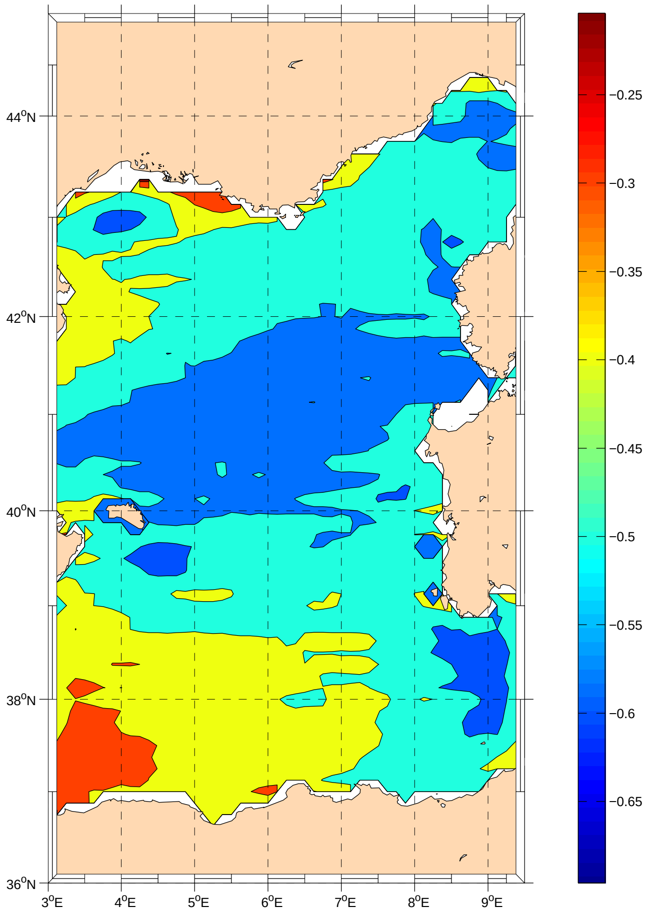

Figure 1.25: Heterogeneous correlation map for the first SVD mode (SLA expansion coefficients Vs Chl data)

then confirming that the relation between SLA and Chl, although present, is weaker in the AC area than in the central and northern ones.

1.3.5 SST–Chl covariability

As for SLA, the analysis of the covariability with the Chl has been conducted at first by the analysis of the spatial distribution of the linear correlation coefficients, r, between the two variables.

The correlation map between SST and Chl of Fig. 1.27, shows only negative values (anti-correlations is found, as expected) ranging from -0.1 to -0.8.

High anticorrelation values, as for SLA, are found in the central part of the

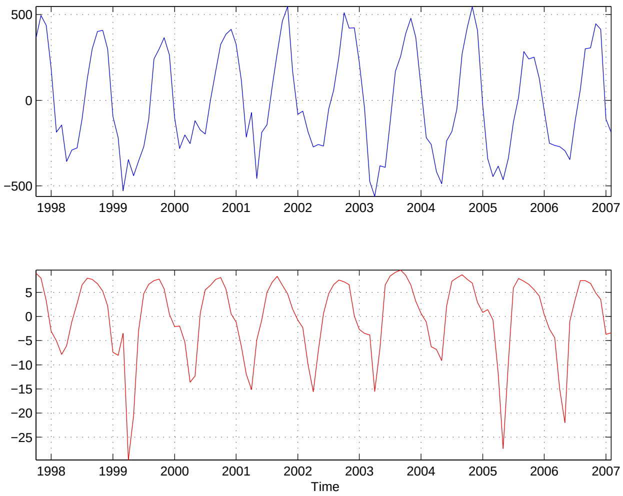

Figure 1.26: Expansion coefficients of first SVD mode: up SLA and bottom Chl expansion coefficients

basin but, in contrast to what we found for SLA, the highest values have been observed near to the Ligurian coast, along the path of the LC. On the contrary, over the area of sub-basin cyclonic circulation of the LPB (the MEDOC area) we show a large off-shore area were low values of anti-correlation (i.e. values of the coefficient approximating zero) are reached. A weak signal of the MAW flow is also present in the south-western area of the domain, altough really weak if compared to that visible in the SLA–Chl correlation map. The SVD-1 pair for SST–Chl datasets explains more than 0.99 SCF, i.e. almost all the co-variability of the two fields. The so called *left* and *right* SVD-1 maps (SLA and Chl respectively) roughly show the same patterns seen in the EOF-1s. Heterogeneous correlation maps of this SVD-1 mode are shown in figure 1.28. They are computed, as described in Bjornsson and Venegas (1997), by calculating correlation coefficient vectors between k^{th} expansion coefficients of one variable and the values of other variable at each grid point. This kind of representation of SVD modes permits to show the distribution of the covariability patterns of the mode (and their centers of action) scaled as correlation coefficients.

The *right* (SVD-1-SST vs Chl values, Fig. 1.25) heterogeneous map substantially shows the same features observed in the simple correlation map. The center of action of the first SVD mode for this pair of variables is located in the central part of the basin, between the Balearic islands and Sardinia, drawing a pattern which includes the Sardinia Channel. The main difference with the

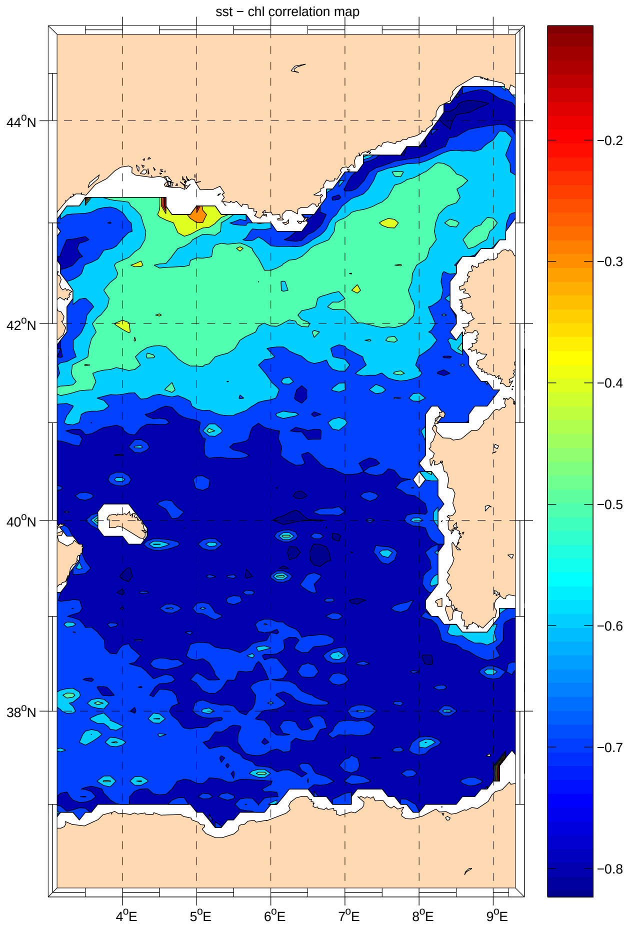

Figure 1.27: SST–Chl correlation map. The values of r are negative on the whole basin

simple correlation map is that the AC and AEs signature is enhanced.

The fact that r correlation map and SVD heterogeneous correlation map almost give the same spatial information is not surprising because the variability of SST, as we have seen in the EOF analysis, is explained almost entirely by the first mode of (co-)variability. The SVD-1 expansion coefficients (Fig. 1.29) show clear annual cycles similar to those observed for PC-1s of the two variables.

By combining the spatial and temporal information from the SVD analysis we can tell that the covariability between SST and Chl is characterized by a seasonal cycle having its maximum in the central and SE areas (Sardinia

Channel) of the basin, with an absolute and localized maximum located along the Ligurian coast.

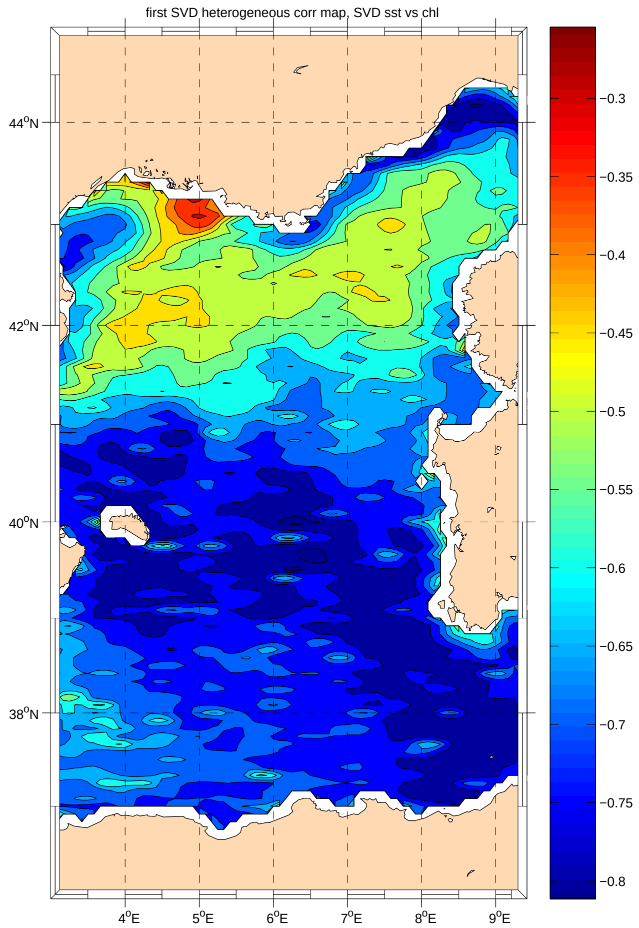

Figure 1.28: Heterogeneous correlation map for the first SVD mode (SST expansion coefficients Vs Chl data)

1.4 Discussion

Satellite estimates of chlorophyll-a (Chl) concentration collected by SeaWiFS radiometer, AVHRR Sea Surface Temperature (SST) data and Sea Level Anomaly (SLA) AVISO/CLS satellite maps in the Algerian Basin, during a 10 years period (September 1997 to January 2007), have been analyzed. The study addresses to detect the main patterns of spatial and temporal variability

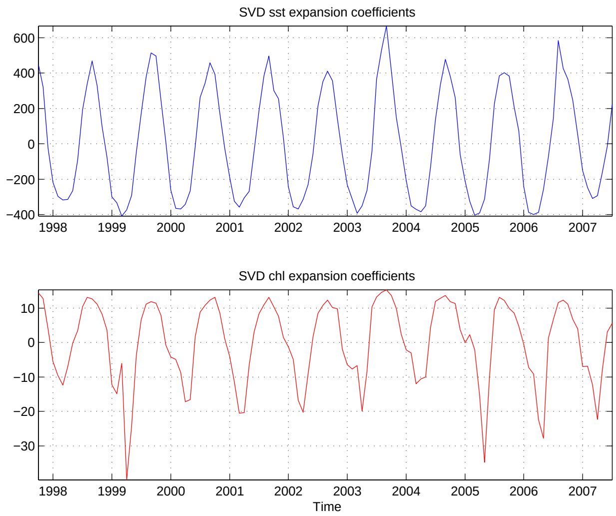

Figure 1.29: Expansion coefficients of first SVD mode: up SST and bottom Chl expansion coefficients

of Chl and SLA fields. This in order to investigate the covariability of biological and physical fields at seasonal and interannual scales and to describe different areas of the basin in terms of the observed bio-physical coupling.

The time series of SLA shows a marked seasonality with maxima in autumn, probably due to steric effect as discussed by Bouzinac et al. (2003). The anomalies of the SLAs can be hardly interpreted, also with the help of the wavelet analysis. The main anomaly (in terms of anomalies normalized by monthly standard deviation) seems to be due to a relative maximum occurring in spring 2000. Lacking information on spatial patterns variability of SLA, a deeper analysis is therefore conducted through EOF decomposition. The EOF-1 of SLA series (3/4 of total variance), related to the seasonal cycle (shown in PC-1), showed the highest variability in the central and southern part of the basin. While the high loadings in the area between the Algerian coast and $\sim 40°$N can be attributed to the variability of the spreading and intensity of the MAW flow and of the mesoscale features generated from the AC, the high variability of the area between 40°N and 41.5°N could be due to the dynamics of the Balearic Front, particularly of the Frontal Eddies (Fuda et al., 2000), both cyclonic and antyciclonic, detaching from the front. The signature of (semi-)permanent features (the Liguro Provençal Current and the South East Sardinian Gyre) are recognized by the minima of variability of this EOF-1. The EOF-2 and EOF-3 (together about 7% of variance) are related to the interannual variability of the SLA. The EOF-2 is the most interesting of the two showing an eddy-like shape at about 36°N - 6°E which corresponds to the formation and presence of a large and intense AE, occurring non-periodically but several times in the decade, in some cases persisting for several months (in 2001 and 2006) as seen in the wavelet spectrum of the related PC. The long-period signal recognized in PC-2 spectrum and centered in 2003, is due to anomalous low values of SLA due to a long-period absence of that hydrodynamic feature and probably indicating modifications (reduction) on MAW flow. The summer part of this anomaly can be related to the anomalous persistence of high atmospheric pressure determining a strong heatwave in summer 2003 (Black et al., 2004; Schär et al., 2004; Olita et al., 2007), which could explain the lower SLAs than normally in summer. The seasonal cycle of variability of the two main coastal currents of the domain, the AC and the LPC, is separated in the EOF-4 then explaining only about the 2% of the variance. The signal of the two currents is in phase and the analysis of the related PC shows that the signature two currents reach its maximum in winter-time, suggesting also a maximum in the currents intensity.

The SST basin-averaged time series shows a marked seasonality with the main anomaly centered in summer 2003, in coincidence with the European heatwave (Black et al., 2004; Olita et al., 2007). The decomposition of the SST dataset performed by EOFs finds a first mode explaining almost 97% of the variance (including the heatwave footprint). The second mode is more related to the southern gradient due to latitude differences and accounts for 0.6% of the variance only.

The decomposition of SeaWiFS data showed an EOF-1 (almost half of the total variance) characterized by a clear seasonal cycle. The main spatial pattern draws the contours of the seasonal spring bloom occurring in the MEDOC area, whereas the second mode (about 1/6 of total variance) shows the signal related to the advection of phytoplnktonic biomass-rich waters from coastal shelf to off-shore areas (up to about 40°N) performed by AC and AEs. It is also interesting to underline that this two modes are timewise shifted: the former is temporally located in early spring; the second, related to the off-shore advection performed by the Algerian Current and to the Algerian Anticyclonic Eddies, occurs in late winter, when the AC reached its highest sea level variability, as shown in PC-4 of SLA.

The correlation map generally shows anticorrelation between SLA and Chl, as expected. The maximum anticorrelation is reached in the central part of the basin, between Sardinia and the Balearic islands, showing the highest SLA–Chl covariability in some patches just north of 41°N. We showed, through correlation map and SVD analysis, that the highest anticorrelation is reached in the central part of the basin, between Sardinia and the Balearic islands, assessing the strongest dependence of Chl by the SLA roughly across 41°N. In this area the deepening/shoaling of the isopycnae, mainly due to the action of mesoscale eddies which are predominant in this area (Fuda et al., 2000; Ribotti et al., 2004), and the related vertical fluxes of nutrients seem to have a larger influence on total Chl concentration than in areas where horizontal advection processes are much more consistent, due to the presence of important coastal currents. The coupled maps produced by SVD and their respective expansion coefficients drew the spatial and temporal patterns driving the observed covariability. The first pair of maps explain more than 98% of SCF of the two fields, depicting spatial patterns similar to respective EOF-1s, therefore drawing structures in large part not co-located. The heterogeneous correlation map between SLA-SVD-1 expansion coefficients and Chl data showed that the behavior of SLA in time can "predict" the Chl concentration especially in the area of the Balearic Front. We guess that mesoscale cyclonic and anticyclonic eddies detaching from the Balearic Front and called Frontal Eddies from Fuda et al. (2000), substantially contribute to this signal. In fact in this area the shoaling/deepening of the isopycnae, and the related vertical fluxes of nutrients, seem to have a larger influence on total Chl concentration than in areas where horizontal advection processes are much more important due to the presence of important coastal currents.

The analysis of the SST–Chl correlation shows negative values of r ranging from -0.1 to -0.8. The largest correlation is found along the Ligurian coast and is related to the upwelling generated by the Liguro-Provençal Current, rising cold and nutrient rich waters and enhancing the new production. Other wider areas of high correlation are the central part of the basin and the Sardinia Channel. In the Sardinia Channel, the strong coupling between the two variables could be due to the presence of a cyclonic gyre which determines, as for the coastal upwelling, the co-existence of cold and nutrient-rich waters. SVD analysis conducted on SST–Chl coupled datasets does not add significant spatial information to the correlation map, because of high seasonality of the SST data which are quite all explained by the first single mode of variability. Timewise, the analysis confirms that the patterns of correlation between the two variables are typically seasonal and enclose all the covariability ($SCF = 0.99$) of the datasets.

Both the analysis of the variability of the single datasets and also the analysis of the covariability between physical and biological fields support the idea that the APB might be divided in three main regions, in the perspective of the physical-biological coupling: the southern, the northern and the central one. The southern region is characterized by moderately chlorophyll-rich waters (in winter), transported by the AC and the AEs up to about 39-40°N, as shown by EOF2 and PC-2 of Chl and by EOF4 of SLA. At these spatial and temporal scales the horizontal advection, performed by AC, is probably the main forcing of the observed concentration of Chl, considering that SLAs (and related variations of thermocline and nutricline depth) have the lowest (near to zero) correlation with Chl. The second pair of SLA–Chl SVD (not shown) also confirms that the AC (and its variability in intensity and path) is correlated to the intensity and extension of the (weak) seasonal bloom occurring along the Algerian Coast in winter, although this pair of coupled modes explain a very small part of the total covariance. The seasonal spring-bloom occurring in the MEDOC area accounts for almost half of the total variance of Chl (EOF-1). The mechanism of this annual phenomenon is well reported in literature (Jacques et al., 1973), and briefly described in the introduction of this chapter, involving a complex sequence of physical processes. The coupling between SLA and Chl in this region, although present, is relatively important for the seasonal bloom as shown in the heterogeneous correlation map of SVD analysis. In this area the mesoscale processes (having a SLA signal) seems to be important for the fine-scale (in space and time) modulation of the bloom and for the redistribution of water masses, as discussed by Levy et al. (1998, 2000), but this is outside of the focus of this chapter.

The Balearic Basin, which hydrodynamically can be seen as the buffer area between MEDOC area and Algerian Basin, shows the strongest SLA–Chl and SST–Chl anti-correlation. This suggests a clearer biological response to the shoaling and deepening of the thermocline/nutricline, mainly performed by the eddies (Frontal and Algerian). In this area any other physical forcing does not mask the effect of SLA variability (footprint of the eddies action) on the Chl concentration. Results also suggest that the central part of the basin may constitute a good location to conduct further investigations on the biological effects of vertical displacement of isopycnae (and therefore of thermocline and nutricline) performed by eddies. This last aspect has been studied in Chapter 3 by means of the analysis of hydrological and fluorometric data collected during two oceanographic cruises conducted in the Sardinian Sea.

Chapter 2

Satellite based estimates of Primary Production, in the decade 1997-2007: seasonal and interannual variability

2.1 Introduction

The understanding of the mechanisms controlling primary production (PP, hereafter) in seas and oceans is essential for the study of the marine ecosystems at all spatial scales.

There are two main reasons motivating the efforts done by scientists in this direction in the last years, as stated by McGillicuddy et al. (2007), having practical implications: the role of PP in controlling the amount of energy available for higher trophic levels (assuming the dominance of a top/down control); the importance of marine PP in the removal of carbon dioxide from the atmosphere by means of photosynthesis, and therefore its role in controlling global warming by carbon sequestration.

A huge number of measurements of marine PP has been collected from the introduction of ^{14}C method (Steeman-Nielsen, 1952). However these local measurements, because of their lack in synopticity and spatial continuity, can be hardly used to evaluate budgets as well as spatial distribution of PP at basin scales.

The turning point in the assessment of spatial and temporal variability of marine biomass and PP was the launch of satellite sensors able to acquire Ocean Color data (see Box 1 in the General Introduction). From that moment successful efforts have been done to develop mathematical tools able to "relate" remotely sensed chlorophyll-a (Chl hereafter) estimates to PP at the surface or integrated over the euphotic layer (hereafter PP_{eu}). Models of PP_{eu} based on satellite Chl concentration, spanning in a range of different complexity, from simple empirical parameterizations to complicated bio-optical models, have been developed since the late '70s (e.g. Morel, 1978; Falkowsky, 1981; Eppley et al., 1985; Platt, 1986; Platt and Sathyendranath, 1988; Morel and Andrè, 1991; Behrenfeld and Falkowski, 1997a,b).

In this study we make use of the Vertically Generalized Production Model (VGPM, Behrenfeld and Falkowski, 1997b), and its following modifications, which uses remotely sensed chlorophyll-a, Photosyntetically Available Radiation (PAR), daylength and the $P^{B}{}_{opt}$ parameter [the maximum primary production per chlorophyll-a unit $(mgC(mgChl)^{-1}h^{-1})$] as first order constraints for PP_{eu} computation. We chose this model in virtue of its good skill to reproduce PP_{eu} at various scales (Behrenfeld and Falkowski, 1997b; Mizobata and Saitoh, 2004; Kameda and Ishizaka, 2005) and because all the parameters used in the model can be directly or indirectly derived from remotely sensed data.

We applied the model to the Algero-Provençal Basin (APB) area which was broadly investigated about its hydrology and hydrodynamics (e.g. Vignudelli, 1997; Levy et al., 1999; Millot et al., 1999; Levy et al., 2000; Bouzinac et al., 2003; Isern-Fontanet et al., 2004). The biological response to the physical forcing at the first trophic level over the basin has been also analyzed in many studies (e.g. Lohrenz et al., 1988; Raimbault et al., 1993; Levy et al., 1998, 2000; Garcon et al., 2001; Moran et al., 2001; Taupier-Letage et al., 2003), no one making use of time series longer than 4 years. Seasonal and interannual variability of modeled PP over the entire Mediterranean sea have been investigated by Bosc et al. (2004) which used the satellite based model of Antoine et al. (1996) to estimate the variability and the annual budget over the period 1998-2001.

Despite this previous study, the assessment of spatial and temporal variability of PP_{eu} in the APB requires an analysis spanning over a longer period. The main forcing influencing PP variability have to be investigated and a continuous monitoring of PP_{eu} is required, in the light of the increasing anthropogenic inference in the Mediterranean ecosystems (Turley, 1999; Bosc et al., 2004).

The present availability of 10 years-long remotely sensed time series for all the parameters required by PP_{eu} satellite based models allowed us to accomplish such investigation.

This chapter aims to:

- setup the PP model for the APB area;
- estimate the temporal and spatial variability of PP_{eu} in APB along a decade, icluding periods of strong surface forcing anomaly, like the summer 2003 overheating (Black et al., 2004; Olita et al., 2007);
- compare the results, when and where possible, with previous findings obtained through different methods/models.

2.2 Methods

2.2.1 Satellite Data

Level-3 Chl and PAR monthly composite data acquired from the SeaWiFS satellite (O'Reilly et al., 1998), processed and provided by NASA Goddard Space Flight Center through the Ocean Color Web portal (reprocessing 5.2), have been used. A set of 118 monthly SeaWiFS Chl and PAR composite maps from September 1997 to June 2007 has been obtained as starting point for the PP_{eu} modellization.

Level-2 Chl and K_{490} data from SeaWiFS have been used to compare and validate the Chl regional and standard products with our *in situ* dataset, collected during oceanographic cruises.

SST data used to model the PP_{eu} are the pathfinder SST version 5. The pathfinder SST data are derived from the 5-channel Advanced Very High Resolution Radiometers (AVHRR) on board of the NOAA-7, -9, -11, -14, -16 and -17 polar orbiting satellites. The monthly averaged data for the ascending pass (daytime) on equal-angle grids of 8192 pixels/360 degrees (nominally referred to as the 4 km resolution) have been used. Data have been provided by the US National Oceanographic Data Center (NODC) of the National Oceanic and Atmospheric Administration (NOAA) and downloaded via ftp (data.nodc.noaa.gov).

2.2.2 Regional algorithm for chlorophyll

The algorithm developed by Bricaud et al. (2002) was applied to standard NASA Level 3 SeaWiFS products to compute regional Chl. This algorithm constitutes an optimization of SeaWiFS standard L3 products for oligotrophic Mediterranean waters. It is particularly useful, compared to other regional algorithms, because it can be retrieved directly from L3 NASA standard products, without involving re-computation of Chl values from L1 single swaths.

Bricaud et al. (2002) showed that the regional algorithm permits to obtain better estimates of the Chl content for oligotrophic waters of the Mediterranean. In facts a systematic error (overestimation) was observed by the Authors in the SeaWiFS standard products (reprocessing 3 and 4) for Mediterranean waters with Chl $< 0.4\ mgm^{-3}$, due to presence of atmospheric aerosols (mainly desert dust). The Bricaud et al. (2002) algorithm partially corrects this error and reduces the values of Chl lower than this threshold, leaving substantially unchanged larger values.

Following the method of Bosc et al. (2004), the regional Chl estimates (rChl) are directly derived from the standard (Level2 or Level3) products by:

$$rChl = 10^{0.366-3.067\rho+1.930\rho^2+0.649\rho^3-1.532\rho^4} \tag{2.1}$$

where ρ is the maximum reflectance ratio, given by:

$$\rho = log_{10}[R_{rs}(\lambda)/R_{rs}(555)] \tag{2.2}$$

and $R_{rs}(\lambda)$ is the highest value between $R_{rs}(443)$ and $R_{rs}(490)$.

2.2.3 Chl algorithms validation

However the two chlorophyll (regional and standard) products have been locally validated making use of a dataset of *in situ* chlorophyll measurements partly covering our area of interest.

For validation purposes we used fluorometric chlorophyll concentration values, derived by calibration of fluorometer with bottle measurements of chlorophyll concentration, collected during two oceanographic cruises in spring and autumn 2001 (Medgoos-2 and Medgoos-3, respectively).

In Fig. 2.1 the distribution of the 39 validation points is shown.

Methods applied for bottle Chl measurements are explained in details in Chapter 3. The Chl_m, the mean chlorophyll concentration into the penetration

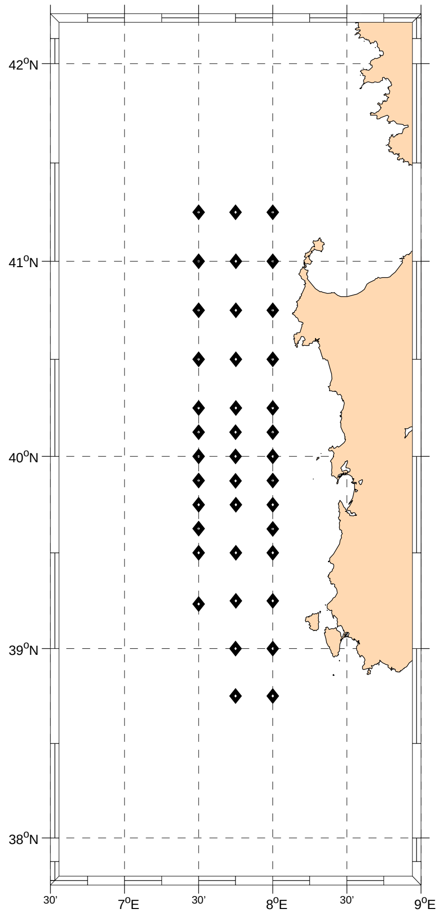

Figure 2.1: Distribution of Chl validation data

depth (Z_{pd}), is computed to be compared with satellite retrievals and is given by:

$$Chl_m = \frac{\int_0^{Z_{pd}} Chl(z)\, exp(-2Kz)\, dz}{\int_0^{Z_{pd}} exp(-2Kz)\, dz} \tag{2.3}$$

where Kz is the attenuation coefficient of light at depth z.

Z_{pd} values are empirically derived from the K_{490} parameter, which is the attenuation coefficient of the light at $\lambda = K_{490}$, using the following parameterization:

$$Z_{pd} = \frac{1}{K_{490}} \tag{2.4}$$

The satellite data used for validation purposes are Level 2 SeaWiFS Chl images (single swaths) overpassing the sampling point the same day of the water samples. A box of 3x3 pixels of satellite Chl have been averaged for each single sample, and the mean value has been calculated to compare it with the bottle measurement, in order to reduce time/space mismatching problems. Satellite Chl values are therefore transformed using the regional algorithm. The performances of both global and regional products in reproducing the "real" values have been tested.

The validation is performed by linear regression of satellite (Chl and rChl) with *in situ* data. The r^2 value is used as principal indicator of the skill of satellite products to reproduce *in situ* measurements. Additionally two statistics of the goodness of the fitting are computed to give a more complete picture of the skill score of the global and regional products. They are the root mean square (RMS) and the mean relative percentage difference (RPD), defined as reported by Volpe et al. (2007).

The RMS indicates the spread of the data as compared to the best agreement, and is given by:

$$RMS = \sqrt{\frac{\sum_{i=1}^{N} (Chl_i - Chl_{mi})^2}{N}} \tag{2.5}$$

The RPD gives the uncertainty as function of the Chlorophyll value, and is given by:

$$RPD = \frac{1}{N} \sum_{i=1}^{N} \frac{(Chl_i - Chl_{mi})}{Chl_{mi}} 100 \tag{2.6}$$

The regional Chl algorithm showed better performances than the standard one using our validation dataset. In Fig. 2.2 the two datasets of satellite Chl, regional and standard, are linearly regressed with *in situ* data obtaining respectively a r^2 of 0.8 and 0.75.

The RPD values are -24.8 for the regional and 37.3 for the standard products while the RMS are 0.033 and 0.045, respectively. Therefore, for all the

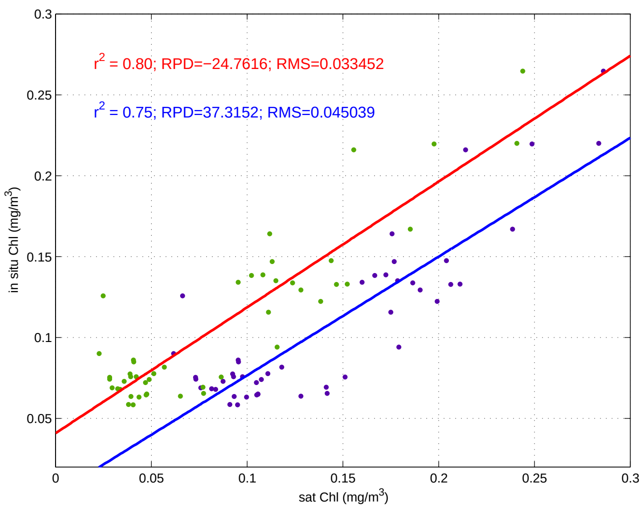

Figure 2.2: Regression of regional (red line) and global (blu line) satellite chlorophyll data with *in situ* measurements. Regional algorithm shows better performances.

three skill scores, the regional algorithm showed better performances than the standard one.

2.2.4 Vertically Generalized Production Model

The estimates of PP have been obtained through the Vertically Generalized Production Model (VGPM) developed by Behrenfeld and Falkowski (1997b), and following modifications suggested by Kameda and Ishizaka (2005) concerning the P^B_{opt} parameter modellization.

As mentioned in the introduction, all the parameters required by the VGPM model can be obtained, directly or indirectly, by remote sensing: Chlorophyll-a (Chl), Photosyntetically Available Radiation (PAR), Sea Surface Temperature (SST) and the euphotic depth Z_{eu}.

The main equation of the VGPM is:

$$PP_{eu} = Chl\, Z_{eu}\, DL\, P^B_{opt}\,(0.066125\,\frac{PAR}{PAR + 4.1}) \tag{2.7}$$

where DL is the daylength analytically computed for the 15^{th} of each month, the euphotic depth Z_{eu} is derived from the Chl following Morel and Andrè

(1991) and $P^B_{opt}k$, modellized following Kameda and Ishizaka (2005), is:

$$P^B_{opt}k = \frac{0.071\,T - 3.2\,10^{-3}\,T^2 + 3.0\,10^{-5}\,T^3}{Chl} + \\ + (1.0 + 0.17\,T - 2.5\,10^{-3}\,T^2 - 8.0\,10^{-5}\,T^3) \quad (2.8)$$

while the classical P^B_{opt} model of (Behrenfeld and Falkowski, 1997b) is:

$$P^B_{opt} = -3.27\,10^{-8}\,T^7 + 3.4132\,10^{-6}\,T^6 - 1.348\,10^{-4}\,T^5 + 2.462\,10^{-3}\,T^4 - \\ -0.0205\,T^3 + 0.0617\,T^2 + 0.2749\,T + 1.2956 \quad (2.9)$$

Four different setups of the VGPM have been compared in order to understand the effects of the use of rChl and of the two different parameterizations of P^B_{opt}:

- A) Classical VGPM with standard Chl SeaWiFS products
- B) Classical VGPM with regional Chl calculated by means of a regional algorithm for Mediterranean proposed by Bricaud et al. (2002)
- C) VGPM with P^B_{opt} modelled as in Kameda and Ishizaka (2005, $VGPM_k$ and $P^B_{opt}k$) and Chl standard product
- D) $VGPM_k$ with regional Chl

It is obvious that the VGPM setups using regional algorithm (rChl) produce lower estimates of PP_{eu} (holding P^B_{opt} constant) than using the standard Chl products, although these differences are quantitatively small in percentage terms (less than 5%). Should be noticed that the effects of the two different satellite Chl on PP_{eu} estimates also depend on the P^B_{opt} modellization. In $VGPM_k$, where $P^B_{opt}k$ is function of both Chl and SST, the effect of the use of regional Chl is weaker (the monthly-averaged value of PP is reduced by 5% over the 1997-2007 period) than when using classical VGPM, where P^B_{opt} is only function of SST (monthly-average of PP is reduced by 15% over the same period).

From the comparison, the two models of P^B_{opt} used in VGPM and $VGPM_k$ (A vs C and B vs D) show larger differences than only changing the Chl algorithm (regional or standard). The classical modellization of P^B_{opt}, function of temperature, produces higher annual estimates of PP than the $VGPM_k$, where $P^B_{opt}k$ is function of the temperature and of the Chl.

The Kameda and Ishizaka (2005) $P^B_{opt}k$ model has been developed by the authors assuming a schematic two-sized phytoplankton community; it is also assumed, in accordance with literature, that big-size phytoplankton predominates at lower biomass and small-size individuals predominate at high biomass. Unpublished data (Polonelli et al., PhD thesis) shows that this schematic description of the phytoplankton community can be roughly adopted also in the APB, justifying the choice of the $P^B_{opt}k$ modellization. However Kameda and Ishizaka (2005) showed that the improved estimates of $P^B_{opt}k$ and PP of $VGPM_k$ are obtained for meso-eutrophic waters ($Chl > 0.1 mg/m^2$) while for oligotrophic waters (less than $0.1 mg/m^2$) the classical VGPM gives better results.

For these reasons, we adopted a hybrid version of VGPM by applying the Kameda and Ishizaka (2005) $P^B_{opt}k$ model for Chl concentrations higher than $0.1 mg/m^2$, and the classical one (Behrenfeld and Falkowski, 1997b) for lower concentrations. The Chl retrieved through the regional algorithm was used in the model, thanks to its better fitting with the *in situ* data. Thanks to its better fitting with *in situ* data, the Chl retrieved through the regional algorithm was used in our setup.

2.2.5 Data analysis

Empirical Orthogonal Functions (EOF) decomposition has been applied to the $VGPM_k$ results to decompose the variability of the PP_{eu} dataset into orthogonal (uncorrelated) modes of variability. These modes of variability, here rapresented by maps of loadings, are physically interpreted together with the related time-expansion coefficients, or Principal Components (PCs), as explained in details in Chapter 1. The PCs suggest the temporal behaviour of the related EOF modes. The visual interpretation of the modes of variability is necessary because of EOF method can potentially produce physically-inconsistent results, especially for the highest-order modes. A percentage of total variance explained is associated to each mode of variability. For a detailed description of the EOF decomposition method, and equations, please see Preisendorfer (1988). Seasonal, interannual and spatial variability of PP is therefore depicted for the ten years period 1997-2007.

2.3 Results

2.3.1 Annual budgets of PP

The climatological PP_{eu} map calculated through $VGPM_k$ and averaged over the 1998-2006 period is shown in Fig. 2.3, while the time series of annual budgets is shown in Fig. 2.4. Annual PP_{eu} values are expressed in $gCm^{-2}year^{-1}$. The highest values of primary production in Fig. 2.3 are reached in the shallow waters of the Gulf of Lyon, a well known area where wind induced coastal upwelling and river runoff contribute to the exceptionally high values of biomass and primary production. However the estimates of biomass and PP in such coastal area are potentially lacking of accuracy (with an order of 2 for biomass) because of the high content of Colored Dissolved Organic Matter (CDOM). For this reason, and consistent with the paper purposes, we will concentrate on the basin and regional scale PP. The main feature can be observed at these scales is the high PP value associated to the so called MEDOC area (MEDOC group, 1969), which involves the Ligurian Sea and the Provençal Basin. The southern limit of this area is the Balearic Front, at about 41° N. Here the annual primary production ranges between 150 and 180 $gCm^{-2}year^{-1}$. South of 41° N the values decreases and the area between 39 and 40° N shows the lowest production of the whole domain, about 130 $gCm^{-2}year^{-1}$. Close to the Algerian coast the values increase again (140 to 160 $gCm^{-2}year^{-1}$). This southern area results to be under the inference of the MAW flow and of the Algerian Current which contributes to enhance the productivity along the coast. The time-series of annual PP averaged over the domain (Fig. 2.4) shows a marked interannual variability: the minimum reached in 2003 is particularly evident with an after-effect in 2004 (when the secondary minimum of the series is recorded). Annual budgets (1998-2006) range between about $127gCm^{-2}year^{-1}$ in 2003 and $151gCm^{-2}year^{-1}$, with an average of $142gCm^{-2}year^{-1}$ (standard deviation σ of $6.7gCm^{-2}year^{-1}$).

The annual values computed with $VGPM$ are in good accordance with those calculated for the 1998-2001 period over the whole Western Mediterranean Sea ($163gCm^{-2}year^{-1}$) by Bosc et al. (2004) which used the light-photosynthesis model of Morel and Andrè (1991). The same study estimated annual values of about $153gCm^{-2}year^{-1}$ for the central part of APB, where we estimated averaged values a little lower (about $140gCm^{-2}year^{-1}$) for the same period and area. Other satellite estimates of the Mediterranean PP_{eu}

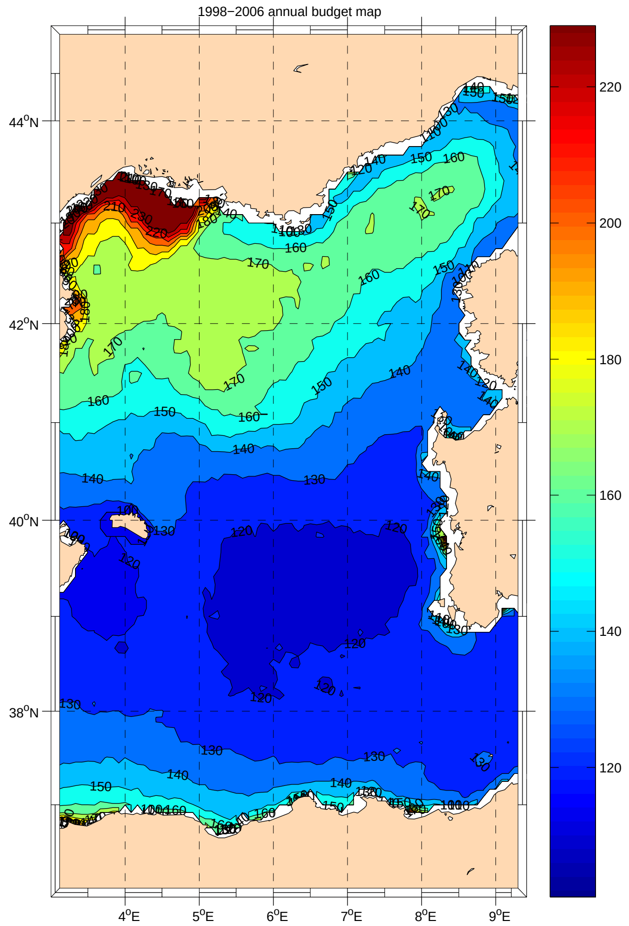

Figure 2.3: Annual PP_{eu} (1998-2006 climatology)

have been provided by Antoine et al. (1996), that calculated an averaged value of $197 gCm^{-2}year^{-1}$ for the Western Basin over the period 1978-1981 using CZCS data and the same algorithm used by Bosc et al. (2004). As stated by Bosc et al. (2004) it is hard to understand if the differences in the budgets of these two previous study are due to an actual drift or to an improvement of the quality of the satellite dataset (radiometric resolution; simultaneity of PAR, SST and Chl observations; development of regional Chl algorithms). However, we consider the study of Bosc et al. (2004) as the main term of comparison also because its period of investigation is partially superimposed with the present study.

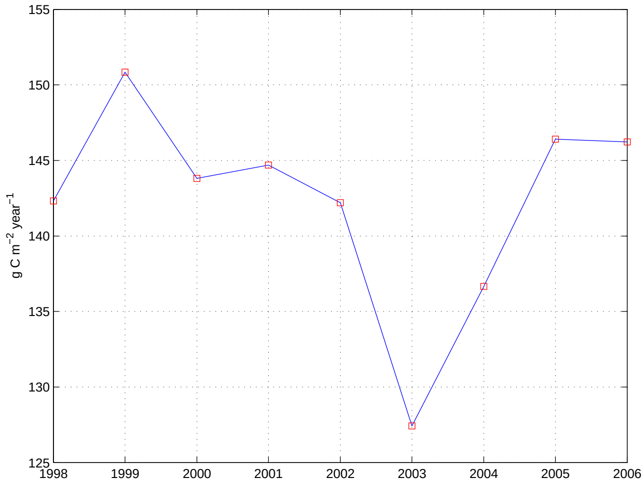

Figure 2.4: Annual budgets of PP_{eu} (1999-2006)

2.3.2 Seasonal and interannual variability

The time series of monthly PP expressed as $mgCm^{-2}day^{-1}$ from September 1997 to June 2007 is shown in Fig. 2.5.

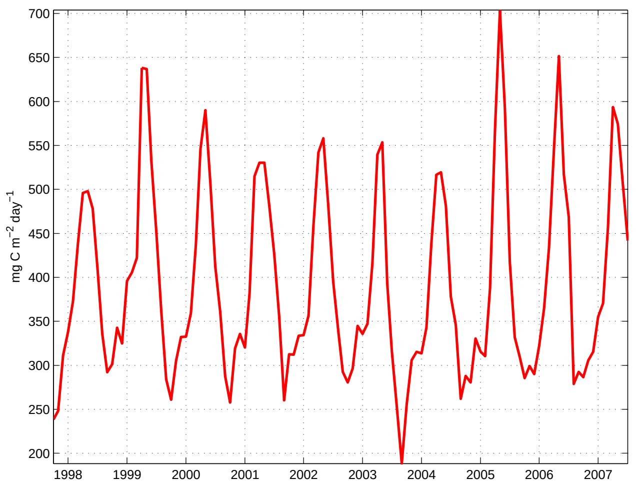

Figure 2.5: Monthly time series of PP

Monthly values range between 188 and 704 $mgCm^{-2}day^{-1}$ with a standard deviation σ of 108 $mgCm^{-2}day^{-1}$. The seasonal cycle clearly dominates the variability of PP in the basin and strictly reflects timewise variations in biomass (with Chl as proxy for biomass, not shown). Especially the timing of the bloom of MEDOC area seems to influence the relative maxima of the monthly series of PP. There is also an evident interannual variability superimposed on the seasonal one. The maximum of the monthly series in recorded in 2005, mainly due to an exceptionally intense bloom occurred in the MEDOC area in that year. The minima of PP_{eu} are located in summer or autumn, depending on the year (function of the balance between lower biomass, decreased efficiency in summer and the significatively shortened daylength of autumn), with an absolute minimum in late-summer 2003 of $188 mgCm^{-2}day^{-1}$. This signal is probably related to the heatwave of summer 2003, which caused an anomaly of SST up to 4°C in North-Western Mediterranean (Marullo and Guarracino, 2003), and also affected surface dynamics in the central Mediterranean (Olita et al., 2007). This increase in temperatures strongly affects the P^B_{opt} parameter which decreases for values of SST larger than 20°C.

A multivariate analysis of model output has been applied, to better understand seasonal and interannual variability of PP_{eu}. As stated above, the dataset variability has been decomposed using EOFs. Only the first three EOF modes have been considered, accounting for about 85% of total variance.

The first EOF mode (EOF1, Fig.2.6) explains about 68% of variance with the highest loadings (strongest signal) in the MEDOC area: this mode therefore clearly separates the seasonal bloom occurring in the North-Western Mediterranean. It is also interesting to note that part of the interannual variations are still retained in this mode of variability, suggesting that they matches the main seasonal variations of this mode of variability in time and space. So, it seems that the anomaly of summer 2003 is also included in the EOF1 (see PC1 in top panel of Fig. 2.9) because of its synchronicity with the usual summer-autumn minima of PP, even if the value of this 2003 minimum is largely lower than in other years (with a residual from the mean of $204 mgCm^{-2}day^{-1}$).

As for Chl (see Chapter 1, the loadings of the first mode for PP_{eu} are in phase over the whole domain, meaning that the seasonal variations related to this mode are synchronous even if characterized by different magnitudes. On the contrary a phase opposition of the loadings of EOF2 is shown in Fig. 2.7. This second orthogonal mode explains about 13% of variance and is characterized by the signal of the weak winter bloom along the AC path, as shown in Chapter 1. The seasonality of this signal seems to be related to the seasonal cycle of MAW flow, which increases in winter. The central panel of Fig. 2.9 shows the PC2, where the seasonal cycle of this mode is clearly visible, with

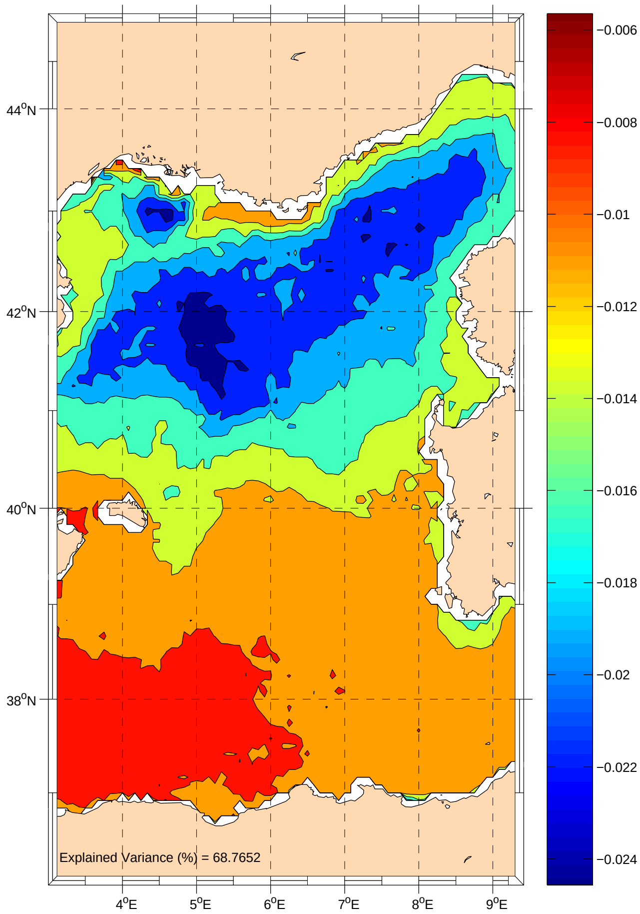

Figure 2.6: EOF-1 of PP. About the 68% of variance is explained by this mode of variability

its winter-time peaks.

EOF3, accounting for the 3% of total variance, shows patterns which can be brought back to anomalies in the strength and location of the MEDOC spring bloom in the LPB (Fig. 2.8), as observed by Bosc (2002). In fact this mode shows positive loadings of PP_{eu} located in the north-eastern part of the basin, close to the Sardinia and Corsica islands. Timewise these two maxima are indentified by PC3 (bottom panel of Fig. 2.9) which localizes them in spring 1999 and 2005, respectively.

This two interannual events certainly contribute to explain the maximum of annual PP_{eu} reached in 1999 and the secondary maximum in 2005 we have

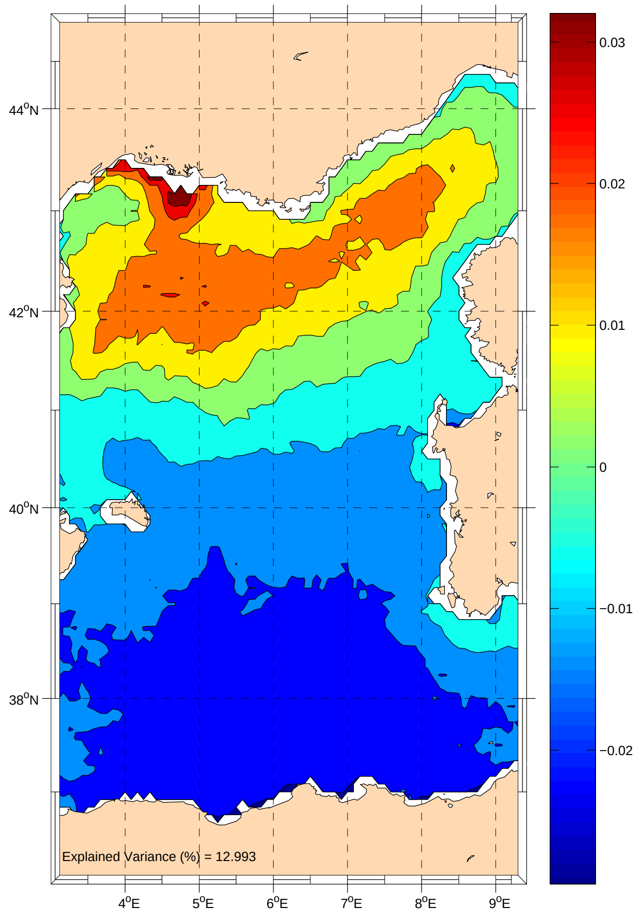

Figure 2.7: EOF-2 of PP. 13% of variance is explained by this mode, showing a seasonal behaviour

seen in annual budgets and in monthly time series.

2.4 Discussion

In this chapter the primary production of the APB over a decade has been estimated and analyzed. Particularly, we used a satellite based model to estimate the primary production integrated over the euphotic layer, PP_{eu}. To do this, we made use of the Vertically Generalized Production Model (VGPM) developed by Behrenfeld and Falkowski (1997b), adopting the modifications proposed by Kameda and Ishizaka (2005), concerning the parameterization of

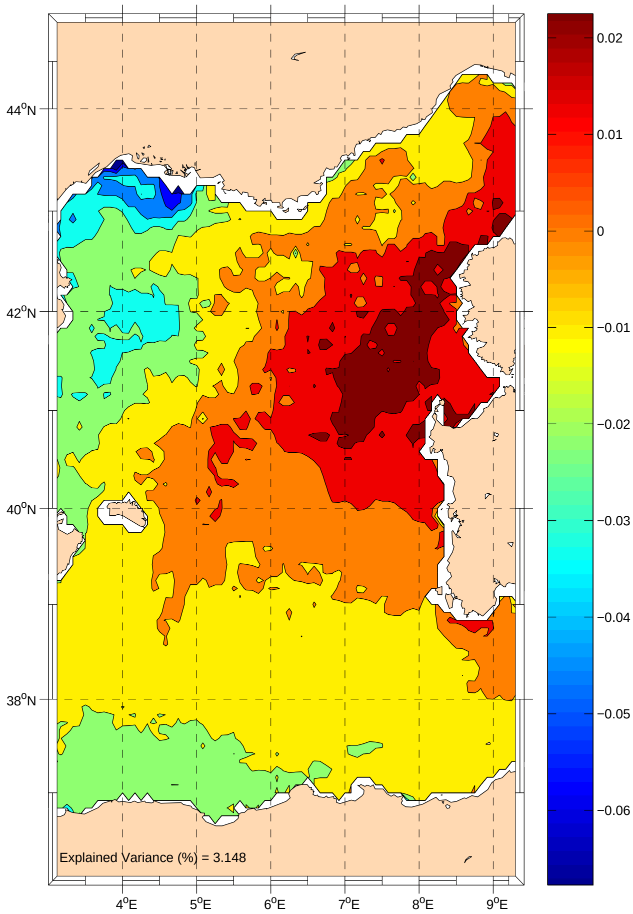

Figure 2.8: EOF-3 of PP. 0.6% of variance is explained by this EOF, related to interannual variability patterns

P^B_{opt} (the maximum production per unit of chlorophyll). In this form P^B_{opt} is function both of SST and Chl. We compared different setups of the model using different parameterization of P^B_{opt} and different Chl estimates. In facts we tested the model either using the Chl Seawifs NASA standard products and the regional Chl directly obtained from standard products through the algorithm developed by Bricaud et al. (2002). Through these different setups of the model, we observed its different sensitivities due to the variation of the P^B_{opt} and Chl parameters. The model proved to be more sensitive to P^B_{opt} variations than to the use of different Chl estimates. The final setup of VGPM for our study of variability the parameterization of P^B_{opt} of Kameda and Ishizaka

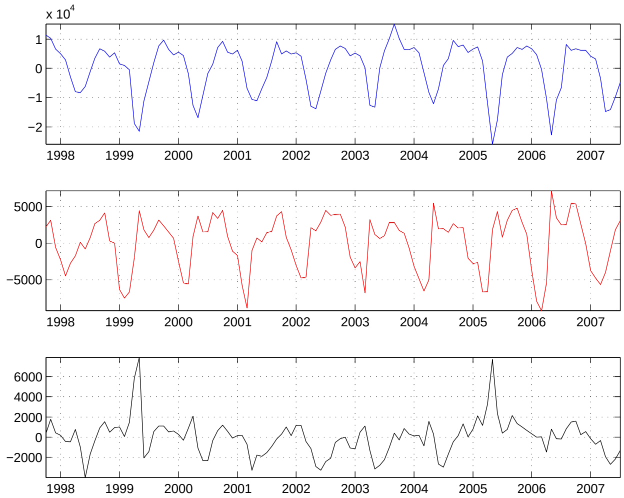

Figure 2.9: Top to bottom, PC-1, 2 and 3 of PP dataset

(2005) for Chl higher than $0.1mg/m^3$ and the classical parameterization for lower values. We used the regional Chl which, as in Bosc et al. (2004), better reproduces Mediterranean Chl concentrations in oligotrophic conditions and moreover showed a better fitting with our *in situ* dataset, compared to the standard SeaWiFS product.

The basin averaged values we found (9-years average is $\sim 142gCm^{-2}year^{-1}$ with a σ of $6.7gCm^{-2}year^{-1}$) are quite in good accordance with the values previously estimated by other authors (Antoine et al., 1996; Estrada, 1996; Bosc et al., 2004) for the western Mediterranean, with a marked interannual variability. No evident trends, neither negative nor positive, have been found in terms of annual budgets. The decadal monthly time series show peaks in 1999 and 2005 which are due, as observed by the EOF decomposition, to anomalous intensity of the spring bloom in the MEDOC area. In particular EOF-3 mode suggests that the 1999 and 2005 spring maxima could be related to the eastward and southward expansion of the spring-bloom area. This extension, mainly occurring in March, is probably due to the strong winds recorded also by Bosc et al. (2004) for the year 1999, which contributed to the eastward and southward displacement of the BF, and to an exceptionally strong mixing of upper layers in the northern area.

It is also noteworthy the strong anomaly of the 2003 when the lowest primary production over the decade has been recorded. This minimum is related to extremely low values of Chl and to a maximum in SST, as we have seen in

Chapter 1, both having a negative impact on the P^B_{opt} parameter and therefore on the primary production itself. We remind that exceptional SST values are due to the summer heatwave event which stroke western continental Europe and the Mediterranean sea in 2003 (Black et al., 2004). The absolute minimum of monthly PP_{eu} is reached in summer 2003 with a value of $188 mgCm^{-2}day^{-1}$. This event however has not been separated through the EOF analysis in a different mode of variability, but is included as an oscillation in amplitude of the first mode, which is related to the seasonal variability of the basin enclosing almost 65% of the total variance of PP_{eu} dataset. Gomez and Souissi (2008), for the North Eastern English channel, did not find any particular signature of the 2003 heatwave on annual phytoplanktonic primary production, guessing that this was because the summer generally is characterized by a low phytoplanktonic biomass. On the contrary we found, in our study area, that the impact of the heatwave on the annual budgets is really evident notwithstanding the low biomass of the summer period. We guess that, nevertheless the low biomass, the summer (in our study area) is characterized by higher PAR and daylength than during other periods of the year, so that the daily production remains quite high even in summer. The method we adopted proved to be suitable to investigate the seasonal and interannual variability of the PP at basin scales, and to localize anomalous events. The VGPM setup we adopted showed its affordability in estimating PP, with values comparable to the literature.

Chapter 3

Mesoscale eddies and chlorophyll distribution in the Sardinian Sea

3.1 Introduction

Many authors showed in the last 20 years that mesoscale eddies influence, through several mechanisms, the primary production and/or the chlorophyll concentration and distribution in the pelagic domain (e.g. Yentsch and Phinney, 1985; McGillicuddy et al., 1998; Martin and Richards, 2001; Moran et al., 2001; Martin, 2003; Taupier-Letage et al., 2003; Martin, 2003; McGillicuddy et al., 2007).

The Sardinian Sea (SaS), located in the eastern part of the Algero-Provençal basin along the western Sardinian coast, is strongly interested by the presence of mesoscale features, particularly antyciclonic eddies as stated by Ribotti et al. (2004). The eddies of the SaS can have different origin. They can be AEs (Anticyclonic Algerian Eddies) detatching from the Algerian current as described by Puillat et al. (2002).The AEs can approach the Sardinian coast several times during their lifetime. The eddies can also be shorter-life and locally-formed eddies generated, for example, from the Balearic Front area with mechanisms which are still not deeply understood (Fuda et al., 2000).

The main objective of this chapter is to understand how these eddies, and other mesoscale processes and features, infer on the phytoplanktonic distribution of the Sardinan Sea. The knowledge of the relationships between mesoscale structures and phytoplaktonic biomass distribution may substantially help to interpret and explain the findings and the bio-physical characteristics we have seen in the previous chapters, concerning the bio-physical variability at wider scales.

To do this, a set of hydrological and fluorometric *in situ* data, collected during two oceanographic cruises with a mesoscale resolving sampling strategy conducted in 2001 and 2002 in the Sardinian Sea and Sardinia Channel (SaC, located between Sardinia and African coast), has been analysed.

3.2 Methods

The two oceanographic cruises are named MedGOOS-2 and MedGOOS-4, respectively conducted in March 2001 and May 2002 on board the R/V Urania. In Tab. 3.2 the geographic boundaries, the period and the number of casts for the two cruises are indicated.

Table 3.1: Period and area sampled during the two cruises

Cruise	Lat	Lon	Casts	Date
MedGOOS-2	38°– 41.5°N	7.5°– 9°E	66	23 Mar - 3 Apr 2001
MedGOOS-4	38°– 41.5°N	7.5°– 9°E	62	10 - 18 May 2002

The cruises have been conducted on a large across-shelf area, encomprising the whole length of the western Sardinian coast and part of the Sardinian Channel (Fig. 3.1). The sampling area, for both the cruises, was covered by a grid of about 1/4°of resolution in latitude and longitude. The sampling resolution was increased in front of the Gulf of Oristano (centra-western coast of Sardinia), close to the coast at about 40°N.

3.2.1 Hydrological measures and water samples

Profiles of potential temperature, salinity and density have been obtained by a SBE 911 plus CTD used on the hydrographic stations. SBE-3/F (temperature), SBE-4 (conductivity), 4000 Digiquarz (pressure), and SBE-13 (oxygen) sensors were installed on the probe. The chlorophyll fluorescence was measured by means of a Seatech 90S fluorometer connected to the SBE carousel. Data were archived, processed and reduced using SeaSoft vers. 5.26.

Fig. 3.1 shows the sampling points of the two cruises and the location of the transects along which the vertical sections have been analysed. The longitudinal position of the three meridional transects is the same for the two cruises. The transects are, inshore to offshore, T1, T2 and T3, respectively.

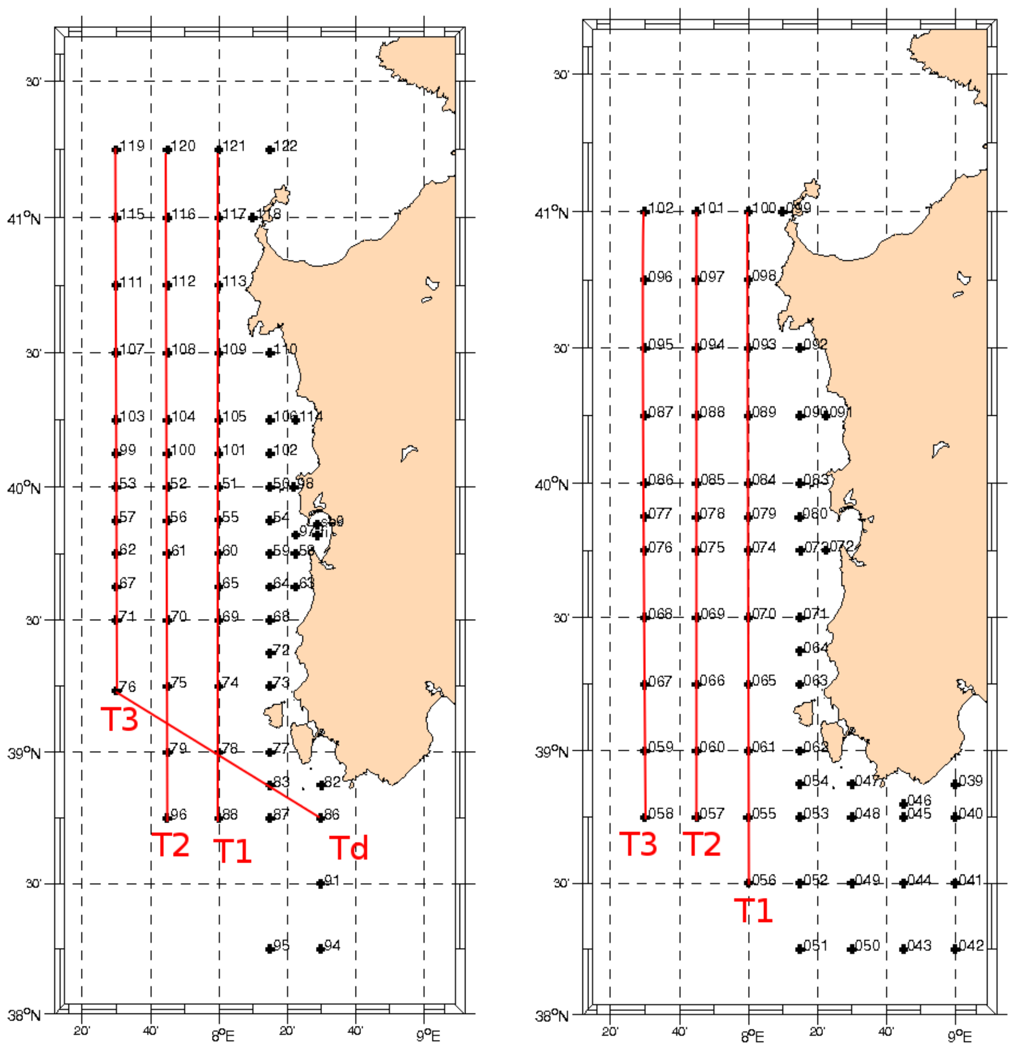

Figure 3.1: Sampling scheme of MedGOOS-2 (left) and MedGOOS-4. The transects along which vertical sections have been coduced, are also indicated.

A standard G.O. 1016I, 10 lt 24 Niskin bottle carousel was used for the water sampling. In a reduced subset of stations, 38 for MedGOOS-2 and 40 for MedGOOS-4, at fixed depths and in correspondence of the DCM (Deep Chlorophyll Maximum) and DSM (Deep Salinity Maximum), the samples for photosynthetic pigments were collected. For pigments extraction, a water sample of $4dm^3$ was filtered through Whatman GF/F filters ($47mm$) using a glass in-line filter holders and a vacuum pump. Filters, immediately placed in acetone for chlorophyll-a extraction, have been stored until on-shore analysis according to the general procedures of Lazzara et al. (1990). The fluorescence of these pigments was measured, before and after acidification with HCl, by a Perkin-Elmer LS 5B spectrofluorometer (excitation at $430nm$ and emission at $671nm$), following the method of Holm-Hansen et al. (1965). The chlorophyll-a concentrations have been used to calibrate the Seatech 90S fluorescence data collected on field by means of linear regression. Hereafter in the chapter when we use Chlf, we indicate the fluorometrically derived chlorophyll-a concentration.

3.2.2 Satellite Data

As previously mentioned, the SaS is dominated by mesoscale features, in particular anticyclonic eddies which in some season have stronger signature in salinity than in temperature (Ribotti et al., 2004). In facts, the core of the anticyclonic eddies of Atlantic origin is often well identified by a minimum of salinity. On the contrary, in some periods, the horizontal temperature gradient is very low, and the thermic signature of the AC and of the AEs is hardly detectable. For this reasons, the use of remotely- sensed SST does not permit, in some cases, to clearly identify the oceanographic mesoscale structures.

We observed that, in the SaS and in spring period, the Ocean Color imagery can be used to better identifie these mesoscale structures. The analysis of the correlation between chlorophyll and salinity (good indicator of mesoscale features of the area, as stated above), statistically confirms (see Section 3.3) the reliability of the relationship existing between the Ocean Color features and the hydrodynamics in the area. For this purpose Level-2 SeaWiFS images (single swaths) of chlorophyll-a concentration, temporally and spatially matching the *in situ* samplings, have been downloaded and used.

3.3 Results

3.3.1 Chlorophyll–salinity correlation

We analysed the correlation between salinity, which at first approximation represents a good signature for mesoscale structures (Ribotti et al., 2004), and the chlorophyll-a concentration, as measured by CTD casts and fluorometric measurements, to justify the use of Ocean Color data to detect hydrodynamical features.

We discarded from this analysis the casts close to the coast. In facts in coastal areas the Chlf concentration may be conditioned by local-scale phenomena (above all in proximity of small gulfs) which could hide the effect of the mesoscale features.

We build two subsets of casts, in function of the observed differences in the stratification of the water column, north and south of a strong salinity and density front located at about 40.5° N. In this way we separated the norhtern zone with the deeper and well formed mixed layer from the southern one characterized by the presence of mesoscale eddies and by a well structured DCM.

The Mixed Layer Depth (MLD) distribution over the domain has been obtained calculating the MLD for each station and then interpolating MLD values on a regular grid. Here we used the definition of Sprintall and Tomczak (1993) of MLD, i.e. the depth at which the $\Delta\sigma_\theta$, referred to the surface density value, is equal to -0.2.

The map of Fig. 3.2 clearly shows two different areas in which MLD is strongly different. The main difference is between northern and southern areas, with a *frontal* zone located north of A1 eddy (at about 40.5°N).

Once identified the subsets of casts, we computed the Pearson correlation coefficient (r) between the two variables for each sub-area separately. The r coefficent may assume values between -1 and $+1$ and is associated to a probability P value (r is significant for $P < 0.05$) which indicates the probability that the Null hypothesis (no- correlation) is true. If the result is significant ($P < 0.05$), low r values indicate anticorrelation, high r value correlation and 0 value no-correlation. Vertically the data have been grouped every 10 meters, in order to reach a sufficient number of observations for each layer. The analysis performed on the southern subset shows (Fig. 3.3) that the Chlf is negatively (r about -0.4) and significatively ($P < 0.05$) correlated to salinity in the upper $30m$. Between 30 and 70 meters the correlation becomes positive and/or non-significant, suggesting that at DCM level the chlorophyll is statistically uncorrelated with dynamical features, although the dynamics modulate the depth of UML and therefore of the DCM itself. Between 70 and 100 meters of depth, the bottom limit of our analysis, the correlation comes back negative and significant.

A different behaviour can be observed analysing the correlation results

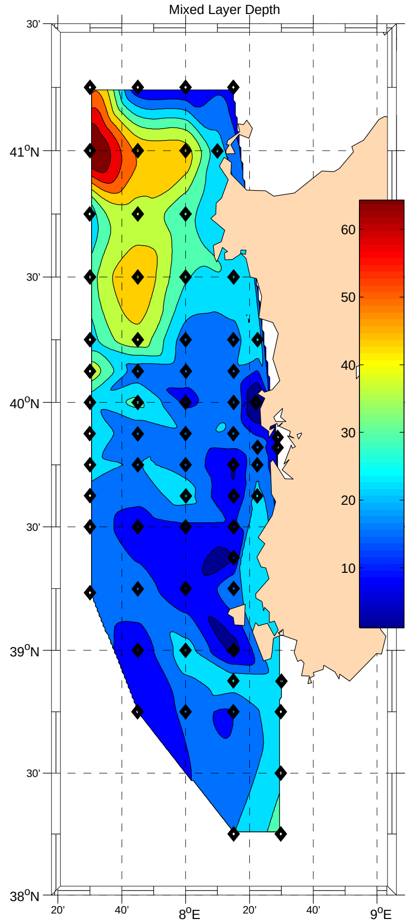

Figure 3.2: Map of Mixed Layer Depth (MLD). MLD values (meters) for single stations have been calculated using the $\Delta\sigma_\theta$ criterion of Sprintall and Tomczak (1993)

for the northern subset. Here the correlation, always significant, is strongly positive in the upper 30 meters ($r > 0.7$) than decrease at $+0.3$ between 30 and $55m$. The deepest (55 to $100m$) strata show anticorrelation ($r \sim 0.4$ in average) between the two variables, similar to that observed in the southern zone.

The correlation, always significant for the upper layers for both the subsets, supports the idea that Ocean Color data can be used for the identification of mesoscale features in this area.

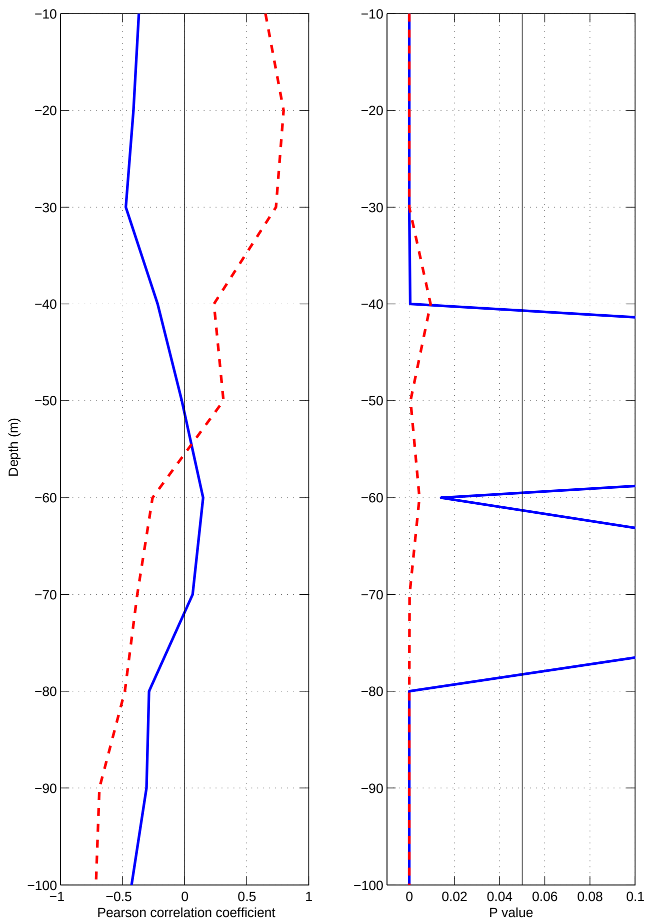

Figure 3.3: Chlorophyll-salinity correlation profiles (left) and correspondent P value (right) for the two zones, north (blue) and south (red) of the density front at 40.5°N

3.3.2 March 2001: hydrology and Chlf distribution

In Fig. 3.4, clockwise from top-left corner the potential temperature, the salinity, the Chlf and the density maps at the surface ($5m$) are presented, obtained horizontally interpolating the values collected in the casts at $5m$ depth.

These maps, and especially the salinity and density fields, suggest the presence of two mesoscale eddies located south of 40.5° N, as reported in previous hydrological studies (Puillat et al., 2002; Sorgente et al., 2003; Ribotti et al., 2004). These eddies are recognised in surface by quasi-circular isolines having fresher, lighter and warmer core. Another smaller sub-mesoscale eddy, A3, is

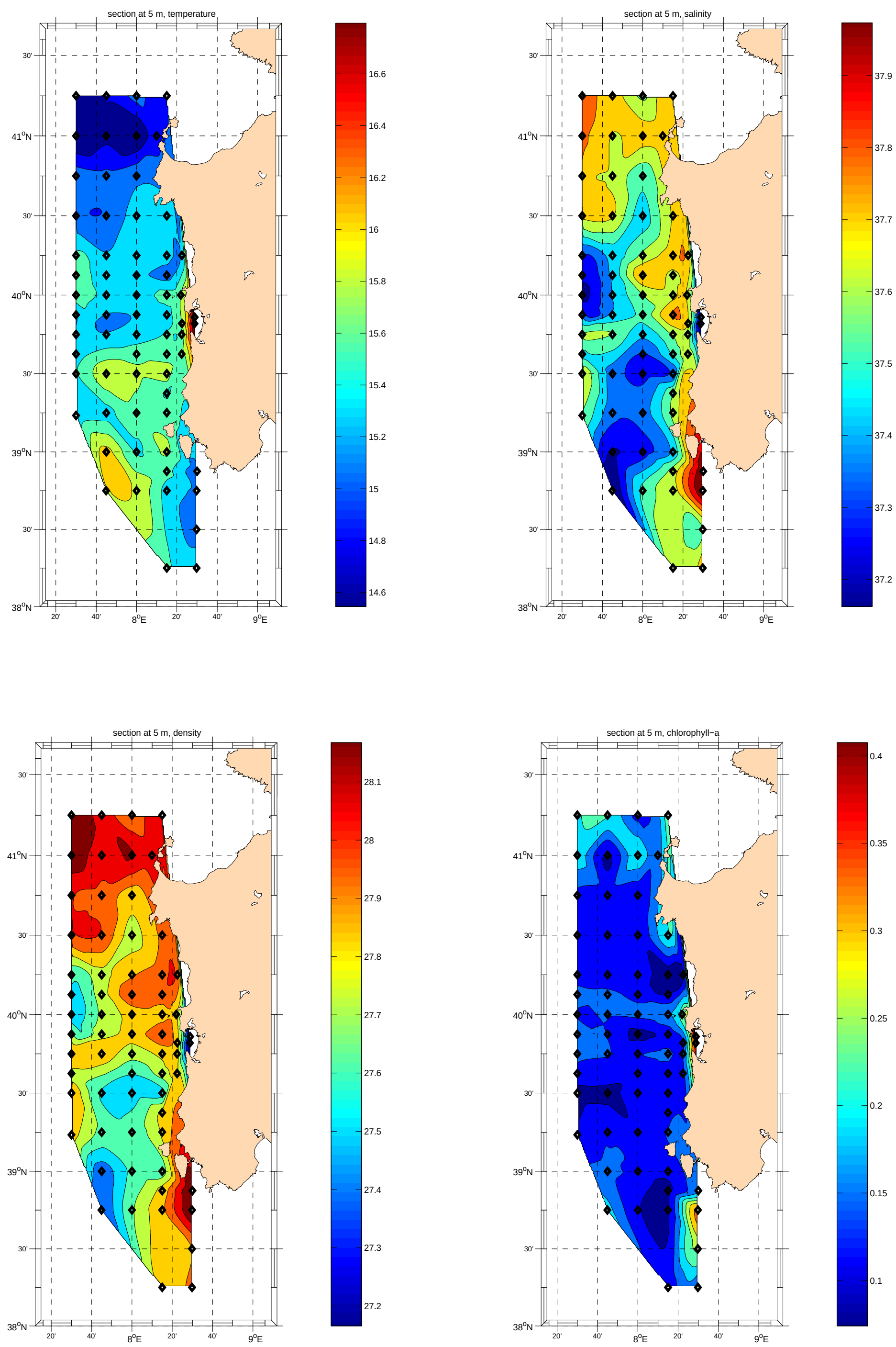

Figure 3.4: Clockwise from the left-top corner, 5 m maps of: temperature, salinity, chlorophyll-a and density. The maps are obtained by cubic interpolation on equally spaced grid

located closer to the coast, at about 39.6° N. The two largest eddies, denominated A1 and A2, have been clearly identified by the satellite Ocean Color image (Fig. 3.5). In this image a less clear signature of the smaller coastal eddy, A3, is visible. The image has been collected by the SeaWiFS sensor on 31 March 2001.

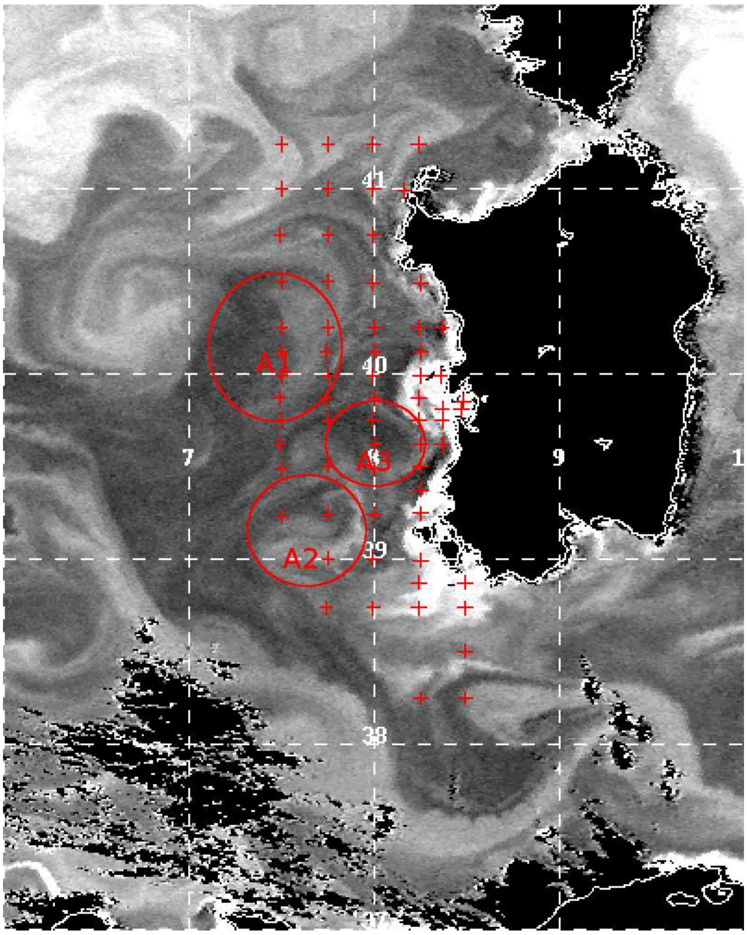

Figure 3.5: The three eddies A1, A2 and A3, found by the analysis of CTD casts, have been also observed in the Ocean Color image.

The northern eddy (A1) is located off-shore, between 39.75°N and 40.50°N. The diameter of this structure is estimated to be about 100 km. At the surface the centre of the northern anti-cyclone is characterised by a temperature $T > 15.6°C$, salinity $S < 37.3$ and density $\sigma\theta < 27.60$ (Fig. 3.4).

The southern eddy, A2, is located at 38.90°N and 7.60°E and extends northward until a latitude of approximately 39.2°N. The core of A2 is characterised by $S < 37.2$, $\sigma\theta < 27.45$ and $T > 15.8°C$. So, A2 is characterised by lower salinity and density than A1.

At the surface (Fig. 3.4), the Chlf is very low throughout the whole sampling field ($< 0.20 mg/m^3$) with the exception of two regions. The highest values (about $0.30 mg/m^3$) are detected in the south-east limit of the survey area, centered in the station 86. This area is characterised by a colder, saltier and denser water, probably due to presence of a coastal upwelling. The other high-Chlf patch is detected in the northern part of the survey area, not interested by the eddies, and mainly due to the presence of a thicker UML.

The Chlf map at $30m$ (Fig. 3.6) presents two intense patches, having $Chlf > 0.6 mg/m^3$. The first patch is located at the eastern margin of A2, within a region of high horizontal salinity and density gradient.

The second one is located at the south of the Sardinia Island, in the South-East limit of the sampling field (38.9° N, 8.5° E) detected also at the surface (centered over the station 86), confirming that this signal could be due to upwelled waters. Relationships between the two patches of Chlf may be supposed by considering the moderately high values of Chlf in the stations located between the two patches. The vertical section coduced along the diagonal transect Td, as defined in Fig.3.1, confirms both the presence of the coastal upwelling and the link between the two patches of Chlf at $\sim 30m$ depth (Fig. 3.7).

This observation may be helpful, jointly with vertical sections (see below), to explain the highly different Integrated Chlf (Chl-int) distribution, over the first 150 m, between A1 and A2 (Fig. 3.8).

In correspondence of A2 the highest values of Chl-int for the entire sampling area are observed. Furthermore, the values are especially higher in the center of the anticyclone, while A1 shows lower values, mainly distributed at the margins. We think that the caption of high-nutrients and high-chlorophyll waters performed by A2 may be the reason of the higher values of Chl-int in this normally oligotrophic area.

The map at 50m (Fig. 3.9) shows the spatial variability of Chlf at the DCM level. It presents a complicate chlorophyll patchiness having $Chlf > 0.5 mg/m^3$. In particular the patch with the highest concentration is located between the two anti-cyclonic eddies, A1 and A2.

This area has the typical structure of an upwelling area (although it does not reach the surface) with temperature minimum and a relative maximum of density and salinity. This structure includes the stations 70 and 71. The interaction of the two eddies, producing this convergence area, may be the

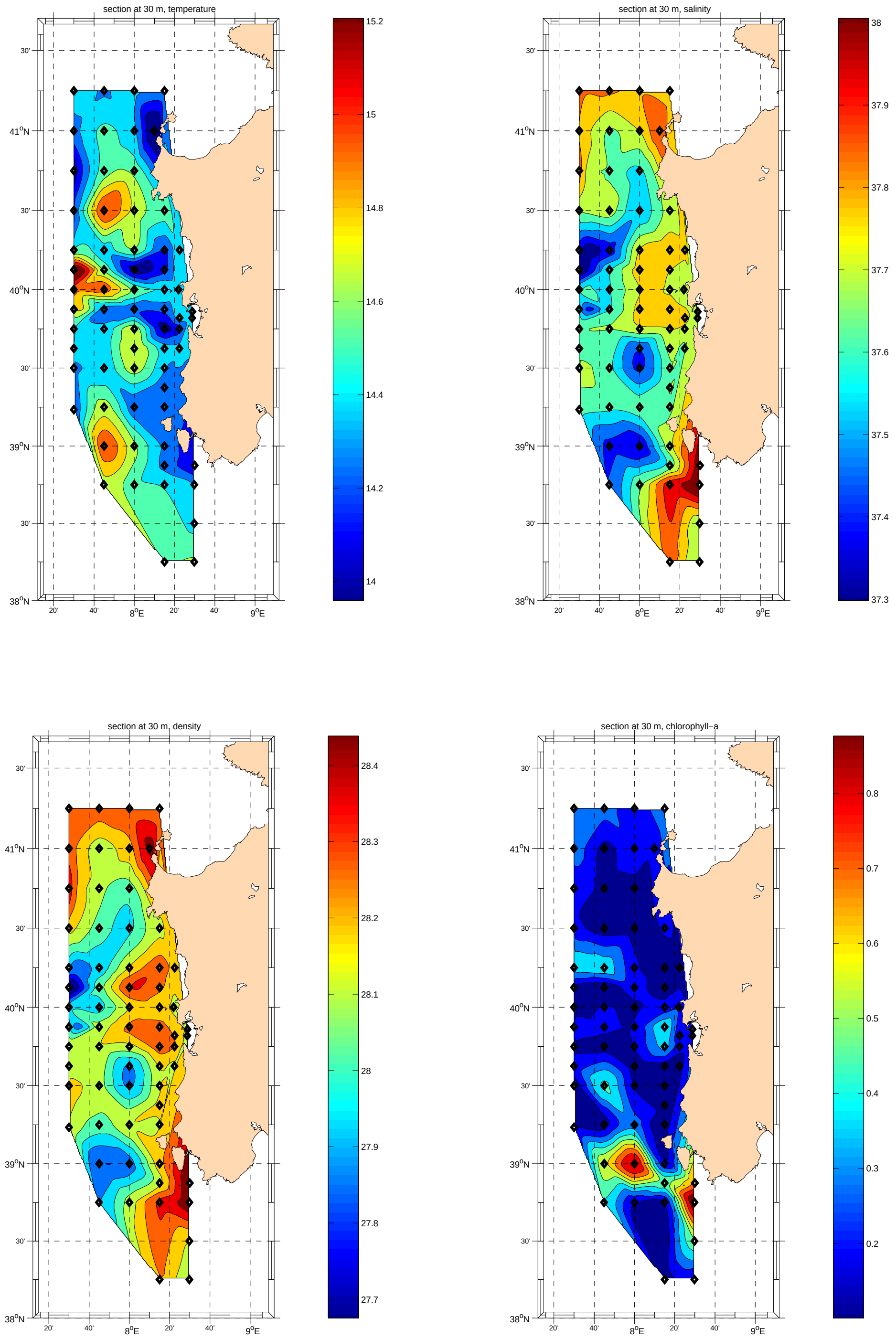

Figure 3.6: March 2001, clockwise from the left-top corner, 30 m maps of: temperature, salinity, chlorophyll-a and density. The maps are obtained by cubic interpolation on equally spaced grid

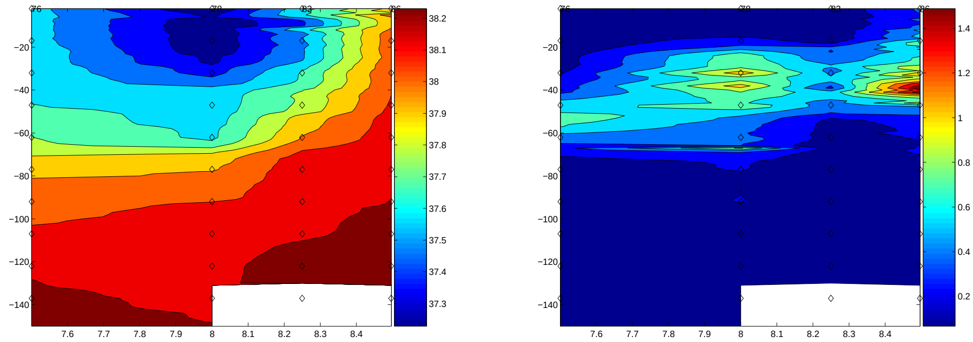

Figure 3.7: March 2001, vertical section, between stations 76 and 86 (diagonal transect Td), identifying the coastal upwelling south of Sardinia. The rise of isoalines (left) and the connection between the two Chlf patches (right) seen in the 30m map are evident

cause of this intense chlorophyll patch.

At the depth of 80 m the Chlf is, in mean, lower than 50 m with few small areas having $Chlf > 0.5mg/m^3$. The highest chlorophyll values are detected close to the centre of the two eddies (not shown), because of the convergence of isopycnae.

The Chlf and the salinity vertical sections along three meridional transects T1, T2 and T3 for the upper 150 m are shown in Figs. 3.10, 3.11 and 3.12, respectively.

The analysis of the features along the transect T1 evidences the typical vertical structure of an anticyclone in the northern area (Fig. 3.10). This signal is probably due to the northern elongation of A1. The structure of eddie A2 can be recognised in the left part of the plots. The transect just covers the peripheric area of A2 eddy. In this region we can see the patch of the highest values of Chlf along the trasect, precisely at about 30-40 meters of depth. Such a patch is probably caused by the entrapement of upwelled and rich waters from the SaC area, as we have also observed through Fig. 3.7. It is also evident the modulation of the UML and of the DCM caused by the eddy, and the distribution of the Chlf in the periphery along iso-lines, due to the effect of the isopycnal mixing.

The border of the eddy A1 is detected in the central transect T2 (Fig. 3.11). The eddy A2 is crossed by the southern part of T2. In this case the transect cuts-off the core of the structure. The classical vertical modulation of the DCM performed by the eddy can be seen, deeper in the center than at the

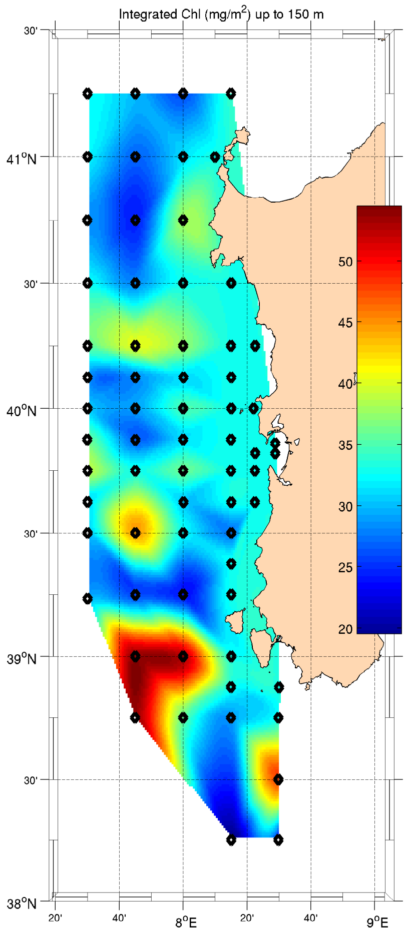

Figure 3.8: March 2001, Integrated chlorophyll in the upper 150 m

border, as well as a moderate concentration of chlorophyll in the upper layers at $\sim 30m$ of depth. Again, this last can be due to the entrapement of richer upwelled coastal waters which, once captured by the eddy, are advected to its central area by convercence.

The effect of the anti-cyclone on spatial distribution of chlorophyll is well clear in the offshore transect T3 that cuts across the core of A1 (Fig. 3.12). The rotational forces affect the vertical distribution of isolines between stations 71 to 111. The central sinking of the anticyclone is well visible below 50m depth. In this case the chlorophyll is classically distributed in a single and well defined DCM, more intense and shallower at the borders, deeper and weaker in the center of the structure. The patch with the highest concentration is located in

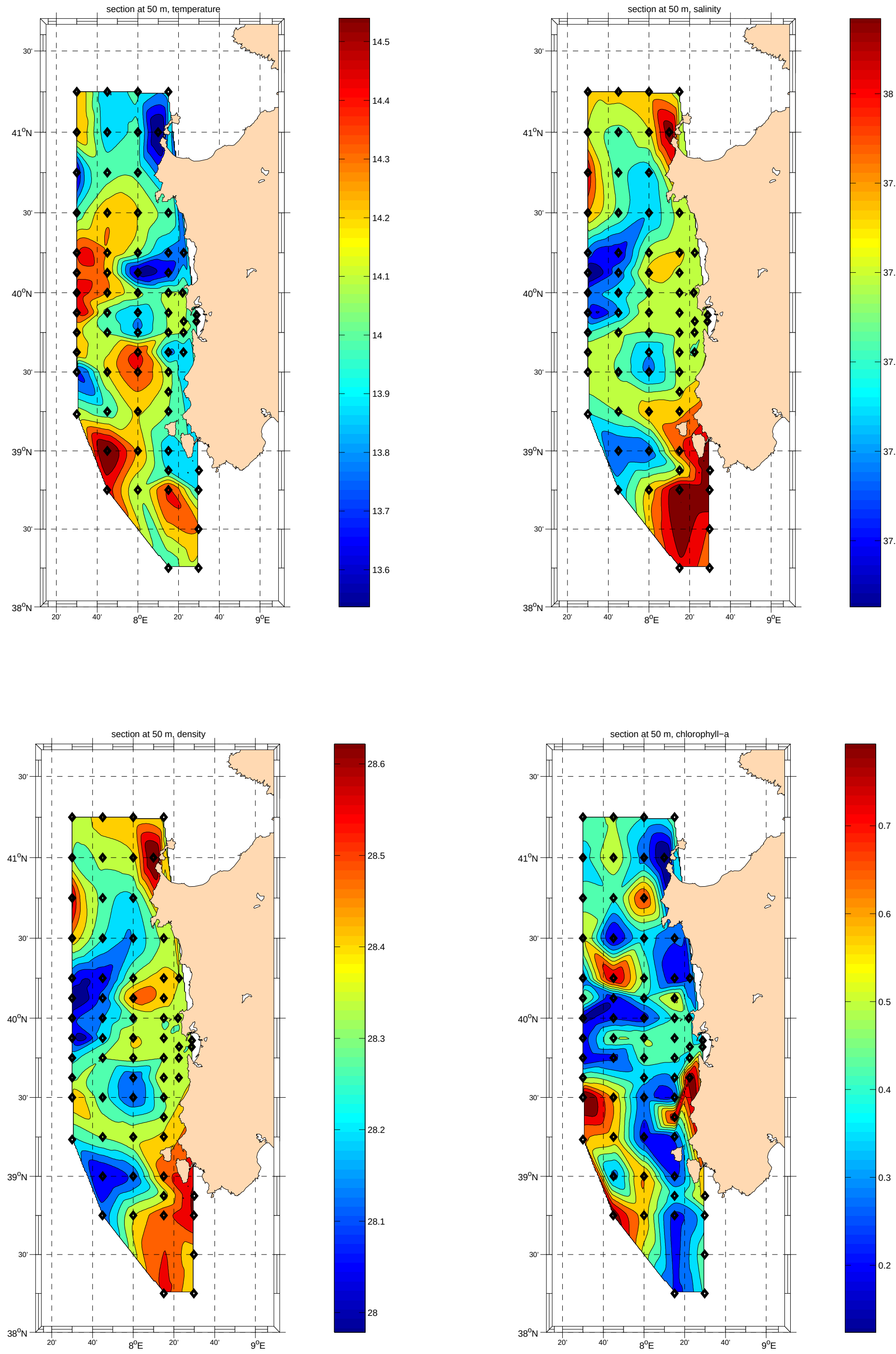

Figure 3.9: March 2001, clockwise from the left-top corner, 50m (DCM depth) maps of: temperature, salinity, chlorophyll-a and density. The maps are obtained by cubic interpolation on equally spaced grid

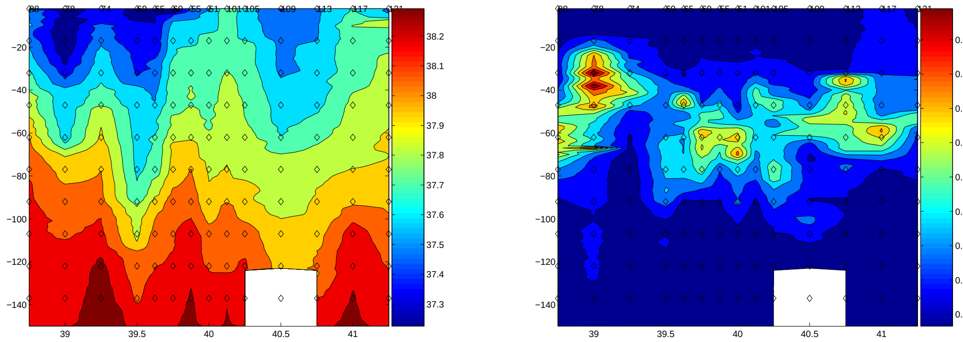

Figure 3.10: March 2001, salinity (left) and chlorophyll sections along transect T1. Salinity is expressed in *psu* and chlorophyll-a in mg/m^3

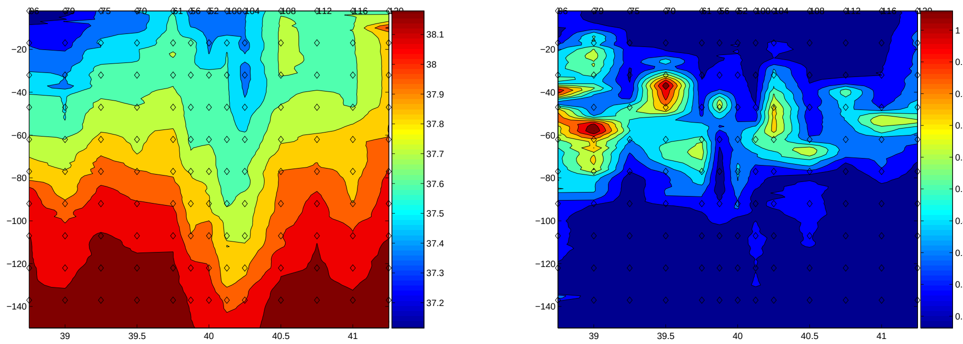

Figure 3.11: March 2001, salinity (left) and chlorophyll sections along transect T2. Salinity is expressed in *psu* and chlorophyll-a in mg/m^3

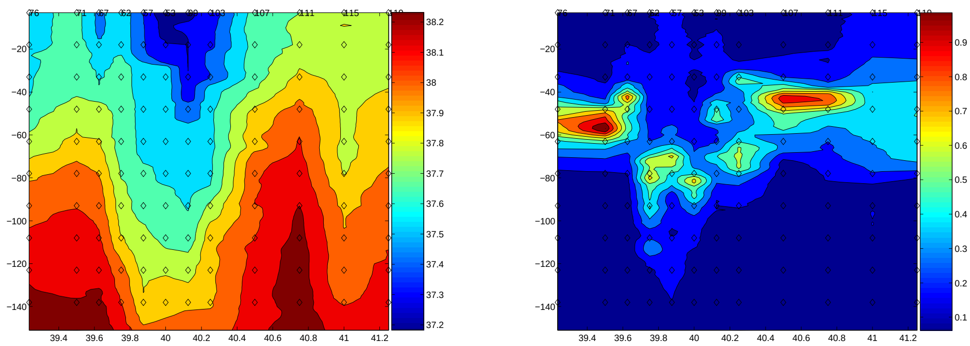

Figure 3.12: March 2001, salinity (left) and chlorophyll sections along transect T3. Salinity is expressed in *psu* and chlorophyll-a in mg/m^3

the southern part of the eddie, in correspondence of a dome of isolines. This is probably due to the proximity of A1 and A2, whose interaction enhances the rise of rich waters contributing to the formation of this high Chlf patch. In the northern area, above ∼40.5°N the surface layers, down to about 70m, are well mixed and the chlorophyll-a is distributed in a more uniform way, which does not show any DCM structure because of the stronger surface mixing (see right side in Fig. 3.12). The wider UML of this northern area is clearly visible also in Fig. 3.2.

3.3.3 May 2002: hydrology and Chlf distribution

During the cruise conducted in May 2002, at the surface (Fig. 3.13) the Chlf field shows lower values than in March 2001 during the MedGOOS-2 (Chlf<$0.18 mg/m^3$). The surface hydrological fields of Fig. 3.13 clearly show the signature (especially in salinity) of an antyciclonic eddy, as in Ribotti et al. (2004), localized at about $40.2°N$ and $7.5°E$. This northern eddy (A4) is located almost in the same position of A1, a little closer to the coast and partially interesting the continental shelf. Possible signatures of other anticyclones (low surface salinities, characteristic slope of isolines) are also detected in the southern part of the sampled domain, but it is hard to understand the size and the position of these anticyclones without considering satellite and vertical sections along the three meridional transects.

The Chlf and the salinity vertical sections along three meridional transects T1, T2 and T3 for the upper 150 m are shown in Figs. 3.14, 3.15 and 3.16, respectively.

In the vertical sections conducted along each meridional transect (T1, T2 and T3) the footprint of eddy A4 north of $\sim 40°N$ is clearly detectable (in salinity). The signature of other anticyclonic structures in the southern part of the sampling field is also clear, by considering the characteristic slope of isoalines. The satellite image of Fig. 3.17 (SeaWiFS image of May 15 2002) suggests that the salinity signal and the convergence of isoalines observed in the southern area are due to two distinct anticyclonic eddies, A5 and A6, that are sampled by the CTD casts only at their boundaries. T3 and T2 meridional transects intercept A5 on its western margin. A5 eddy could be defined an *open sea* eddy [as defined by Puillat et al. (2002)] considering its position and size. T1 transect, closer to the coast, intercepts only the very external northern border of A6, which, from satellite, appears a wide structure (more than $150km$ of diameter) still connected to the AC flow.

The chlorophyll distribution along the three sections is patchy and appears deeply modulated and influenced by the anticyclones. In T1 transect, which cuts across the eastern periphery of the eddy just above the continental shelf, the highest values of Chlf ($\sim 0.8mg/m^3$) are reached at the margins of the eddy, especially at its southern boundary, at $\sim 70m$ depth. The two high-Chlf patches shown in T1 (Fig. 3.14) are located where the isoalines have the strongest slope. The signal, in Chlf and salinity, of the boundary of A6 eddy

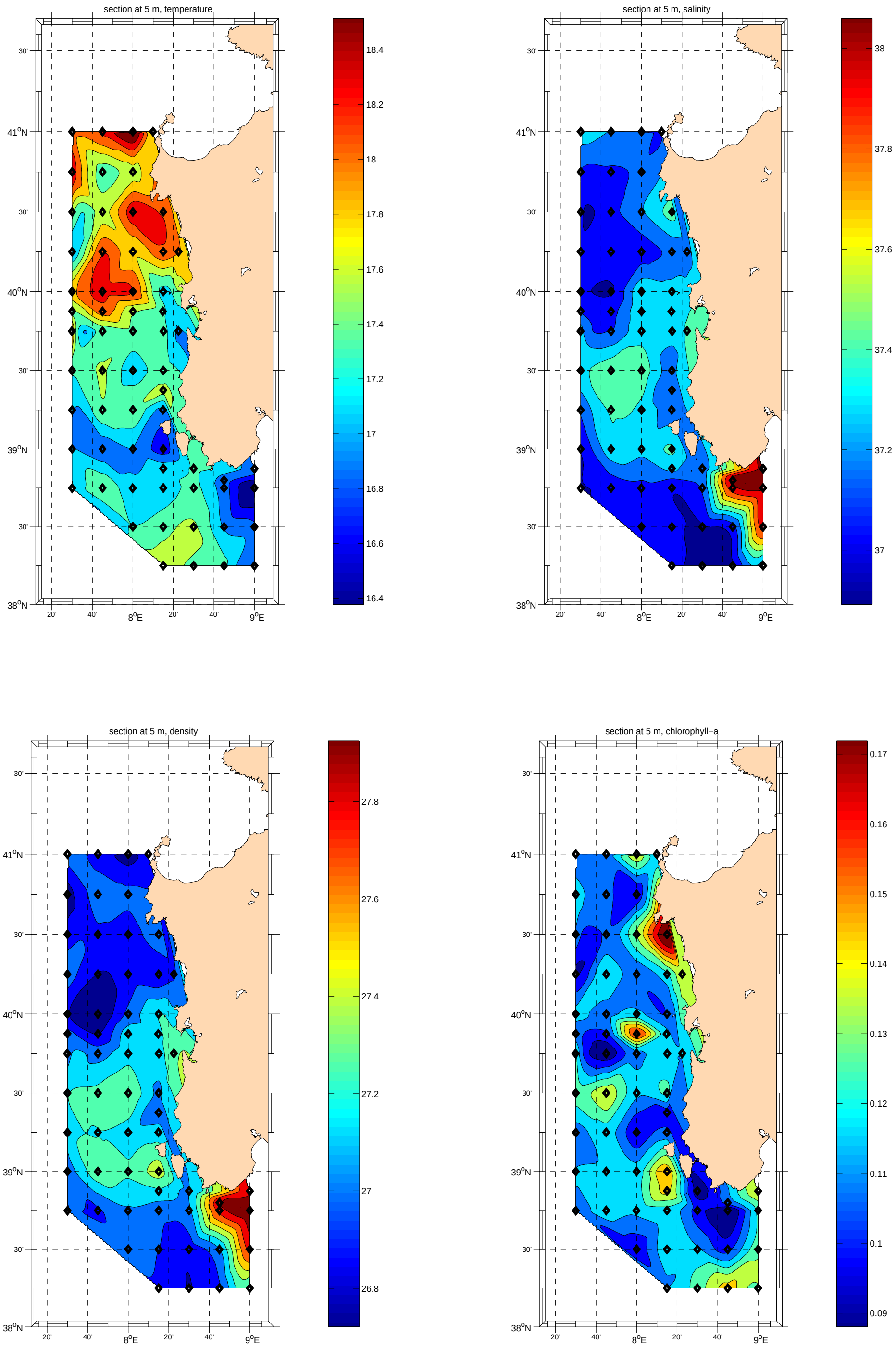

Figure 3.13: May 2002, clockwise from the left-top corner, 5m maps of: temperature, salinity, chlorophyll-a and density. The maps are obtained by cubic interpolation on equally spaced grid

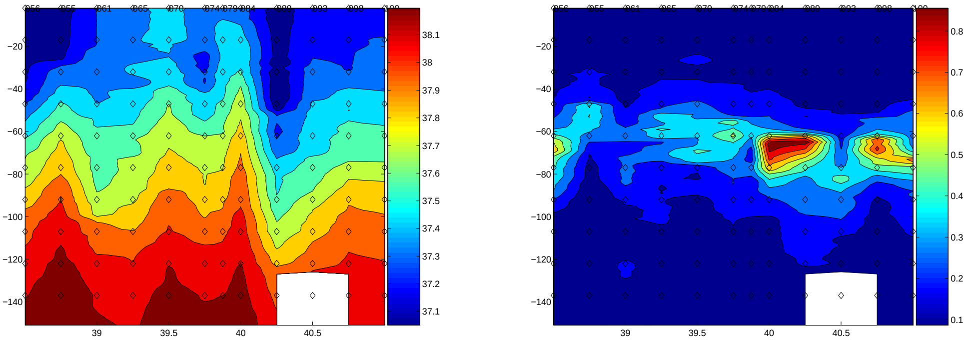

Figure 3.14: May 2002, salinity (left) and chlorophyll sections along transect T1. Salinity is expressed in *psu* and chlorophyll-a in mg/m^3

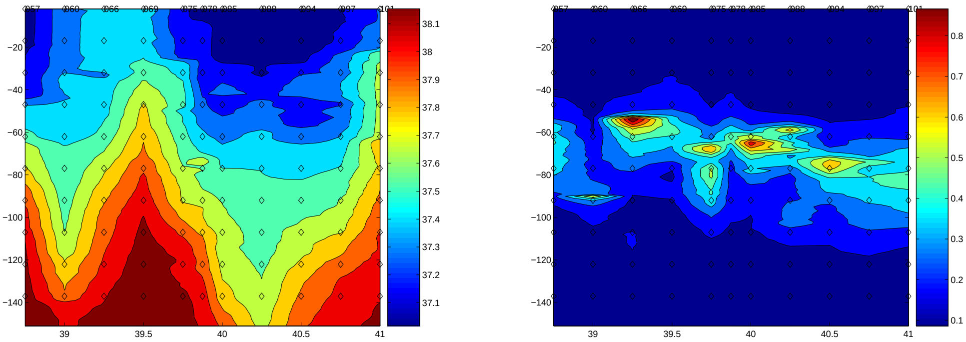

Figure 3.15: May 2002, salinity (left) and chlorophyll sections along transect T2. Salinity is expressed in *psu* and chlorophyll-a in mg/m^3

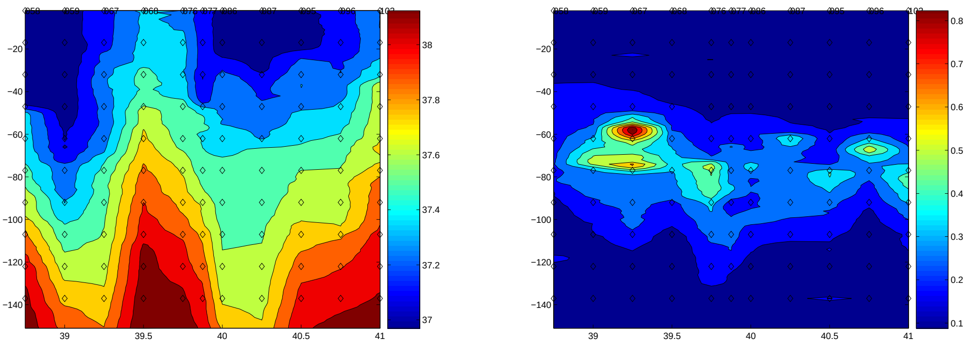

Figure 3.16: May 2002, salinity (left) and chlorophyll sections along transect T3. Salinity is expressed in *psu* and chlorophyll-a in mg/m^3

is also evident (left side of the plots), with the sinking of the DCM caused by deepening of UML and a correspondent moderate increase, in respect to the sourrounding points, of Chlf. The T2 transect (Fig. 3.15) passes through the center of A4 and touch the eastern margin of A5. The highest values ($\sim 0.8mg/m^3$) are found, as in T1, in areas where the slope of isolines is maximum, at DCM depth. T3 crosses the western margin of A4 and the peripheral eastern area of A5. Once again near to the zone with the largest slope of the isoalines of A5, the highest chlorophyll patch is found.

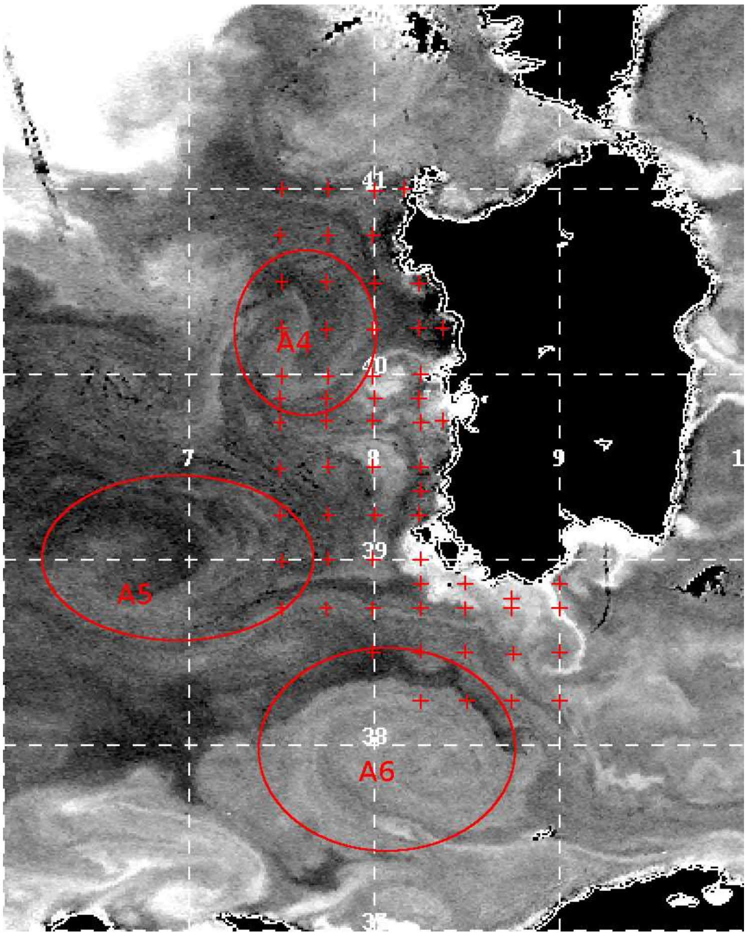

Figure 3.17: The anticyclonic eddies A4, A5 and A6 are indicated in the Ocean Color image (May 25 2002).

The Chlf map at 30m (Fig. 3.18) show generally low values of Chlf (less than $0.15mg/m^3$). The two patches with highest are not related to the action of mesoscale eddies, but are due to local coastal upwelling events occurring in the SW of the Sardinia.

The horizontal map at DCM level (Fig. 3.19), confirms the hypotesis that at this level the Chlf is distributed along the isolines which are convergent towards the center of the anticyclone. This is evident above all for A4.

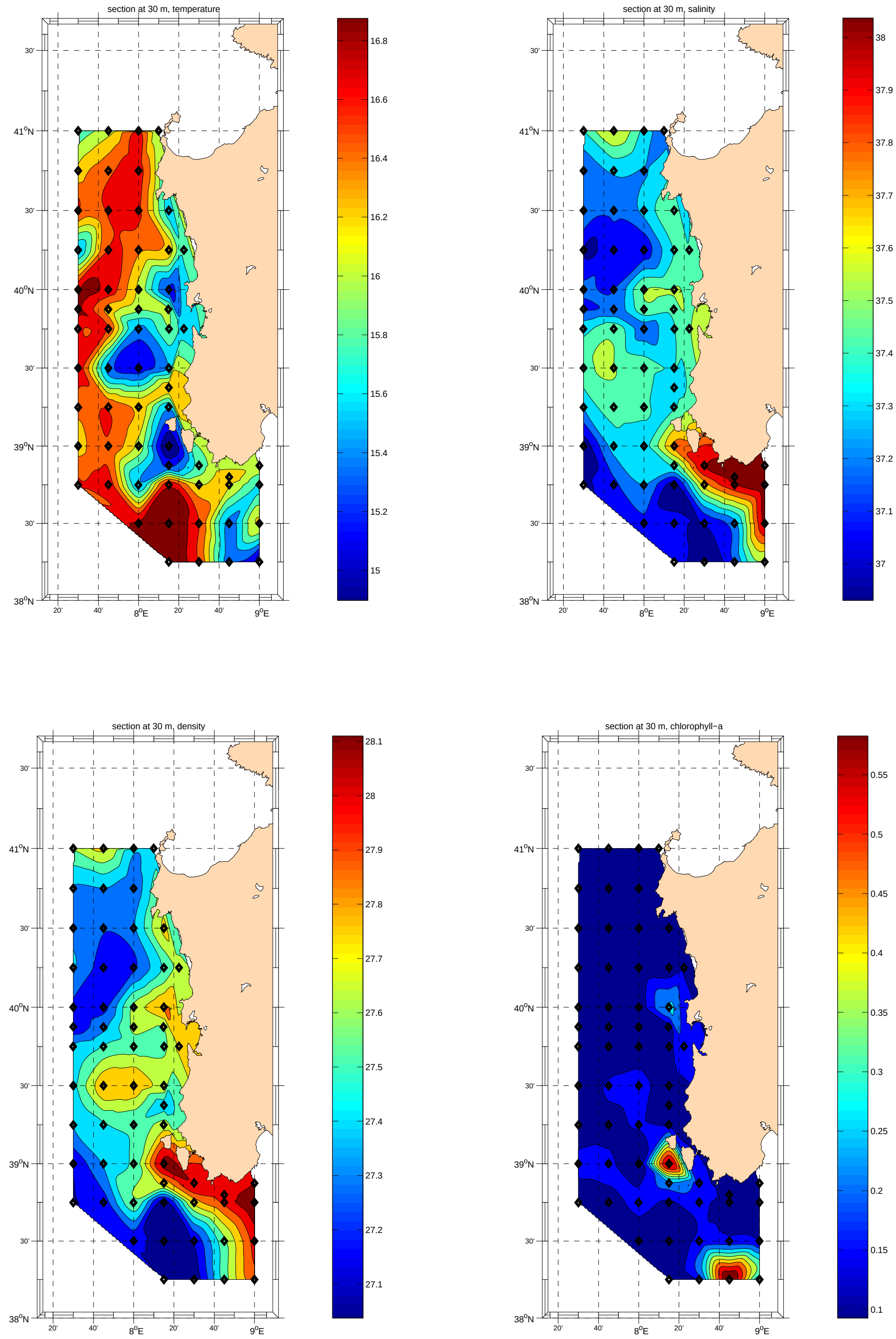

Figure 3.18: May 2002, clockwise from the left-top corner, 30m maps of: temperature, salinity, chlorophyll-a and density. The maps are obtained by cubic interpolation on equally spaced grid

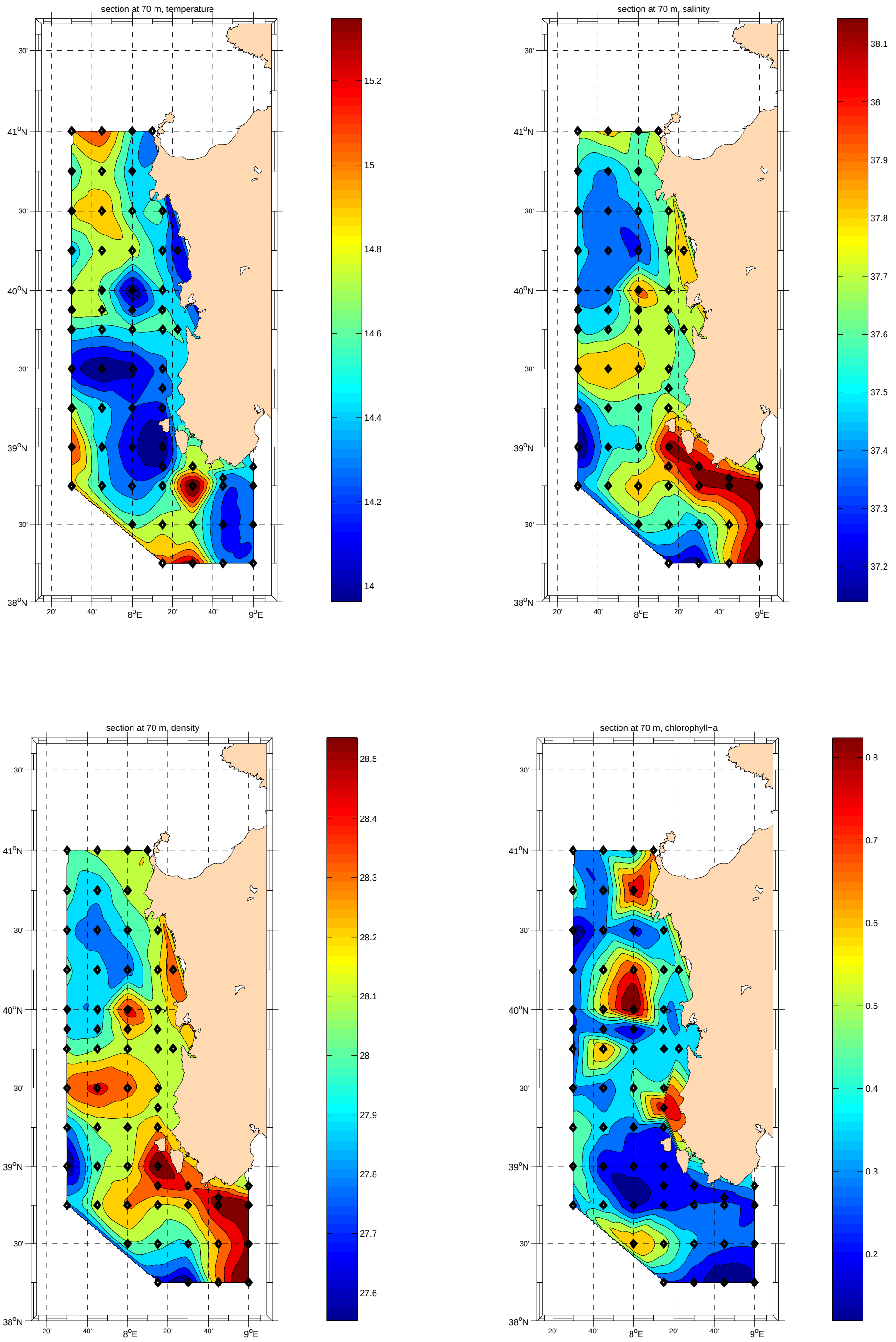

Figure 3.19: May 2002, clockwise from the left-top corner, 70m (DCM depth) maps of: temperature, salinity, chlorophyll-a and density. The maps are obtained by cubic interpolation on equally spaced grid

The map of integrated chlorophyll over the upper $150m$ (Fig. 3.20) well resumes the partial informations about Chlf patchiness and distribution deduced by horizontal maps and vertical sections we have seen. The highest values ($36mg/m^2$) of integrated Chlf are reached on the eastern boundary of A4, where the eddy iteract with the continental shelf.

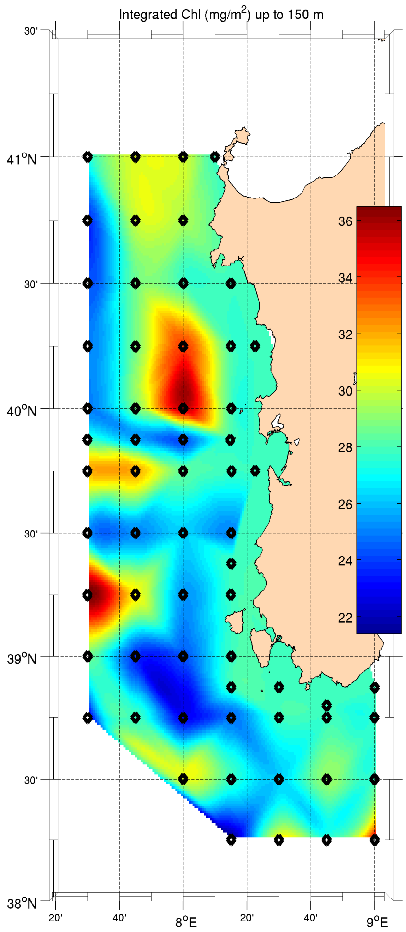

Figure 3.20: May 2002, integrated chlorophyll in the upper 150 m

3.4 Discussion

The measurements clearly show that the SaS dynamics are dominated by mesoscale eddies, as previously seen by other authors (Ribotti et al., 2004), which potentially infer on chlorophyll distribution. During MedGOOS-2 (March 2001), two mesoscale anticyclonic eddies have been detected in the survey area, A1 and A2, while a smaller one, which can be classified as sub-mesoscale eddie (A3) has been observed close to the Sardinian coast. The three eddies in 2001, cover the main part of the surveyed area south of 40.5°N. During MedGOOS-4, in may of 2002, two mesoscale eddies (A4 and A5) have been identified almost in the same position than the previous year, with the northern one partly interesting the continental shelf. An anticyclonic eddy, A6, still connected to the AC flow, was marginally intercepted by the samplings. The localization and identification of all these eddies has been possible thorugh the synergistic use of *in situ* and satellite data.

In March 2001, the salinity values at the surface seem to indicate that A2 is younger than A1, if we consider the same *Algerian* origin for both. However it was not possible to directly determine if A1 and A2 eddies are properly Algerian anticyclonic Eddies (AEs, *millot sensu*) or Frontal Eddies as described by Fuda et al. (2000). We tried to track A1 and A2 with weekly satellite altimetric maps of SLA, but they resulted out of the limits of the sensor capabilities because of their proximity to the coast and/or cause of their reduced life-time. However we speculate that A1, due to its position and size, might actually be a Frontal Eddy (FE). Concerning the MedGOOS-4 cruise, we observed that A4 shoud have the same origin of A1, considering that it has the same position (a little closer to the coast) and size. It is noteworthy that, as clearly visible by satellite imagery, both A1 and A4 seem part of a coupled cyclone/anticyclone system. In facts a cyclonic eddie is visible for both the A1 and A4 at their western side. On the contrary the Algerian origin of A6 is clear, because of its connection with the AC, as proved by the SeaWiFS image.

In all the cases (FEs or AEs) the core of these eddies is identified by fresher and less dense water. The salinity and density progressively increase from the centre to the periphery, as described in Ribotti et al. (2004). The margins of these eddies, especially in this period of the year, are not easily identified in temperature due to the low horizontal thermic gradients at the surface. For this reason the eddies show a stronger signature in Ocean Color satellite data, used to support the *in situ* measurements, than in SST satellite images. The chlorophyll proved (by means of the Chlf-salinity correlation) to be a good indicator for the identification of the eddies in the Sardinian Sea.

In March 2001, at first approximation, we distinguished two different areas, north and south of $\sim 40.5°$ N, where we identified a well defined frontal structure (in salinity and density) separating the waters of Atlantic origin from the local saltier waters of the northern zone, also characterized by a wider UML. This front can be considered the eastern elongation of the Balearic Front. The two zones are characterized by two different profiles of correlation between Chlf and Salinity (Fig. 3.3), and can be easily identified observing the MLD map (Fig. 3.2) and the surface hydrology maps (Fig. 3.4). In the southern zone anticorrelation at the surface is shown. In this area, which encloses the three antyciclonic eddies, the surface layer has higher algal biomass in corrispondence of the center of the eddies. The relatively higher Chlf may be due to the off-shore advection of phytoplaktonic biomass from coastal zone performed by the eddies, as observed in south-western area. On the contrary, in the northern zone Chlf and salinity are positively correlated from surface down to $60 - 70m$. Here we can note the absence of a DCM, due to the presence of a deeper UML. The correlation tell us that areas with higher salinity have higher chlorophyll, probably due to the effect of upwelled waters determined by cyclonic circulation. An interesting intense patch of Chlf has been detected, at about $30 - 50m$ depth, in correspondence of the area of interaction of A1 and A2, producing a well defined *dome* of the isopycnae, with a consequent rise of nutrient-rich waters up to the photic layers. This iteraction of the two eddies created the most intense patch of Chlf. Big differences between A1 and A2 have been evidenced in terms of integrated Chl. The southern A2 resulted richer than A1 in integrated Chlf. This can be due to the entrapement of algal biomass from the south-west Sardinia, were a coastal upwelling has been detected.

During the 2002 cruise, the DCM along the three meridional transects is deeper ($\sim 60-70m$ vs $\sim 40-50m$) than in March 2001. This is because of the increased stratification of this period of the year, which in turn determines a complete depletion of nutrients (injected at the surface during winter mixing) in the surface layers. The integrated chlorophyll map shows the highest values in correspondence of the eastern margin of A4, where the eddy interact with the continental shelf. In this area, as seen by the plots of the T1 transect, the strong slope of the isopycnae contributes to the rise of rich-waters from the depth of $\sim 120m$ to teh photic layer, determining the formation of these high-chlorophyll patches.

So, results suggest that the algal biomass distribution in the Sardinian Sea is strictly related to mesoscale eddies as presumed. The eddies seem to enhance the concentration processes and in some cases the production of phytoplakton by means of different mechanisms. The interaction of the eddies with continental shelf (as for A4) may determine the direct caption of nutrients rich-waters from deep layer and their rising to euphotic layer. Furthermore, when the eddies get close to the coast (as for A2), they may capture the algal biomass locally produced by coastal upwelling, transporting it off-shore by advection. Finally we observed that the interaction between two anticyclonic eddies (A1 and A2), sufficiently close each other, may cause pronounced domes of isopycnae and strong divergence at the surface, which force the rise of biomass rich waters from DCM to upper layers.

Therefore it is proved that the mesoscale anticyclonic eddies are one of the main drivers of the Chlf distribution, depending on their position (off-shore or in-shore), size and inter-relationships (i.e. relative position of the eddies).

Mesoscale resolving modeling studies, making use of coupled physical and ecological models, are needed to assess these hypotesis and to better understand the processes determining the observed algal distribution.

Chapter 4

Conclusions

The manuscript was devoted to the study of the spatial and temporal variability of the algal biomass and of the primary production in the central part of the western Mediterranean, namely the Algero-Provençal Basin (APB), and to the study of their relationships with physical and hydrodynamical processes at different temporal and spatial scales. We know that physical processes and hydrodynamical features infer in the primary production and in the phytoplankton distribution through different mechanisms, also depending from the spatial and temporal scales (e.g. Martin, 2003; McGillicuddy et al., 2007). We approached this multiscale problem by using remotely sensed and *in situ* datasets, having different spatial and temporal resolution and covering multiple temporal and spatial scales. In particular, by means of the satellite data we studied the seasonal and interannual variability of physical (temperature and sea level) and biological (algal biomass and production) variables on the whole domain, while the *in situ* data allowed us to investigate the mesoscale processes influencing the algal distribution in the central-eastern area, the Sardinian Sea, which represents one of the less known regions of the domain and which shows, in the light of the results of the satellite time series analysis, the strongest relations between hydrodinamical and chlorophyll variability. The integration of the informations coming from the mesoscale/short-term study (Chapter 3) and the basin-scale/long-term study (Chapter 1 and 2) was helpful to better interpret the partial results of each chapter, and to give as much as possible a complete picture of the bio-physical relationships of the area.

4.1 Objectives achieved

The seasonal and interannual variability of the chlorophyll fields has been studied through the statistical analysis of Seawifs monthly Level-3 dataset, covering the decade 1997-2007. The study of the variability of physical fields, namely Sea Level Anomalies (SLA) and Sea Surface Temperature (SST), has been accomplished analyzing the AVISO/CLS SLA and the Pathfinder AVHRR SST datasets. The main sesonal and interannual patterns have been identified through EOF decomposition and wavelet analysis, while covariability was studied trough SVD and the analysis of the correlation coefficient maps.

In this framework, we found that:

- Mainly related to the the seasonal spring bloom of the MEDOC area, the first EOF accounts for ∼44% of the total variance. A second seasonal cycle, discretized by the second mode, is timewise and spacewise shifted in respect to the first one. This is related to a weak winter-time increase on algal biomass, mainly localized in the area of the Algerian Current (∼17% of variance).

- Interannual events on Chl dataset have been also identified. Two relative maxima have been grouped by EOF-3 mode (only 4% of total variance), localized in 1999 and 2005. They are due to anomalously strong spring-blooms in the MEDOC area, which in turn are probably caused by stronger than normal winds. These winds, as reported in literature, contributed to strenghten the bloom and to expand it southward and westward, by the displacement of the BF.

- Constrained by the phase coincidence of the anomalous event with the seasonalilty of the Chl variability, the EOFs tecnique did not reach to separate the signal of the summer 2003 heatwave in the Chl dataset. The 2003 footprint has been detected thorugh the wavelet analysis, with a significant minimum in Chl recorded for that period. This is the first time that the footprint of a summer heatwave has been recognised on the algal biomass in Mediterranean. In this case the wavelet analysis demonstred its ability in detecting anomalous events, where the EOF failed.

- Has been proved that the heatwave also affected the SLA. A clear signature of the summer 2003 was recognized in the SLA dataset, detected either by wavelet and EOF analyses. The same event is also recognized in the SST fields, with a warming of 3-4 C°(basin average) in respect to the decadal monthly climatology. The seasonal variability of SLA is splitted in two modes, the former due to the seasonality of the atmospheric pressure, the second one related to the Algerian Current flow which shows its maximum in winter, while the seasonal cycle of SST (EOF-1) accounts for ∼98% of the total variance.

- Eddies action is probably the main driver of the observed SLA–Chl co-variability in the central part of the domain, just between the Balearic Front and the AC area-of-inferece. Significant and high anti-correlation has been found between the two variables in this area. This suggests that the Chl is highly influenced by the vertical displacement of the isopycnae (with consequent injection/reduction of nutrients into the photic layer).

- Lower bio-physical correlation is found in northern and southern areas, probably because of the importance of horizontal advection of biomass, which can partially hide the response of the phytoplankton community to the action of the mesoscale eddies on the nutricline depth.

- Evinced by different patterns of variability and co-variability, a simple zonation of the domain has been done. Three main zones have been identified. The northern one, enclosing the so called MEDOC area, is characterized by a strong seasonality and by the highest algal biomass. The central zone shows the lowest trophic level and, at the same time, the highest correlation between mesoscale dynamics (deduced by SST and SLA patterns of variability) and algal biomass. The southern zone is characterized by the footprint, in Chl fields, of the AC and AEs path and by their seasonality.

Once the main spatial and temporal patterns of variability of the algal biomass have been indentified, the successive step was the assessment of the Primary Production (PP) budget and variability. In particular our interest focused on the seasonal and interannual variability of PP and on the estimation of the summer heatwave footprint, already detected both in physical and biomass fields. The PP integrated over the euphotic layer (PP_{eu}) has been estimated over the decade, by using a satellite based model. The model makes use of satellite Photosyntetically Available Radiation (PAR), SST and surface chlorophyll, the daylenght and a photosynthetic efficiency parameter (per chlorophyll unit). Once again, the results have been statistically analysed through EOFs and wavelets.

Our conclusions are that:

- The annual basin averaged PP_{eu}, for the years 1998-2006, is estimated to be $\sim 142 gCm^{-2}year^{-1}$, with a pronounced interannual variability and no evident trends. The results obtained are in good agreement with findings of other studies making uses of different models or *in situ* data.

- The first mode of variability encloses more than 68% of total variance (sesonal cycle). The highest varaibility was found in the Gulf of Lyons and in the whole MEDOC area, where the highest values of annual PP have been detected too.

- We recognised in the model results (by means of the time series analysis) the footprint of the 2003 European heatwave, which determined a marked decrease of PP in summer 2003. Although the summer istantaneous PP is low, we observed that this event determined a marked minimum in monthly and also annual budgets, mainly because the daylenght and PAR are quite large in summer. Addictionally, the anomalously high temperatures and low chlorophyll (indentified in Chapter 1) determined a decreased efficiency of the PP per unit of chlorophyll, modellized by the P^B_{opt} parameter.

The conclusions drawn in Chapter 1 emphasized the effects of an anomalous extreme event, the summer 2003 heatwave (Black et al., 2004), on the physical and biological fields, which footprint in terms of production has been studied in Chapter 2. On the other hand the analyses conduced in Chapter 1 clearly evidenced the different relationtships, depending on the area, between physics and biology, and the strongest correlation between chlorophyll and SLA variability localized in the central zone. We guessed that this higher correlation was due to the effect of mesoscale features, particularly eddies, largely present in the area. A set of hydrologic and fluorometric data, collected during two oceanographic cruises conducted in 2001 and 2002 in the Sardinian Sea (the Eastern part of the APB), has been analysed to better understand the relationships we hypothesized between mesoscale eddies and chlorophyll distribution.

The analysis of the oceanographic data proved that:

- Mesoscale eddies have a predominant role in modulating and redistributing the algal biomass, especially south of the Balearic Front, confirming the assumptions we done in previous chapters about the strong influence of mesoscale hydrodynamics in the algal biomass distribution.
- The interaction of the eddies with continental shelf (as for A4) may determine the direct caption of nutrient-rich waters from deeper layers and their rising up to the euphotic layer.
- The closeness of two antyciclonic eddies determines strong domes of isopycne in the interaction area, and the production of a surface divergence that enhances the advection to the surface of rich waters from the underlying DCM.
- The eddies approaching the coast (as for anticyclone A2) may capture algal biomass locally produced by coastal upwellings, and entrape this biomass rich waters transporting it off-shore.
- A point of concern is that satellite based PP models, like the VGPM, might uderestimate the PP integrated over the euphotic layer when the column is higly stratified. In this case the Deep Clorophyll Maximum (DCM) has a major role in the total integrated biomass, and the satellite might be unable to correctly estimate the actual biomass and therefore the primary production. This point should be verified by analyzing the primary production along the water column by means of direct measurements.

4.2 Perspectives

The synergistic use of satellite and *in situ* data allowed us to investigate some of the relationships existing between hydrodynamics and algal biomass distribution and production in the area. The main patterns of variability and covariability, as well as the effects of mesoscale eddies on biological fields have been successfully observed through our diagnostic/statistical approach. Some uncertainity on the reliability of the use of satellite based PP still persists, above all considering the strong stratification of the water column observed in certain zones/periods and the relevance of DCM's in the integrated chlorophyll values, which cannot be observed from satellite. For this reason direct measures of PP along the water column should be accomplished, integrated and compared with the satellite based model outputs, to verify if the supposed underestimation of PP during the stratified period is an actual issue.

On the other hand, by usign such an approach, in many cases we could just hypotesize or speculate about the hydrodynamical and ecological processes underlying the observed patterns of chlorophyll and PP. We tried to give a *rationale* for each relation and correlation (both in statistical and common sense) observed, but inferring causality from correlation is often hard and not always a successful exercise.

For this reason the natural development of the present research will be the progressive shift towards a deterministic/prognostic approach to the probelm. The hydrodynamic modeling tools became by now quite reliable, while the ecological modeling based on the deterministic modelization of the biogeochemical cycles in the sea is still in embrional phase, cause this branch of the marine sciences is only few years old. The computer power is still increasing esponentially, permitting to improve in the next future the spatial and temporal resolution and to increase the number of state-variables modelized. The ecological numerical tools still need a lot of research, study and increase of basic knowledges.

We developed during the last 10 years a long experience in modeling the hydrodynamics in the central and western Mediterranean at regional and mesoscales. First steps in the development of the knowledges of the biogeochemical models have been also accomplished by our group. The effort in this direction will also imply the prosecution of the analysis of satellite and *in situ* measurements, which are fundamental to calibrate and validate the models and, eventually, to improve model results through *Data Assimilation* tecniques.

Bibliography

Antoine, D., Andrè, J., Morel, A., 1996. Oceanic primary production : Ii. estimation at global scale from satellite (coastal zone color scanner) chlorophyll. Global Biogeochemical Cycles 10, 57–69.

Astraldi, M., Conversano, F., Civitarese, G., Gasparini, G. P., Ribera d'Alcalà, M., Vetrano, A., 2002. Water mass properties and chemical signatures in the central mediterranean region. Journal of Marine Systems 33-34, 155–177.

Baldacci, A., Corsini, G., Grasso, R., G., M., Allen, J. T., Cipollini, P., Guymer, T. H., Snaith, H. M., 2001. A study of the alboran sea mesoscale system by means of empirical orthogonal function decomposition of satellite data. Journal of Marine Systems 29, 293–311.

Bartolacci, D. M., Luther, M. E., 1999. Patterns of co-variability between physical and biological parameters in the arabian sea. Deep-Sea Research II 46, 1933–1964.

Behrenfeld, M. J., Falkowski, P. G., November 1997a. A consumers's guide to phyoplankton primary productivity models. Limnology and Oceanography 42 (7), 1479–1491.

Behrenfeld, M. J., Falkowski, P. G., 1997b. Photosynthetic rates derived from satellite-based chlorophyll concentration. Limnology and Oceanography 42 (1), 1–20.

Bjornsson, H., Venegas, S., A., 1997. A Manual for EOF and SVD Analyses of Climatic Data. Department of Atmospheric and Oceanic Sciences.

Black, E., Blackburn, M., Harrison, G., Hoskins, B., Methven, J., 2004. Factors contributing to the summer 2003 european heatwave. Weather 59(8), 217–222.

Bosc, E., 2002. Variations saisonnières et interannuelles de la biomasse phytoplanctonique et de la production primaire en mèditerranèe : Evaluation et utilisation des donnèes satellitales de couleur de le ocèan (seawifs, polder et octs). Ph.D. thesis, Universitè Pierre et Marie Curie.

Bosc, E., Bricaud, A., Antoine, D., 2004. Seasonal and interannual variability in algal biomass and primary production in the mediterranean sea, as derived from 4 years of seawifs observations. Global Biogeochemical Cycles 18.

Bouzinac, C., Font, J., Johnny, J., 2003. Annual cycles of sea level and sea surface temperature in the western mediterranean sea. Journal of Geophysical Research 108.

Bretherton, C. S., Smith, C., Wallace, J. M., 1992. An intercomparison of methods for finding coupled patterns in climate data. J. Clim. 5, 541–560.

Bricaud, A., Bosc, E., Antoine, D., 2002. Algal biomass and sea surface temperature in the mediterranean basin - intercomparison of data from various satellite sensors, and implications for primary production estimates. Remote Sensing of Environment 81, 163–178.

Clarke, G. L., Ewing, G. C., Lorenzen, C. J., Feb. 1970. Spectra of Backscattered Light from the Sea Obtained from Aircraft as a Measure of Chlorophyll Concentration. Science 167, 1119–1121.

Eppley, R. W., Stewart, E., Abbot, R. M., Heyman, V., 1985. Estimating ocean primary production from satellite chlorophyll, introduction to regional differences and statistics for the southern california bight. Journal of Plakton Research 7, 57–70.

Estrada, M., 1996. Primary production in the northwestern mediterranean. Scientia Marina 60 (Suppl.2), 55–64.

Falkowsky, P. G., 1981. Light-shade adaptation and assimilation numbers. Journal of Plankton Research 3, 203–216.

Fuda, J., Millot, C., Taupier-Letage, I., Send, U., Bocognano, J., 2000. Xbt monitoring of a meridian section across the western mediterranean sea. Deep-Sea Research I 47(11), 2191–2218.

Fulton, E. A., Smith, A. D., Johnson, C. R., 2004. Biogeochemical marine ecosystem models i: Igbem-a model of marine bay ecosystems. Ecological Modelling 174 (3), 267–307.

Garcon, V. C., Oschlies, A., Doney, S. C., McGillicuddy, D., Waniek, J., 2001. The role of mesoscale variability on plankton dynamics in the north atlantic. Deep-Sea Research II 48, 2199–2226.

Gian-Reto, W., Post, E., Convey, P., Mnzel, A., Parmesan, C., Beebee, T., Fromentin, J., Hoegh-Guldberg, O., Bairlein, F., 2002. Ecological responses to recent climate change. Nature 416, 389–395.

Gomez, F., Souissi, S., 2008. The impact of the 2003 summer heat wave and the 2005 late cold wave on the phytoplakton in the north-eastern english channel. C.R. Biologies 331, 678–685.

Holm-Hansen, O., Lorenzen, C., Holmes, R., Strickland, J., 1965. Fluorometric determination of chlorophyll. J. Cons. Perm. Int. Explor. Mar. Sci. Commun. 30, 3–15.

Isern-Fontanet, J., Font, J., Garcia-Ladona, E., Emelianov, M., Millot, C., Taupier-Letage, I., Dec. 2004. Spatial structure of anticyclonic eddies in the algerian basin (mediterranean sea) analyzed using the okubo-weiss parameter. Deep Sea Research Part II: Topical Studies in Oceanography 51, 3009–3028.

Jacques, G., Minas, H., Minas, M., Nival, P., 1973. Influence des conditions hivernales sur les productions phyto et zooplanctoniques en mèditerraneè nord-occidentale. ii: Biomasse et production phytoplanctonique. Marine Biology 23, 251–265.

Kahru, M., Fiedler, P., Gille, S., Manzano, M., B.G., M., 2007. Sea level anomalies control phytoplankton biomass in the costa rica dome area. Geophys. Res. Lett. 34.

Kameda, T., Ishizaka, J., 2005. Size-fractionated primary production estimated by a two-phytoplankton community model appllicable to ocean color remote sensing. Journal of Oceanography 61, 663–672.

LaViolette, P. E., Tintoré, J., Font, J., Feb. 1990. The surface circulation of the Balearic Sea. Journal of Geaphysical Research 95, 1559–1568.

Lazzara, L., Bianchi, F., Falcucci, M., Hull, V., Modigh, M., Ribera D' Alcalà, M., 1990. Metodi nell'ecologia del plancton marino. Nova Thalassia, Ch. Pigmenti clorofilliani., pp. 207–235.

Legaard, K. R., Thomas, A. C., Jun. 2006. Spatial patterns in seasonal and interannual variability of chlorophyll and sea surface temperature in the California Current. Journal of Geophysical Research (Oceans) 111 (10), 6032–+.

Levy, M., Memery, L., Madec, G., 1998. The onset of a bloom after deep winter convection in the northwestern mediterranean sea: mesoscale process study with a primitive equation model. Journal of Marine Systems 16, 7–21.

Levy, M., Memery, L., Madec, G., 1999. The onset of the spring bloom in the medoc area: mesoscale spatial variability. Deep-Sea Research I 46, 1137–1160.

Levy, M., Memery, L., Madec, G., 2000. Combined effects of mesoscale processes and atmospheric high-frequency variability on the spring bloom in the medoc area. Deep-Sea Research I 47, 27–53.

Lohrenz, S. E., Wiesenburg, D. A., DePalma, I. P., Johnson, K. S., Gustafson, Daniel E., J., 1988. Interrelationships among primary production, chlorophyll, and environmental conditions in frontal regions of the western mediterranean sea. Deep-Sea Research, 35(5A), 793–810.

Lopez-Calderon, J., Manzo-Monroy, H., Santamaria-del Angel, E., Castro, R., Gonzales-Silvera, A., Millan-Nunez, R., 2006. Variabilidad de mesoescala del pacifico tropical mexicano mediante datos de los sensores topex y seawifs. Ciencias Marinas 32, 539–549.

López Garciá, M. J., Millot, C., Font, J., García-Ladona, E., 1994. Surface circulation variability in the Balearic Basin. Journal of Geophysical Research 99, 3285–3296.

Lorenz, E., 1956. Empirical orthogonal functions and statistical weather prediction. Tech. rep., Department of Meteorology, Massachusetts Institute of Technology, Cambridge, MA.

Martin, A., 2003. Phytoplankton patchiness: the role of lateral stirring and mixing. Progress in Oceanography 57, 125–174.

Martin, A., Richards, K., 2001. Mechanisms for vertical nutrient transport within a north atlantic mesoscale eddy. Deep-Sea Research II 48, 757–773.

Marullo, S., Guarracino, M., 2003. La anomalia termica del 2003 nel mar mediterraneo osservata da satellite. Energia, Ambiente e Innovazione 6/03, 48–53.

McGillicuddy, D., Anderson, L., Bates, N., Bibby, T., Buesseler, K., Carlson, C., Davis, C., Ewart, C., Falkowski, P., Goldthwait, S., Hansell, D., Jenkins, W., Johnson, R., Kosnyrev, V., Ledwell, J., Li, Q., Siegel, D., D.K., S., 2007. Eddy/wind interactions stimulate extraordinary mid-ocean plankton blooms. Science 316, 1021–1026.

McGillicuddy, D., Robinson, A., Siegel, D., Jannasch, H., Johnson, R., Dickey, T., McNeil, J., Michaels, A., Knap, A., 1998. Influence of mesoscale eddies on new production in the sargasso sea. Nature 394, 263–266.

McGillicuddy, D. J., Robinson, A. R., 1997. Eddy-induced nutrient supply and new production in the sargasso sea. Deep-Sea Research I 44, 1427–1450.

MEDOC group, 1969. Observation of formation of deep water in the mediterranean sea. Nature 227, 1037–1040.

Millot, C., 1985. Some features of the Algerian current. Journal of Geophysical Research 90, 7169–7176.

Millot, C., Gacic, M., Astraldi, M., La Violette, P. E., 1999. Circulation in the western mediterranean sea. Journal of marine systems 20(1-4), 423–442.

Mizobata, K., Saitoh, S.-I., 2004. Variability of bering sea eddies and primary productivity along the shelf edge during 1998-2000 using satellite multisensor remote sensing. Journal of Marine Systems 50, 101–111.

Moran, X. A. G., Taupier-Letage, I., Vazquez-Dominguez, E., Ruiz, S., Arin, L., Raimbault, P., Estrada, M., 2001. Physical-biological coupling in the algerian basin (sw mediterranean) : Influence of mesoscale instabilities on the biomass and production of phytoplankton and bacterioplankton. Deep-sea research I 48, 405–437.

Morel, A., Aug. 1978. Available, usable, and stored radiant energy in relation to marine photosynthesis. Deep Sea Research Part II: Topical Studies in Oceanography 25, 673–688.

Morel, A., Andrè, J. M., 1991. Pigment distribution and primary production in the western mediterranean as derived and modeled from coastal zone color scanner observations. Journal of Geophysical research 96, 685–698.

Nieves, V., Llebot, C., Turiel, A., Solé, J., García-Ladona, E., Estrada, M., Blasco, D., Dec. 2007. Common turbulent signature in sea surface temperature and chlorophyll maps. Geophysical Research Letters 34, 23602–+.

Olita, A., Sorgente, R., Natale, S., Gaberšek, S., Ribotti, A., Bonanno, A., Patti, B., 2007. Effects of the 2003 european heatwave on the central mediterranean sea: surface fluxes and the dynamical response. Ocean Sci. 3, 273–289.

O'Reilly, J. E., Maritorena, S., Mitchell, B. G., Siegel, D. A., Carder, K. L., Garver, S. A., Kahru, M., McClain, C., Oct. 1998. Ocean color chlorophyll algorithms for SeaWiFS. Journal of Geophysical Research 103, 24937–24954.

Peng, S., Fyfe, J., 1996. The coupled patterns between sea level pressure and sea surface temperature in the mid-latitude north atlantic. J. Clim. 9, 1824–1839.

Pinardi, N., Masetti, E., 2000. Variability of the large scale general circulation of the mediterranean sea from observations and modelling: a review. Palaeogeography, Palaeoclimatology, Palaeoecology 158, 153–173.

Platt, T., Feb. 1986. Primary production of the ocean water column as a function of surface light intensity: algorithms for remote sensing. Deep Sea Research Part I: Oceanographic Research 33, 149–163.

Platt, T., Sathyendranath, S., Sep. 1988. Oceanic Primary Production: Estimation by Remote Sensing at Local and Regional Scales. Science 241, 1613–1620.

Preisendorfer, R., 1988. Principal Component Analysis in Meteorology and Oceanography. Elsevier, Amsterdam.

Puillat, I., Taupier-Letage, I., Millot, C., 2002. Algerian eddies lifetime can near 3 years. J. of Marine Systems 31, 245–259.

Raimbault, P., Coste, B., Boulhadid, M., Benyahia, B., 1993. Origin of high phytoplankton concentration in deep chlorophyll maximum (dcm) in a frontal region of southwestern mediterranean sea (algerian current). Deep-Sea Research I 49, 791–804.

Ribotti, A., Puillat, I., Sorgente, R., Natale, S., 2004. Mesoscale circulation in the surface layer off the southern and western sardinia island in 2000-2002. Chemistry and Ecology 20(5), 345–363.

Rivas, A. L., Dec. 2006. Quantitative estimation of the influence of surface thermal fronts over chlorophyll concentration at the Patagonian shelf. Journal of Marine Systems 63, 183–190.

Schär, C., Vidale, P. L., Lüthi, D., Frei, C., Häberli, C., Liniger, M. A., Appenzeller, C., 2004. The role of increasing temperature variability in european summer heatwaves. Nature 427, 332–336.

Smith, R., Ainley, D., Baker, K., Domack, E., Emslie, S., Fraser, B., Kennett, J., Leventer, L., Mosley-Thompson, E., Stammerjohn, S., Vernet, M., 1999. Marine ecosystem sensitivity to climate change. Bioscience 49, 393–404.

Somot, S., Sevault, F., Déqué, M., Dec. 2006. Transient climate change scenario simulation of the mediterranean sea for the twenty-first century using a high-resolution ocean circulation model. Climate Dynamics 27, 851–879.

Sorgente, R., Drago, A. F., Ribotti, A., 2003. Seasonal variability in the central mediterranean sea circulation. Annales Geophysicae 21, 299–322.

Sprintall, J., Tomczak, M., Apr. 1993. On the formation of central water and thermocline ventilation in the southern hemisphere. Deep Sea Research Part I: Oceanographic Research 40, 827–848.

Steeman-Nielsen, E., 1952. The use of radioactive carbon (14c) for measuring organic production in the sea. Journal du Conseil 18, 117–140.

Taupier-Letage, I., Puillat, I., Millot, C., Raimbault, P., 2003. Biological response to mesoscale eddies in the algerian basin. Journal of Geophysical Research 108.

Torrence, C., Compo, G. P., 1998. A practical guide to wavelet analysis. Bull. Am. Meteor. Soc. 79, 61–78.

Turley, C. M., 1999. The changing mediterranean sea - a sensitive ecosystem? Progress in Oceanography 44, 387–400.

Venegas, R. M., Strub, P. T., Beier, E., Letelier, R., Thomas, A. C., Cowles, T., James, C., Soto-Mardones, L., Cabrera, C., Mar. 2008. Satellite-derived variability in chlorophyll, wind stress, sea surface height, and temperature in the northern California Current System. Journal of Geophysical Research (Oceans) 113 (12), 3015–+.

Vichi, M., Masina, S., Navarra, A., Jan. 2007a. A generalized model of pelagic biogeochemistry for the global ocean ecosystem. Part II: Numerical simulations. Journal of Marine Systems 64, 110–134.

Vichi, M., Pinardi, N., Masina, S., Jan. 2007b. A generalized model of pelagic biogeochemistry for the global ocean ecosystem. Part I: Theory. Journal of Marine Systems 64, 89–109.

Vignudelli, S., 1997. Potential use of ers-1 and topex/poseidon altimeters for resolving oceanographic patterns in the algerian basin. Geophys. Res. Lett. 24(14), 1787–1790.

Volpe, G., Santoleri, R., Vellucci, V., M., R. D., Marullo, S., D'Ortenzio, F., 2007. The colour of the mediterranean sea: Global versus regional bio-optical algorithms evaluation and implication for satellite chlorophyll estimates. Remote Sensing of Environment 107, 625–638.

Wilson, C., Adamec, D., 2001. Correlations between surface chlorophyll and sea surface height in the tropical pacific during 1997-1999 el nino-southern oscillation event. Journal of Geophysical Research 31, 175–188.

Wilson, C., Adamec, D., Apr. 2002. A global view of bio-physical coupling from seawifs and topex satellite data, 1997-2001. Geophysical Research Letters 29, 98–1.

Yentsch, C. S., Phinney, D. A., 1985. Rotary motions and convection as a means of regulating primary production in warm core rings. Journal of Geophysical Research 90, 3237–3248.

Zavatarelli, M., Pinardi, N., 2003. The adriatic sea modelling system: a nested approach. Annales Geophysicae 21, 345–364.

Acronyms and abbreviations

AB	Algerian Basin
AC	Algerian Current
AE	Anticyclonic Algerian Eddy
APB	Algero-Provençal Basin
AVHRR	Advanced Very High Resolution Radiometer
AW	Atlantic Water
BF	Balearic Front
Chl	Chlorophyll-a concentration
Chlf	Fluorometrically derived Chlorophyll-a concentration
Chl-int	Chlorophyll-a concentration depth integrated
CDOM	Colored Dissolved Organic Matter
CWT	Continous Wavelet Transform
DA	Data Assimilation
DCM	Deep Clorophyll Maximum
DUACS	Data Unification and Altimeter Combination System
EOF	Empirical Orthogonal Function
FE	Frontal Eddy
FT	Fourier Transform
LPB	Liguro-Provençal Basin
LPC	Liguro-Provençal Current
MAW	Modified Atlantic Water
MLD	Mixed Layer Depth
NOAA	National Oceanic and Atmospheric Administration
NODC	National Oceanographic Data Center
PAR	Photosyntetically Available Radiation

PC	Principal Components
PCA	Principal Components Analysis
PP	Primary Production
PP_{eu}	Integrated Primary Production over the euphotic layer
rChl	Chlorophyll-a concentration computed with regional alghoritm
SaC	Sardinian Channel
SaS	Sardinian Sea
SCF	Squared Covariance Fraction
SLA	Sea Level Anomalies
SST	Sea Surface Temperature
SVD	Singular Value Decomposition
UML	Upper Mixed Layer
VGPM	Vertically Generalized Production Model